Volume 3
Number 5
September 2025
Pages 873–1170

EES Catalysis

rsc.li/EESCatalysis

ISSN 2753-801X

ROYAL SOCIETY OF CHEMISTRY

REVIEW ARTICLE
Meenesh R. Singh and Joseph Gauthier *et al.*
Advancements in dinitrogen activation for catalytic breakthroughs

EES Catalysis

REVIEW ARTICLE

View Article Online
View Journal | View Issue

Check for updates

Cite this: *EES Catal.*, 2025, 3, 883

Advancements in dinitrogen activation for catalytic breakthroughs

Vamsi Vikram Gande,†[a] Nishithan C. Kani,†[a] Ishita Goyal,†[a] Rohit Chauhan,†[a] Yancun Qi,†[a] Samuel A. Olusegun,†[b] Joseph A. Gauthier*[b] and Meenesh R. Singh*[a]

Activation and catalytic transformation of dinitrogen (N_2) remains a grand challenge at the intersection of global food security, sustainable energy, and chemical manufacturing. The remarkable strength of the N≡N bond poses formidable thermodynamic and kinetic barriers, driving reliance on the century-old Haber–Bosch process-an energy-intensive route that consumes substantial fossil fuels. Recent advances underscore a growing shift toward alternative strategies, including biological and enzymatic pathways inspired by nitrogenase, homogeneous catalysis through transition-metal complexes, plasma-assisted reactions leveraging high-energy species, and diverse electrochemical or thermo-electrochemical methods integrating renewable power. Key breakthroughs in catalyst design, from metal nitrides and single-atom catalysts to next-generation perovskite oxides, highlight the importance of targeted bond weakening, electron back-donation, and multi-electron/proton transfer steps. Concurrently, mechanistic insights gleaned from *in situ* spectroscopy, density functional theory, and machine learning-guided screening are refining our understanding of molecular orbital interactions and reaction intermediates. Looking ahead, the N_2 activation field seeks to unite high efficiency with lower energy footprints by tailoring catalysts for mild conditions, exploring hydrogen sources beyond conventional H_2, and adopting process intensification strategies to curb carbon emissions. By bridging fundamental discoveries with scalable engineering, future research should aim to deliver cost-effective, low-carbon nitrogen fixation, reshaping the global nitrogen economy and paving the way toward sustainable ammonia production and novel nitrogen-based chemicals.

Received 4th February 2025,
Accepted 22nd April 2025

DOI: 10.1039/d5ey00033e

rsc.li/eescatalysis

Open Access Article. Published on 24 4 2025. Downloaded on 2026-02-14 8:12:44.
This article is licensed under a Creative Commons Attribution-NonCommercial 3.0 Unported Licence.

Broader context

Dinitrogen (N_2) activation is at the heart of a sustainable future, influencing global agriculture, energy, and industrial chemistry. The current state-of-the-art, dominated by the Haber–Bosch process, is energy-intensive and heavily reliant on fossil fuels, contributing to high carbon emissions. The imperative to transition toward low-carbon, energy-efficient nitrogen fixation technologies has sparked interest in alternative pathways, including biological, electrochemical, plasma-assisted, and thermochemical approaches. These emerging methods promise greener nitrogen fixation by leveraging advances in catalysis, mechanistic understanding, and computational modeling. Recent breakthroughs in catalyst design—such as single-atom catalysts, transition-metal nitrides, and perovskite oxides—have enabled new strategies for breaking the strong N≡N bond under mild conditions. Additionally, *in situ* spectroscopy, density functional theory (DFT), and machine learning are refining our understanding of catalytic pathways, helping to optimize activity and selectivity. Exploring alternative hydrogen sources, integrating renewable energy, and designing multi-functional catalytic systems will be crucial for next-generation nitrogen activation. This review aligns with global efforts to decarbonize chemical manufacturing and reduce dependence on fossil fuels. By bridging molecular-level insights with scalable engineering solutions, advancements in N_2 activation can pave the way for low-energy ammonia synthesis and novel nitrogen-based chemicals, reshaping the global nitrogen economy.

1. Introduction

Nitrogen, which constitutes most of the Earth's atmosphere, predominantly exists as dinitrogen (N_2), a molecule characterized by its exceptional stability due to the strength of the triple bond between nitrogen atoms (~9.79 eV). This strong bond presents significant challenges for nitrogen activation, converting N_2 into reactive or biologically valuable forms such as ammonia (NH_3).[1] The inert nature of N_2 arises from both thermodynamic and kinetic factors. Thermodynamically, the formation of nitrogen-containing compounds, such as nitrogen oxides, is challenging due to their positive standard free energies of formation, making them less stable than N_2 itself. Kinetically, N_2 activation is

[a] *Department of Chemical Engineering, University of Illinois Chicago, 929 W. Taylor St., Chicago, Illinois 60607, USA. E-mail: mrsingh@uic.edu; Tel: +1 (312) 413-7673*
[b] *Department of Chemical Engineering, Texas Tech University, Lubbock, Texas 79409, USA. E-mail: joe.gauthier@ttu.edu; Tel: +1 806 742 3552*
† Authors contributed equally.

© 2025 The Author(s). Published by the Royal Society of Chemistry

Open Access Article. Published on 24 4 2025. Downloaded on 2026-02-14 8:12:44.
This article is licensed under a Creative Commons Attribution-NonCommercial 3.0 Unported Licence.

sluggish in reactions with most reagents, necessitating high energy input or catalytic intervention. A prominent example is the industrial synthesis of NH_3 from N_2 and H_2, which requires a highly reactive catalyst and elevated temperatures to overcome these barriers. Addressing the challenge of N_2 activation is crucial for advancing sustainable agriculture, as NH_3 and NO_3^- are cornerstones of fertilizers, and their production is currently reliant on energy-intensive processes like the Haber–Bosch method. This review highlights the importance of N_2 activation, explores the challenges involved, and discusses emerging methods to facilitate its chemical transformation.

1.1. Need for N_2 activation (*i.e.*, to form NH_3 and nitrogen oxyanions)

Nitrogen activation is essential for converting atmospheric N_2 into biologically accessible forms such as nitrogen oxyanions (*e.g.*, nitrates (NO_3^-)) and NH_3. This process is critical for several reasons, as outlined below, along with some historical significance:

1.1.1. Fertilizer production. Ammonia and nitrates produced through nitrogen activation are critical components of fertilizers. Given that these forms of nitrogen are rare in nature compared to N_2, nitrogen activation plays a crucial role in supporting global food production. The vast majority of ammonia and nitrates are currently produced *via* the Haber–Bosch process, which consumes about 2% of the world's annual energy,[2] and follows the overall reaction in eqn (1). The process requires an aggressive catalyst, high pressure, and high temperatures to achieve the desired NH_3 synthesis yield. These extreme conditions, particularly the requirement of operation at elevated pressure, increases capital costs, prompting the search for more effective approaches.

The standard free energy formation of ammonia is −16.48 kJ mol^{-1}, and thus, the equilibrium constant of the reaction.

$$\frac{1}{2}N_2(g) + \frac{3}{2}H_2(g) \leftrightarrow NH_3(g) \quad (1)$$

at 25 °C is given by

$$K = e^{-\frac{\Delta G^\circ}{RT}} = 7.7 \times 10^2$$

This equilibrium constant suggests a favorable synthesis for NH_3 at room temperature if equilibrium were achievable at reasonable timescales. However, the extremely stable N–N bond leads to essentially zero forward rate of reaction in an uncatalyzed process at standard conditions despite the favorable equilibrium constant.[3]

1.1.2. Biological nutrient availability. Nitrogen is a vital nutrient for plant and animal growth and a key amino acid component. Since most plants and animals cannot utilize atmospheric nitrogen directly, nitrogen activation converts nitrogen into forms like nitrates and ammonia, making it biologically available for plants and animals to assimilate. Nitrogen is often a limiting nutrient in many ecosystems, meaning that its availability can affect the overall productivity of the ecosystem. Nitrogen activation helps maintain the balance of nutrients in ecosystems, influencing the health and diversity of plant and animal life.

1.1.3. Role in the nitrogen cycle. Nitrogen activation is a key step in the nitrogen cycle, a complex series of processes that involve the transformation of nitrogen through various chemical and biological reactions. Nitrogen activation helps replenish the pool of available nitrogen for living organisms.

1.1.4. Munitions (WWI and development of Haber process). The connection between munitions from World War I and the development of the Haber process is historically significant.[4] During World War I, there was a heightened demand for munitions, including explosives like nitroglycerin. At that time, Germany faced a shortage of nitrates, a key ingredient. This scarcity prompted German chemists, particularly Fritz Haber and Carl Bosch, to develop a process for synthesizing ammonia, a crucial precursor to nitrates. The Haber process was developed around 1909 and later modified by Bosch (Haber–Bosch process) in 1913. Eqn (1) shows the overall reaction for Haber-Bosch process. BASF acquired the invention, and in 1913, Carl Bosch scaled up production to establish the now widely recognized Haber–Bosch process. The process operates at temperatures ranging from 400 to 450 degrees Celsius and 150 to 250 bar pressures, utilizing a multi-promoted fused iron catalyst.[1] This breakthrough addressed the shortage of nitrates for explosives during the war and had profound implications for agriculture and the human population that the planet can support. Before industrial production of NH_3 by the Haber–Bosch process, natural fertilizers came as caliche from Chile and guano from Peru.[1]

1.1.5. Chincha Islands war. Guano, an agriculturally potent fertilizer abundant in nitrogen and phosphorus, commanded immense interest during the 19th century for its significant benefits in farming. The Chincha Islands emerged as a pivotal hub for guano, drawing the attention of nations vying for dominance in the lucrative guano trade. Also known as the Guano War, the Chincha Islands War occurred from 1864 to 1866 and involved a conflict between Spain and a South American alliance consisting of Peru, Chile, Ecuador, and Bolivia. The primary cause of the war was the control and exploitation of valuable guano deposits found on the Chincha Islands off the coast of Peru.

1.1.6. Saltpeter war. In South America, the Atacama Desert boasts substantial saltpeter (*i.e.*, potassium nitrate) reserves, and was the subject of a dispute between Bolivia, Chile, and Peru from 1879 to 1884. Recognized as the War of the Pacific, this conflict stands as a momentous chapter in South American history, its origins intricately linked to the strategic and economic significance of saltpeter.

While the well-established and productive Haber–Bosch process is not expected to be replaced in the immediate future, the reliance on d-block metals as catalysts for the N_2 reduction reaction (N_2RR) in both industry and nature has prompted the exploration of alternative strategies involving transition metals since the mid-1960s.[5] The critical role of ammonia in sustaining human life and societal progress has driven the quest to discover the requirements for efficient N≡N splitting under mild conditions with minimal energy input. Beyond the conventional use of NH_3, it has recently garnered attention as a

© 2025 The Author(s). Published by the Royal Society of Chemistry

Open Access Article. Published on 24 4 2025. Downloaded on 2026-02-14 8:12:44.
This article is licensed under a Creative Commons Attribution-NonCommercial 3.0 Unported Licence.

promising green fuel for fuel cells, elevating academic and industrial interest in achieving its fully sustainable production.

1.2. Challenges inhibiting N_2 activation

Despite the clear need for fixed nitrogen as a source of fertilizer and myriad nitrogen-containing chemical products, large-scale nitrogen activation remains a challenge that requires substantial fossil-derived energy and capital costs. Although the Haber process, given by eqn (1), is exergonic at ambient conditions,[6] state-of-the-art facilities require operation at extreme temperatures and pressure to achieve high production rates. At the heart of this challenge is the N≡N triple bond, among the most stable bonds in nature, with a dissociation energy of nearly 10 eV.[7] The high stability of the bond in N_2 can be understood by its orbital arrangement, illustrated below in Fig. 1. Each atom has five valence electrons in the 2s–2p orbitals. When these orbitals combine, they form eight molecular orbitals: four bonding (two σ and two π) and four antibonding (two σ* and two π*), as shown in Fig. 1.

The N_2 molecule has a total bond order of three, with electrons shared in both σ and π orbitals, a characteristic unique to N among diatomic elements. In addition to its high bond dissociation energy, N_2 has over a 10 eV gap between the highest occupied molecular orbital and the lowest unoccupied molecular orbital under standard conditions.[8] The triple bond encompasses one sigma (σ) bond and two pi (π) bonds, with the sigma bond formed by a head-on overlap of atomic orbitals and the pi bonds resulting from lateral overlap.

In N_2, the molecular orbitals include the highest occupied molecular orbital (HOMO), housing electrons in the sigma bond (σ), and the lowest unoccupied molecular orbital (LUMO), involving the π* antibonding orbitals. The activation of N_2 involves overcoming the high bond dissociation energy associated with the triple bond – a challenging process usually addressed industrially with the assistance of transition metals acting as catalysts. Initiating the nitrogen reduction reaction (NRR) is thermodynamically challenging due to several factors like dominant side reaction (HER), the large HOMO–LUMO gap that inhibits e^- transfer,[8] the high enthalpy change needed for proton transfer,[9] and the significant energy requirement to break the N≡N triple bond.[10,11] Transition metals, commonly used as catalysts, play a critical role in facilitating the activation of N_2. The metal catalyst provides a site for interaction with the electrons of the N_2 molecule, and the metal's d orbitals interact specifically with the π* antibonding orbitals. Through back donation, electrons from the metal catalyst are donated into the antibonding orbitals of N_2, thereby weakening the triple bond by reducing the electron density between the nitrogen atoms.

This interaction leads to the redistribution of electron density within the N_2 molecule, making the triple bond more susceptible to cleavage. During the activation process, intermediate species are formed, representing transitional stages in breaking the N_2 bond. These intermediates contribute to the eventual formation of nitrogen-containing compounds, showcasing the catalytic role of transition metals in driving the activation process. Understanding the principles of molecular

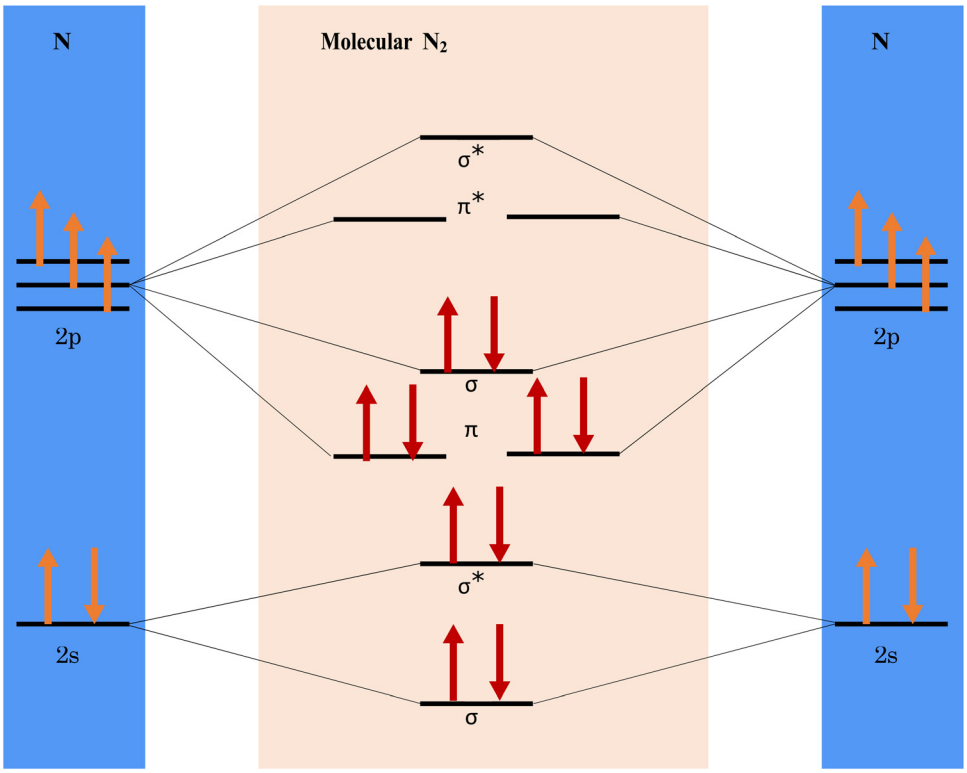

Fig. 1 Molecular orbital diagram for the N_2 molecule.

Open Access Article. Published on 24 4 2025. Downloaded on 2026-02-14 8:12:44.
This article is licensed under a Creative Commons Attribution-NonCommercial 3.0 Unported Licence.

orbital theory and the role of transition metal catalysts is pivotal for unraveling the complex activation of N_2. Such insights are not only fundamental to the understanding of chemical processes but also have practical applications. In this review, we discuss the aspects of the N_2 activation mechanism and the different methods of N_2 activation.

2. Methods for N_2 activation

Although molecular N_2 is abundant in nature, making up nearly 80% of the atmosphere, fixed nitrogen is far less common due to the N_2 molecule's very high stability. Naturally occurring fixed nitrogen is typically the result of complex biological pathways or high-energy plasma (*i.e.*, lightning strikes). Anthropogenic nitrogen activation was a topic of intense scientific interest in the late 19th century due to its importance in food production, chemical synthesis pathways to critical commodity chemicals, and relative rarity in nature. Over the past century, numerous strategies have been developed for efficient artificial nitrogen activation, varying widely in energy efficiency and output. In Fig. 2, we illustrate one efficiency metric comparing anthropogenic and biogenic nitrogen activation methods by plotting energy consumption as a function of the production rate. While the Haber–Bosch reaction is energy-intensive, the optimal heat recovery systems allow the overall energy consumption to be <20 GJ per ton NH_3. The other methods are currently more energy-intensive and have lower production rates. Table 1 shows the optimal and reported energy requirements of different ammonia production technologies.

In the following sections, we categorize the anthropogenic and biogenic strategies for nitrogen activation and provide mechanistic details, challenges, and potential for improvement.

2.1. Thermochemical N_2 activation

Thermochemical processes were among the first anthropogenic sources of fixed nitrogen. Today, thermochemical processes, primarily the Haber–Bosch process, account for the vast majority of fixed anthropogenic nitrogen at a rate of over 200 million tons of ammonia per year.[16] Most of this ammonia is converted into fertilizer and is necessary for sustaining our population, nearing 8 billion people. As such, the discovery of the Haber process has been hailed as the most important innovation of the 20th century.[17] In this section, we begin by discussing the background and history leading to the creation of the Haber process because understanding the context behind its development facilitates understanding the challenges we face as we search for a more sustainable alternative. We then discuss the mechanism underlying the Haber process and end with a future outlook for thermochemical processes.

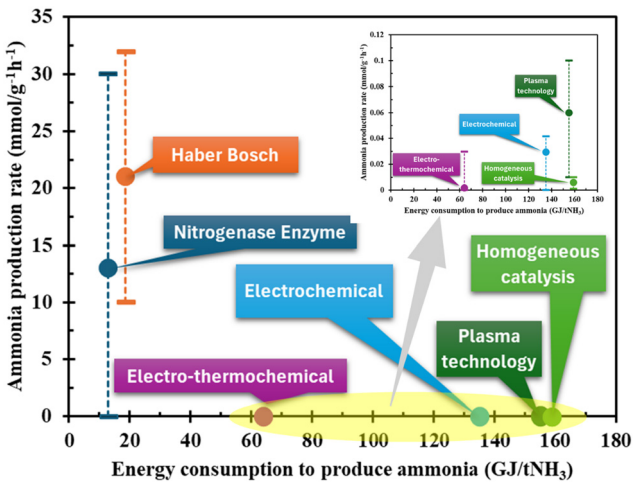

Fig. 2 Illustration of energy consumption *vs.* production rate for several methods of nitrogen activation.[12–15]

Table 1 Optimal and reported energy requirements for different ammonia production technologies[12]

	Energy requirement (GJ per t_{NH_3})	
	Reported	Potential
Brown ammonia		
Steam methane reforming (SMR)	26	26
Naptha	35	—
Heavy fuel oil	38	—
Coal	42	—
Blue ammonia		
SMR with CCS (carbon capture and storage)	33	27
Coal with CCS (carbon capture and storage)	57	—
eSMR	—	26
Green ammonia		
Low temperature electrolysis	33	31
High-temperature electrolysis	—	26
Others		
Benchmark electrolysis-based Haber–Bosch process	33	26
Non-thermal plasma technology	155	60–70
Electrochemical and photochemical synthesis	135	27–29
Electrochemical synthesis	135	27–29
Photochemical synthesis	—	200[a]
Electro-thermochemical looping	64	55
Homogeneous catalysis	900	159

[a] About 199 GJ per t_{NH_3} is required as direct solar energy.

2.1.1. Background and history. Before the development of technologies for producing and transporting natural gas, light hydrocarbons for fuel and lighting were produced on a more local level from coal.[18] The resulting gas, referred to as coal gas, manufactured gas, or town gas, had (among others) ammonia as an important by-product. By the late 19th century, the ammonia by-product was a critical component of the fertilizer and chemical process industry in the United States and Europe.[19] Recognizing the need for improved anthropogenic fixed nitrogen sources, European chemists sought new chemical pathways. Among thermochemical processes, the first successful industrialized process to fix dinitrogen was the Frank–Caro process, developed in 1895, which activates N_2 in the presence of calcium carbide at high temperatures.[20] The overall process is given by eqn (2).

$$CaC_2 + N_2 \rightarrow CaCN_2 + C \quad (2)$$

The process was operated at an extremely high temperature, around 1000 °C, achieved using electrical resistive heating. The

© 2025 The Author(s). Published by the Royal Society of Chemistry

Open Access Article. Published on 24 4 2025. Downloaded on 2026-02-14 8:12:44.
This article is licensed under a Creative Commons Attribution-NonCommercial 3.0 Unported Licence.

tremendous quantities of electricity required to maintain this high temperature limited its operation geographically to areas such as Norway, where dedicated hydroelectric power plants were constructed to supply the needed electricity.[21] Although highly energy inefficient, the Frank–Caro process was exceptionally important as a proof-of-concept: it demonstrated that anthropogenic dinitrogen activation *via* thermo-chemistry was possible on industrial scales. Interest in a more energy-efficient process grew, and in 1901, Le Chatelier discovered what would be later known as the Haber process,[22] in which gaseous nitrogen and hydrogen react to form ammonia at high temperature and pressure over an iron catalyst. Le Chatelier abandoned the research after an explosion in the high-pressure reactor nearly killed an assistant. The process was rediscovered by Haber in 1905.[19] After lab-scale production was demonstrated with an osmium catalyst in Haber's laboratory, BASF purchased rights to the process, with scale-up of the process assigned to Carl Bosch. Owing to its scarcity and tendency to deactivate over time, Alwin Mittasch was tasked with finding a cheaper alternative to the osmium catalyst. After thousands of attempts, Mittasch discovered the promoted iron catalyst that is still used in some ammonia production facilities today.[23]

2.1.2. Mechanism. The overall chemistry of the Haber–Bosch process is given by eqn (1), with an overall reaction enthalpy of -91.8 kJ mol^{-1} at standard conditions.[6] Despite being exergonic, the process must operate at high temperatures due to the high activation barrier to activate the stable N≡N bond.[24] At high temperatures, the reaction Gibbs free energy can shift from negative (spontaneous) to positive (non-spontaneous), even though the reaction enthalpy remains exothermic. This occurs because the negative reaction entropy contributes more significantly to the Gibbs free energy at elevated temperatures. High pressure is then required to favor the forward reaction by countering the entropy-related effects and ensuring a reasonable reaction rate. Fig. 3(a) shows the thermodynamic equilibrium between N_2/H_2 and NH_3 for the Haber–Bosch process. In this manner, the Haber–Bosch equilibrium refers to the chemical equilibrium established in the synthesis of NH_3 from N_2 and H_2 gases shown in eqn (1). This reaction is exothermic ($\Delta H < 0$). It involves a reduction in entropy due to the decrease in gas molecules. As a result, the equilibrium is favored by low temperatures and high pressures, according to Le Chatelier's principle. Industrial processes use moderately high temperatures (400–500 °C) to maintain a practical reaction rate, as lower temperatures significantly slow the kinetics. High pressures (150–300 atm) are applied to push the equilibrium towards NH_3 production. Catalysts, such as iron-based compounds, are utilized to overcome kinetic barriers and enhance the reaction rate under these conditions. The catalytic process and its mechanism are illustrated in Fig. 3(b).

The mechanism of the Haber process on Fe catalysts was largely unraveled by Gerhard Ertl in a series of papers that leveraged low energy electron diffraction (LEED) to estimate sticking coefficients for various intermediate steps along the process,[25–29] partly leading to his receipt of the Nobel Prize in 2007. The mechanism with individual reaction steps is given

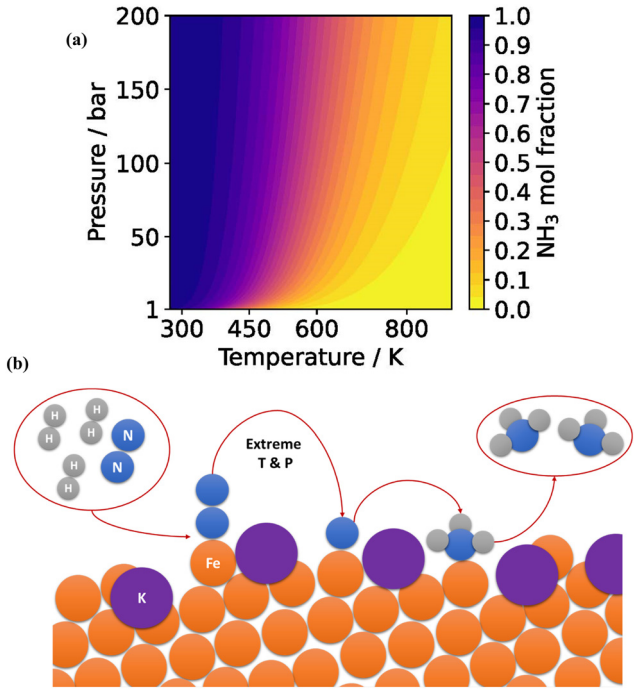

Fig. 3 (a) Thermodynamic equilibrium between N_2/H_2 and NH_3 (Haber–Bosch equilibrium); (b) animated illustration of the Haber–Bosch process, which occurs over a promoted iron catalyst at high temperature and pressure.

below in eqn (3)–(10). The rate-determining step is associated with the activation of bound dinitrogen, *i.e.*, eqn (4).

$$N_2 + * \rightarrow *N_2 \quad (3)$$

$$*N_2 + * \rightarrow 2*N \quad (4)$$

$$H_2 + * \rightarrow *H_2 \quad (5)$$

$$*H_2 + * \rightarrow 2*H \quad (6)$$

$$*N + *H \rightarrow *NH + * \quad (7)$$

$$*NH + *H \rightarrow *NH_2 + * \quad (8)$$

$$*NH_2 + *H \rightarrow *NH_3 + * \quad (9)$$

$$*NH_3 \rightarrow NH_3(g) \quad (10)$$

Later investigations into the Haber process by Nørskov and Chorkendorff demonstrated that activity likely is dominated by step sites[30] instead of the hypothesized terrace sites.[29] Further analysis of the role of the alkali cation promoter has, in time, revealed that the transition state of N_2 activation is stabilized through a dipole–field effect, and the promoter simultaneously reduces the effect of oxygen poisoning and modulates the binding energies of intermediates further down the pathway.[24,31–33]

Dinitrogen can undergo direct reactions with certain metallic elements. For example, the reaction of dinitrogen with lithium yields lithium nitride (Li_3N) which proceeds slowly at room temperature but rapidly at 250 °C.[3] Similarly, dinitrogen reacts with alkaline earth metals to form nitrides like Mg_3N_2, which occurs rapidly at temperatures above 500 °C. At even

Open Access Article. Published on 24 4 2025. Downloaded on 2026-02-14 8:12:44.
This article is licensed under a Creative Commons Attribution-NonCommercial 3.0 Unported Licence.

higher temperatures, dinitrogen reacts with elements such as boron, aluminum, silicon, and various transition metals. Dinitrogen is generally inert around 25 °C, it exhibits direct reactivity with several elements at elevated temperatures.[3]

Nitrogen forms a wide range of nitrides categorized as ionic, covalent, or interstitial. Elements like lithium, alkaline earth metals, zinc, and cadmium from nitrides containing the N_3-ion yield ammonia upon hydrolysis:

$$Li_3N + 3H_2O \rightarrow 3Li^+ + 3OH^- + NH_3 \quad (11)$$

$$Ca_3N_2 + 6H_2O \rightarrow 3Ca^{2+} + 6OH^- + 2NH_3 \quad (12)$$

Nitrogen compounds with elements from groups III, IV, and V are typically covalently bonded nitrides, including BN, Si_3N_4, and P_3N_5.

When nitrogen reacts with finely divided transition metals, it produces interstitial nitrides like W_2N, TiN, and Mo_2N. These nitrides feature nitrogen atoms within the metallic lattice, sharing similarities with interstitial carbides in hardness, high melting points, electrical conductivity, non-ideal stoichiometry, and chemical inertness.

2.1.3. Future outlook for thermochemical nitrogen activation. The Haber–Bosch process has undergone more than a century of optimization. Today it is far more efficient than the initial industrial process implemented by Bosch, which utilized an osmium catalyst and is approaching thermodynamic limits of energy efficiency.

2.1.3.1. Improvement in thermocatalysts. The industrial Haber–Bosch process poses significant challenges, *i.e.*, high pressures and temperatures. A corresponding equation of thermocatalytic N_2 activation suggests that reducing the reaction temperature would be beneficial. If the reaction is conducted at a comparatively low temperature, the rate of reaction of N_2 activation reduces significantly. Therefore, extensive efforts have been made to facilitate this reaction in moderate conditions while maintaining the reaction rate.

Compared to industrial processes, milder conditions can be used to interchange nitrogen atoms between nitrogen molecules and lattice nitrogen. This exchange facilitates the splitting of nitrogen bonds. Additional strategies are needed to reduce the reaction barrier and further enhance the performance of thermocatalytic N_2 activation in ambient conditions. While Ru-based materials have an advantage over Fe-based materials due to less NH_3 poisoning, ruthenium catalysts are susceptible to hydrogen poisoning because of the strong binding of hydrogen atoms. Hosono and co-workers[34] proposed a mechanism of NH_3 production using ruthenium supported on the C12A7:e^- substrate, which allows for reversible release and storage of hydrogen atoms, thereby preventing hydrogen poisoning. Metal hydrides, such as TiH_2, LiH, BaH_2, and CaH_2, have also been crucial in low-temperature thermocatalytic nitrogen activation processes. These hydrides create energy-favored pathways for thermocatalytic NH_3 production in milder environments. Despite the progress made, some thermocatalytic processes still rely on high pressure, which poses a disadvantage due to the need for a source of H_2 gas and N_2.[35–37] Table 2 consists of a few thermocatalysts, which showed great performances for N_2 activation under mild conditions. In addition, the effect of spin promotion on producing NH_3 is studied, and the probable structure of active sites with various promoters is determined. Furthermore, two factors that influence catalytic activity were observed. Firstly, an electrostatic relation occurs between the N–N dissociation transition state and the adsorbed promoter. Additionally, it reported a novel promoter effect in magnetic catalysts, significantly reducing activation energy.[38] These findings open opportunities for discovering new types of thermocatalysts for NH_3 synthesis.

High activity and long-term stability can be achieved by surface modification or alloying. This can potentially reduce

Table 2 Thermocatalysts showed great performances for N_2 activation under mild conditions

Catalyst	Temperature	Remark	Ref.
Ba–Co/C	320–440 °C	The NH_3 concentration rises almost three times.	39
Ru-loaded C12A7:e^-	360–400 °C	The electrode C12A7:e^- is a stable and effective electron donor, acting as a reversible hydrogen-storage material to improve catalytic activity in NH_3 synthesis.	34
Ru/Ca_2N:e^-	300–340 °C	Showed superior catalytic functioning for low-temperature NH_3 synthesis compared to heterogeneous catalysts.	40
Ru/BaO–CaH_2	200–350 °C	NH_3 synthesis at low temperatures with minimal activation energy (41 kJ mol^{-1}).	41
BaH_2–Co/CNTs	250–350 °C	Exceptional catalytic activity at low temperatures, ≈20 and 2.5 times greater than the substantially active Cs–Ru/MgO catalyst.	37
Cr–LiH, Mn–LiH, Fe–LiH and Co–LiH	150–300 °C	The collaboration between transition metals and LiH establishes an energy-efficient route for NH_3 synthesis at moderate conditions.	42
Ni/LaN	350 °C	LaN catalyst with Ni loading demonstrates activity surpassing traditional Ni- and Co-based catalysts, equivalent to Ru-based catalysts.	43
CeN, LaN, and YN,	150–400 °C	Rare earth metal nitrides assist effectively as supports or catalysts in NH_3 synthesis, with nitrogen-vacancy generation significantly influencing catalytic performance.	44
Ru/$Ca(NH_2)_2$	250–350 °C	The excellent catalytic performance is credited to the development of a dense array of flat-shaped ruthenium nanoparticles and the electron-promoting influence of $Ca(NH_2)_2$.	35
Ru/$Ce_xZr_{1-x}O_2$	390 °C	Enhanced electronic metal–support interactions increased NH_3 synthesis catalytic activity and reduced the apparent reaction activation energy.	45
Ru/C in Cs	250–400 °C	Dosing pure metallic Cs *in situ* proves significantly more effective for NH_3 synthesis than conventionally synthesized Ru catalysts, which are promoted *ex situ* with Cs.	46

© 2025 The Author(s). Published by the Royal Society of Chemistry

Open Access Article. Published on 24 4 2025. Downloaded on 2026-02-14 8:12:44.
This article is licensed under a Creative Commons Attribution-NonCommercial 3.0 Unported Licence.

the susceptibility to hydrogen poisoning by altering the electronic and geometric properties of the Ru surface, thus enhancing both catalytic activity and resistance to poisoning. Alternatively, the surface can modify hydrogen adsorption properties, making it less prone to poisoning. For example, combining Ru with oxide supports like Al_2O_3 or TiO_2 can improve stability. These modifications can help reduce the adsorption of hydrogen molecules on Ru while maintaining high catalytic activity for NH_3 synthesis. Electrostatically polar MgO(111) to replace nonpolar MgO as the support can significantly alleviate the hydrogen poisoning and facilitate an unprecedented ammonia production rate by its high intrinsic proton capture ability.[47] Similarly, other refractory metals, or oxide supports, can be explored as future work.

2.1.3.2. More sustainable sources of hydrogen. Today, ammonia producers exhibit greater operational expertise in hydrogen production than all other segments of the hydrogen-producing industry combined.[48] This knowledge is crucial for their success in competitive markets, as it can determine profitability. NH_3 producers are now seeking a new type of hydrogen, one that is decarbonized, sustainable, and renewable. While there will be numerous significant markets for renewable hydrogen in the future, the immediate focus lies on renewable fertilizers, which present a practical and substantial market opportunity that far outweighs existing markets in scale. The production of green hydrogen through low-temperature water electrolysis powered by renewable energy is a critical step toward rapidly reducing carbon emissions in the industrial sector, particularly in ammonia synthesis *via* the Haber–Bosch process. Several challenges currently hinder green hydrogen production's economic viability, including high costs, scalability, energy efficiency, *etc.* Despite these obstacles, this technology is expected to decarbonize chemical transformation processes.

To further enhance its potential, researchers are exploring direct seawater electrolysis, which utilizes abundant seawater resources and eliminates the need for high-purity water, addressing one of the key limitations of conventional electrolysis methods. The world's oceans hold an almost limitless supply of seawater, whereas freshwater is becoming an increasingly scarce resource. Direct seawater electrolysis is an emerging technology for converting and storing electricity into hydrogen in this global context. It proves most valuable in areas with abundant renewable electricity, limited freshwater access, and ample seawater resources. It is also advantageous for offshore hydrogen and mobile maritime-based applications, such as powering unmanned underwater vehicles for offshore maintenance.[49,50] There are few environmental and economic incentives to invest in research and development for current direct seawater electrolysis technology. The costs associated with commercial water electrolysis are significantly higher compared to seawater reverse osmosis (SWRO). The operating and capital costs of SWRO are trivial, resulting in a minimal enhancement in the levelized cost of hydrogen (less than \$\$0.1 per kg of H_2) and CO_2 releases (less than 0.1%) in a seawater reverse osmosis-proton exchange membrane coupled process.[49] Promising catalysts have been identified for anodes and cathodes whereas novel separators and advanced membrane concepts are crucial for enhancing the solidity of direct seawater electrolyzer devices.[51]

The steam-methane reforming (SMR) process is another significant process for producing hydrogen. The production of significant chemicals like NH_3 and hydrogen contributes significantly to CO_2 emissions due to reliance on hydrocarbon combustion for heating during synthesis. SMR is responsible for approximately 50% of the global hydrogen supply and is one of the most significant endothermic processes. The production of hydrogen alone is estimated to contribute 3% of the emissions of CO_2.[52] The Chorkendorff and Mortensen[52] research group presented a highly efficient reformer driven by electricity, utilizing direct resistive (ohmic) heating. This scalable technology is suitable for industrial conditions and capacities. The direct interaction between the electric heat source and the catalyst allows precise reaction control and eliminates thermal constraints. This innovative approach removes the need for a fired section, significantly reducing reactor volume, waste-heat streams, and CO_2 emissions. This breakthrough technology gives existing industrial reformers a competitive edge by enabling the production of environment friendly hydrogen to synthesize crucial chemicals like NH_3. Electrifying SMR opens up new possibilities for reactor design, scalability, and implementation.[52]

Despite the limitations of SMR in terms of economics and the environment, no existing renewable power sources, including electrolysis-based hydrogen, can rival the large-scale H_2 production achieved by SMR. Another option for H_2 production is the pyrolysis of CH_4, which does not generate CO_2 (*i.e.*, $CH_4(g) \rightarrow C(s) + 2H_2(g)$ $\Delta H^\circ = 74$ kJ mol^{-1}).[53] Although this method produces only half the amount of H_2/mole of CH_4 associated with SMR, it requires significantly less energy contribution and produces solid carbon instead of CO_2. This solid carbon can be safely deposited indefinitely and even utilized in various applications such as electrodes or additives in materials like asphalt, concrete, and rubber. Furthermore, straight CH_4 pyrolysis can be carried out in a comparatively simple and potentially cost-effective commercial process, requiring only a single reaction step. Most downstream processes can tolerate small amounts of unconverted CH_4, making it suitable for applications like NH_3 production or use in fuel cells. On the other hand, carbon oxides produced by the SMR process can be detrimental to catalysts and must be eliminated.[53] The McFarland research group[53] has developed a catalytic molten metal method for direct methane conversion into hydrogen and carbon separation. The insoluble carbon of this system rises to the surface for easy removal. The optimal alloy composition, 73% Bi and 27% Ni, enables pure H_2 production without emitting CO_2 or by-products. In addition, Palmer *et al.*[54] and Kang *et al.*[55] synthesized molten Bi–Cu alloy and molten $MnCl_2$–KCl catalyst, respectively, for CH_4 pyrolysis to produce CO_2-free H_2.

2.2. Biological and enzymatic N_2 activation

Biological N_2 activation is a crucial natural phenomenon, possibly second to photosynthesis. The vitality of many natural

Open Access Article. Published on 24 4 2025. Downloaded on 2026-02-14 8:12:44.
This article is licensed under a Creative Commons Attribution-NonCommercial 3.0 Unported Licence.

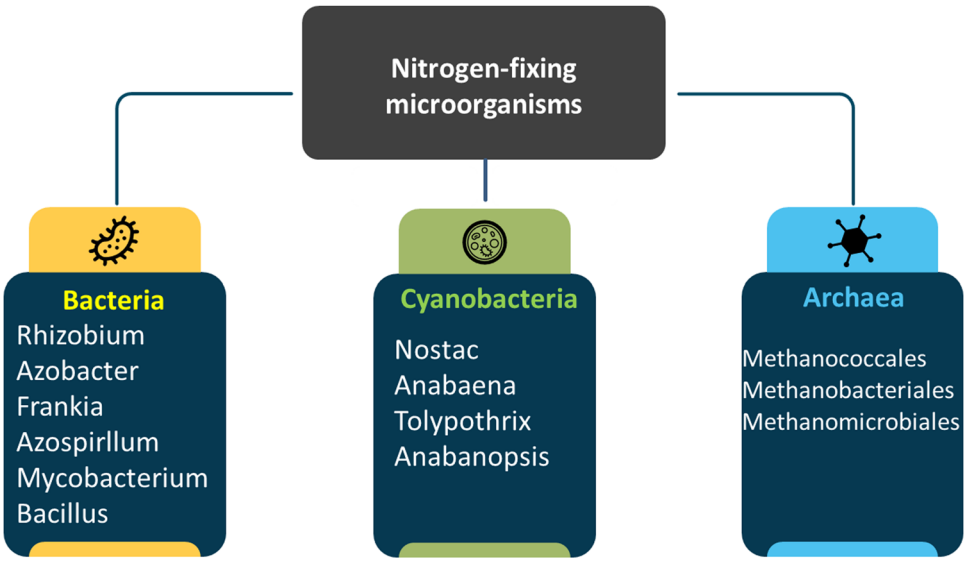

Fig. 4 Classification of nitrogen-fixing microorganism.[58]

ecological systems relies significantly on the biological conversion of atmospheric N_2 into forms that plants and microbes can utilize for growth, all without modern fertilizers or animal waste. Various prokaryotic microbes, including bacteria, archaea, cyanobacteria, and actinomycete *Frankia*, orchestrate this conversion.[56] Fig. 4 shows the classification of nitrogen-fixing microorganisms. The organisms involved in nitrogen activation can either function independently as free-living entities or form associations of varying complexes with other plants, microbes, and animals. These associations range from free connections, such as associative symbioses, to intricate symbiotic relationships (Fig. 5), where precise molecular transfer occurs between the host plant and the bacterium, accompanied by allocated physiological actions. The core of the system is the prokaryotic microorganism that hosts the nitrogenase enzyme complex, which facilitates nitrogen activation by converting N_2 into NH_3. Dinitrogen activation is an exclusive capability of certain prokaryotes. Therefore, when encountering claims about "nitrogen-fixing" plants, it's crucial to recognize that they achieve this through their partnership with prokaryotic organisms, not independently. Organisms that rely on atmospheric N_2 as their primary nitrogen source crucial for growth are diazotrophs. The term "diazo" pertains to N_2, and "trophs" signifies nourishing, a terminology introduced by Burns and Hardy in 1975.[57]

2.2.1. Importance of biological nitrogen activation. The fundamental principle in agriculture and plant physiology directs that plants need significant nitrogen levels for high biomass yield or production. Nitrogen is a necessary element for all living organisms, playing a crucial role in producing proteins, nucleic acids, and other vital biochemicals. In soil, nitrogen often serves as the controlling nutrient for microbial growth and plants. Soil is the primary nitrogen source for the growth of plants in nature, which comes from either atmospheric deposition from rainfall or the biological nitrogen activation process.

The Haber–Bosch process contributes approximately 95 million metric tons per year to global nitrogen supplies, requiring substantial energy inputs, typically as natural gas (Fig. 5).

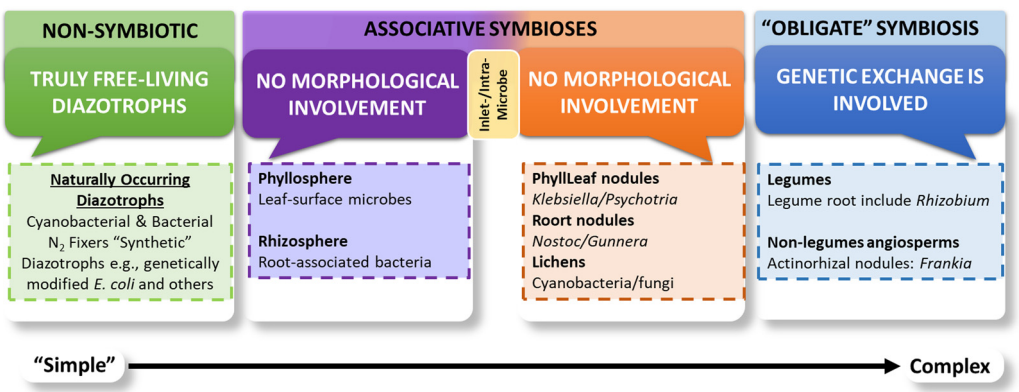

Fig. 5 The exclusive mediation of biological nitrogen activation occurs through free-living diazotrophs prokaryotic and a diverse array of plant-microbe connections with variable degrees of complexity.[56]

© 2025 The Author(s). Published by the Royal Society of Chemistry

Open Access Article. Published on 24 4 2025. Downloaded on 2026-02-14 8:12:44.
This article is licensed under a Creative Commons Attribution-NonCommercial 3.0 Unported Licence.

This quantity is overshadowed by the universal impact of fixed nitrogen obtained within biological nitrogen activation. Pinpointing precise assessments for biological N_2 activation proves challenging.[59] Fowler *et al.*[60] propose that approximately one-third of human-caused nitrogen contribution into terrestrial ecosystems originates from biological nitrogen activation (58 million metric tons ± 50%), while the remaining two-thirds come through fertilizer involvements (120 million metric tons ± 10%). The difficulty in obtaining accurate measurements is emphasized by the wide range of values observed for biological N_2 activation. Symbiotic N_2 activation constitutes the primary source of biological input, but associative and nonsymbiotic N_2 activation also play a notable role in crops like sugarcane and sorghum, particularly in ecosystems where nitrogen is a growth-limiting factor. Rice cultivation, characterized by submerged soils, obtains substantial benefits from free-living cyanobacteria and diazotrophic bacteria. These microorganisms thrive in favorable habitats within flooded soils, such as modest oxygen concentrations and root exudates.[59,60]

Biological N_2 activation offers a cost-effective substitution for expensive nitrogen from NH_3-based fertilizers. Sustaining high-profit agricultural practices in the USA and other regions solely through animal manure and biological nitrogen activation poses significant challenges. The increasing global population necessitates production systems that judiciously incorporate both artificial and, wherever feasible, natural fertilizers. Leguminous plants, alongside further nitrogen fixing methods such as the *Azolla–Anabaena* interaction and potentially naturally transformed vegetation (still in development), will remain integral to ecological agricultural processes. N_2-fixing plants also significantly benefit the restoration of concerned or depleted soils. These have multiple purposes, acting as natural manures, outstanding cover crops, and fodder for cattle. Utilizing nitrogen-fixing crops has the added perspective to mitigate groundwater pollution with NO_3^- and minimize the emission of N-based "greenhouse gases". This multifaceted approach underscores the importance of integrating various strategies to ensure agricultural productivity and environmental sustainability.[59–61]

2.2.2. The complexity of the nitrogenase enzyme: insights into nitrogen activation. Biological nitrogen activation occurs primarily among prokaryotic microbes, encompassing various classes of soil bacteria, *i.e.*, cyanobacteria (known as blue-green algae), and a limited number of actinobacteria, particularly *Frankia*. They demonstrate the capability to fix N_2 in various processes, including as free-living forms independent of plants, in loose associations known as associative symbioses (various grass-bacteria groups) (Fig. 5), and within intricate symbiotic connections with more plants, such as the root-nodule symbioses which are *Frankia* and rhizobia.

All these microbes share a common trait—they generate the complex enzyme known as nitrogenase, facilitating biological nitrogen activation. The term "nitrogenase complex" is aptly applied as it comprises two components of protein, consisting of various subunits, respectively, and accommodates various metallic clusters crucial for catalyzing the reaction of dinitrogen to NH_3.[62] Table 3 represents the nomenclature for nitrogenase enzyme complexes. Fig. 6 illustrates the understanding of the nitrogenase enzyme complex. Unique for its dual proteins, nitrogenase complexes comprise the MoFe and protein known as dinitrogenase and dinitrogenase reductase, respectively. Susceptible to oxygen, it contains Fe and Mo, or V. Activation requires Mg^{2+} and involves the conversion of ATP to ADP. Inhibition by ADP occurs, yet it converts N_2 and various molecules having triple bonds. Remarkably, it reduces protons to dihydrogen even in the presence of dinitrogen.

The biological nitrogen activation reaction utilizing nitrogenase is depicted in Fig. 6. For all e^- transfer from dinitrogenase reductase into dinitrogenase, two MgATPs are necessary. The written reaction demands 16 ATP molecules (112 kcal). An estimated 20–30 MgATP may be required under usual operational conditions, as the procedure is less effective than in optimal lab conditions.[64] Over several years, a consensus has gradually emerged on the universal nitrogenase model.

In summary, the nitrogenase mechanism involves dinitrogenase reductase (*i.e.*, Fe-based protein) receiving e^- from a donor with low-redox, binding two MgATP. It then transfers e^- separately to dinitrogenase (*i.e.*, MoFe-based protein). This complex facilitates electron transfer and hydrolyzing of two

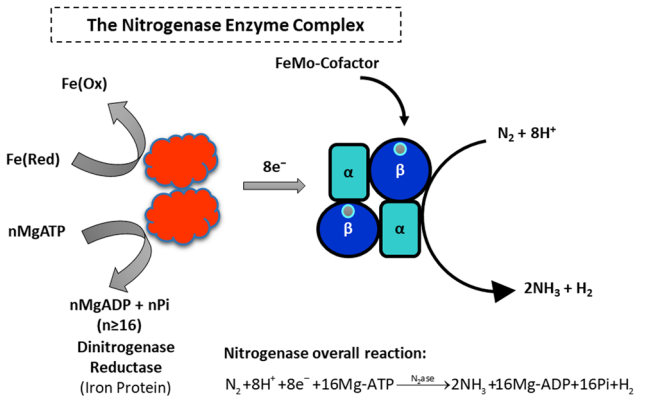

Fig. 6 The nitrogenase enzyme complex is composed of two protein constituents, *i.e.*, dinitrogenase reductase and dinitrogenase.[56,63]

Table 3 Nomenclature for nitrogenase enzyme complex

Nomenclature	Nitrogenase complexes
Nitrogenase	The overall complex
Dinitrogenase	The MoFe protein, which conventionally receives its name based on its substrate (in this case, dinitrogen), plays a crucial role in nitrogen activation.
Dinitrogenase reductase	The Fe protein (the consensus is that its role is to reduce dinitrogenase)

Open Access Article. Published on 24 4 2025. Downloaded on 2026-02-14 8:12:44.
This article is licensed under a Creative Commons Attribution-NonCommercial 3.0 Unported Licence.

MgATP to MgADP + Pi. After dissociation, the process repeats. Once dinitrogenase accumulates adequate e^-, it combines N_2; then, it is reduced into NH_4^+. The dinitrogenase continues the cycle by accepting extra e^- from dinitrogenase reductase.

In each nitrogen activation cycle, dinitrogenase reductase and dinitrogenase combine, hydrolysis of MgATP occurs, and an e^- is shifted. The rate-limiting step is dissociating the MoFe protein–Fe protein complex. Notably slow, the nitrogenase complex takes 1.25 s to convert one enzyme molecule into two NH_3 molecules. To accomplish this, the two proteins must undergo a process of association and dissociation eight times to catalyze the reduction of a single dinitrogen molecule.[65] Due to its sluggish nature, nitrogen-fixing bacteria must produce a substantial amount of the protein. Nitrogenase can make up 10% cell's proteins, with recorded concentrations reaching ≈40%.[65] In the overall reaction illustrated in Fig. 6, it could be noted that for each $8e^-$ transmitted by the nitrogenase complex, the $2e^-$ is utilized in H_2 production. Hydrogen production is essential for nitrogen activation, with each molecule of H_2 (requiring 4 MgATP) supporting the activation of one N_2 molecule, which is then converted into $2NH_3$ molecules (requiring 12 MgATP). Consequently, 25% of the MgATP energy is wasted in the production of H_2, whereas certain diazotrophs understand hydrogenase, enabling oxidation of specific H_2 and producing a reduced e^- carrier or MgATP. This regained energy can be harnessed during the nitrogen activation process, compensating for the small amount of energy initially lost.

2.2.3. Unconventional nitrogenases. Before the 1980s, scientists believed there was only one type of nitrogenase, and molybdenum was crucial for nitrogen activation. In the early 1980s, Dr Paul Bishop and his team in North Carolina made a groundbreaking discovery by isolating a second type of nitrogenase (known as nitrogenase-2) from *Azotobacter chroococcum*.[66] It was generated exclusively with molybdenum-starved conditions.[66] This discovery revealed that Mo was not universally necessary for nitrogen activation and possibly will be replaced by V. Similar to nitrogenase-1, nitrogenase-2 is composed of two proteins – a VFe protein and a Fe protein – and it generates H_2 while being sensitive to O_2. The VFe protein of nitrogenase-2 can bind nitrogen, indicating that metals other than molybdenum can also play a role in nitrogen binding for reduction. Furthermore, a third type of nitrogenase, nitrogenase-3, was later discovered. Interestingly, nitrogenase-3 does not appear to contain molybdenum or vanadium and is synthesized when both metals are deficient due to starvation conditions.

All ''nitrogenases'' consist of a dinitrogenase and dinitrogenase reductase component. Nitrogenases 2 and 3 generate more gaseous hydrogen compared to nitrogenase 1. Instead of converting acetylene to ethylene, they transform it into ethane. In the 1990s, a new putative nitrogenase was reported in *Streptomyces thermoautotrophicus*, a thermophilic and chemoautotrophic actinomycete.[67,68] This unique nitrogenase, not inhibited by CO like others, comprised of three proteins: dinitrogenase, carbon monoxide dehydrogenase and, superoxide oxidoreductase, accountable for the N_2-activation. The enzyme-containing Mn served as a superoxide dismutase, supplying e^- to the dinitrogenase. Remarkably, this nitrogenase, specified as a superoxide-dependent nitrogenase, not only resisted O_2 poisoning but also required O_2 in its reaction mechanism.[67]

In 2016, MacKellar and colleagues, in a collaborative effort across seven laboratories globally, reported conclusive evidence that *S. thermoautotrophicus* cannot fix nitrogen.[69] Despite working with the original isolate and two extra strains, they couldn't validate the combination of ^{15}N-labeled N_2 ($^{15}N_2$) in cell constituents. The authors suggested reclassifying species H1, UBT1, and P1-2 as a non-diazotrophic, non-streptomycete, and facultative chemolithoautotroph. Based on their findings, it was strongly concluded that the presence of the previously suggested oxygen-tolerant nitrogenase is highly improbable.[69] With >99% nucleotide identity to *Hydrogenibacillus schegelii*, a carbon-monoxide oxidizing bacterium, the statement of nitrogen activation by *S. thermoautotrophicus* awaits further verification.

The discovery that N_2 can be fixed without the involvement of molybdenum is remarkable. Before discovering alternative nitrogenases, scientists considered molybdenum an obligatory requirement for N_2 activation. The prevalence of microorganisms with nitrogenase 1 (the enzyme-containing Mo) might be attributed to researchers consistently using Mo-containing enzymes for isolating nitrogen-fixing bacteria. It remains uncertain whether other nitrogenases are widespread. The exploration of alternative nitrogenase systems is in its early stages, and numerous fundamental questions are yet to be answered.[56]

2.2.4. Understanding of the biological N_2 activation through molecular orbitals. The theory of N_2 photoactivation offers the potential to harness sunlight as an energy source for one of the most challenging small molecule activation processes. Simultaneously, this approach allows for energy storage in a practical form by producing valuable chemical intermediates or products. To the best of the author's knowledge, the notion of dinitrogen photoactivation and cleavage was first introduced in 1975 by Fischler and von Gustorf.[70,71] They proposed that specific electronic excitations could trigger significant geometric and electronic transformations in a dinitrogen molecule coordinated to a transition metal, thereby modifying its chemical reactivity. They hypothesized for an end-on Fe–N_2 complex that: (i) d–d transitions would deplete an Fe–N π-bonding orbital while populating an Fe–N σ*-antibonding orbital, effectively weakening the Fe–N bond and promoting its homolytic cleavage (illustrated by the orange arrow in Fig. 7(a)); and (ii) ligand-to-metal charge transfer (LMCT) transitions would populate an N–N π*-antibonding orbital, enhancing the basicity of the nitrogen atoms and enabling their protonation (illustrated by the blue arrow in Fig. 7(a)).

In the conventional biological process of N_2 activation through nitrogenase enzymes, compelling evidence suggests that electron back-donation to π* orbitals facilitates the adsorption and activation of N_2 on the Fe–Mo–S cofactor within the FeMo–protein. The peripheral Fe protein then hydrolyzes MgATP to provide the necessary energy and electrons for the subsequent multiple proton–electron transfer (PET) processes leading to NH_3 generation.[73,74] Throughout these reduction processes, the Fe–protein scaffold around the cofactor functions as a coordination buffer sphere, utilizing H-bonding and redox-active groups to ensure a smooth PET process with a low

© 2025 The Author(s). Published by the Royal Society of Chemistry

Open Access Article. Published on 24 4 2025. Downloaded on 2026-02-14 8:12:44.
This article is licensed under a Creative Commons Attribution-NonCommercial 3.0 Unported Licence.

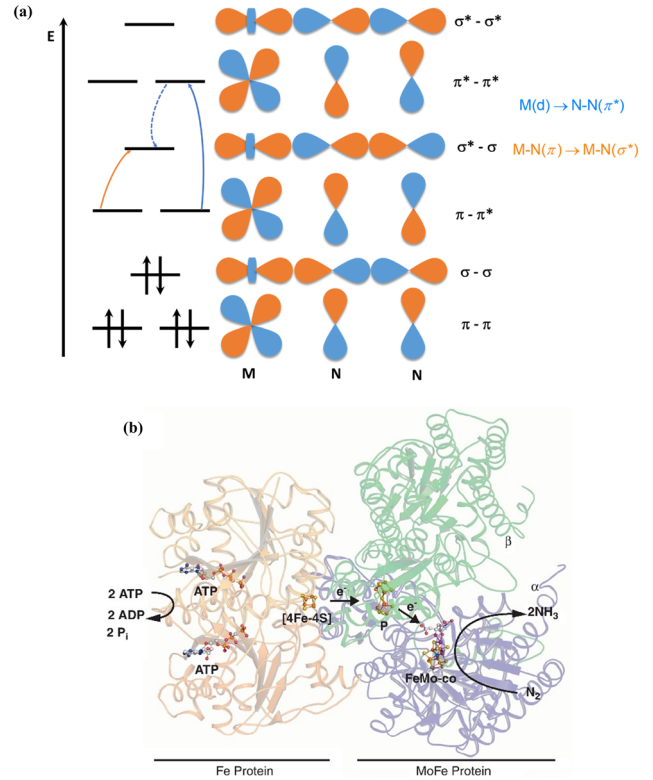

Fig. 7 (a) Two theoretical pathways for N_2 photocleavage, as proposed by Fischler and von Gustorf, involving an Fe-η^1-N_2 complex;[70] (b) reduction of N_2 to NH_3 in nitrogenase complex (reproduced with permission from Elsevier. Copyright © 2012 Elsevier).[72]

energy barrier (Fig. 7(b)).[75,76] Significantly, the active centers capable of adsorbing N_2, such as transition metals Mo and Fe, along with efficient e^- transfer pathways to the antibonding π^* orbitals of N_2, are essential for N≡N bond cleavage in NRR. Although the initial stage of NRR is challenging, the subsequent PET processes are thermodynamically favorable.[10]

The reduction of N_2 to NH_3 by the nitrogenase enzyme involves several crucial steps, with the FeMo-cofactor playing a vital role in weakening the N≡N bond and facilitating electron transfer. N_2 binds to the FeMo-cofactor, where interactions with the metal atoms (such as Fe and Mo) in the cofactor transfer electron density into the antibonding orbitals (π^*) of N_2. This reduces the bond order and makes N_2 more reactive. Furthermore, the back-donation mechanism involves metal atoms, particularly Mo and Fe, donating electrons from their d-orbitals into the π^* orbitals of N_2, further weakening the triple bond and facilitating its cleavage. The reduction process is mediated by the stepwise transfer of electrons from the Fe protein to the MoFe protein, and ultimately to the N_2 molecule, with each electron transfer often coupled with protonation (addition of H^+ ions). As electrons and protons are added, the electronic structure of the intermediates like diazene (N_2H_2) and hydrazine (N_2H_4) changes, leading to further weakening of the N≡N bond and gradual formation of N–H bonds. The final steps in the reduction process involve the complete reduction of N_2 to NH_3. Each protonation step consists of the addition of H^+ to form N–H bonds, accompanied by corresponding e^- transfers to neutralize the added protons. The stabilization of these intermediates and the stepwise reduction pathway culminated in the production of NH_3.[77–80]

2.2.5. Environmental factors affecting nitrogen activation. The energy supply (carbon availability), the presence or absence of enough combined nitrogen, and the amount of molecular oxygen largely dictate the synthesis and level of nitrogenase activity exhibited by bacteria in different environments. While less significant, other environmental factors should not be disregarded. Nitrogenase activity is observed within a narrow temperature range. At lower temperatures (5 °C–10 °C), nitrogenase activity is minimal, and at higher temperatures (37 °C–40 °C), it rapidly decreases due to the enzyme's heat sensitivity. Though most diazotrophs are mesophiles, there are exceptions, like thermophilic cyanobacteria that thrive in hot springs. *Methanococcus thermolithotrophicus*, a methanogen, can fix dinitrogen at a temperature of 64 °C. Various aspects, including adequate phosphorus supply (since nitrogen activation needs high levels of pressure), other inorganic elements (specifically trace metals), and the alkalinity or acidity of the medium, can impact the survival and growth of diazotrophs, therefore influencing N_2 activation indirectly or directly. Table 4 shows the factors influencing nitrogen activation through free-living soil microorganisms, both abiotic and biotic.

Environmental factors significantly impact rhizobial diversity, shaped by microbial species' adaptability to prevailing

Table 4 Factors influencing nitrogen activation by free-living soil bacteria, both biotic and abiotic

Feature	Abiotic or biotic	Effect on N_2 activation
Energy/carbon source	Abiotic/biotic	• The primary controlling factor for nitrogen activation in free-living soil diazotrophs is the absence of an abundant supply of available organic carbon. • This is due to the requirement for substantial amounts of ATP to support nitrogenase activity.
O_2	Abiotic	• In most cases, nitrogenase is conclusively reduced when exposed to oxygen. • For aerobes, the most vigorous nitrogen activation occurs when oxygen levels are significantly reduced, and for anaerobes and facultative anaerobes, oxygen must generally be absent.
Combined N (NO_3^-, NH_4^+, *etc.*)	Abiotic	• Combined nitrogen in the soil, such as NH_4^+, NO_3^-, and organic nitrogen compounds (like amino acids, *etc.*), strongly regulates nitrogenase activity.
Competition	Biotic	• Nitrogen-fixing microbes face competition with other soil bacteria for carbon sources, among other resources. • It is widely accepted that diazotrophs comprise 1% to 10% of the cultivable microbial population.
Others	Biotic/abiotic	• Like other soil microbes, diazotrophs are vulnerable to predation by protozoa and bacterial virus lysis (bacteriophages). • Factors such as temperature, pH, and trace component availability also influence their survival.

Open Access Article. Published on 24 4 2025. Downloaded on 2026-02-14 8:12:44.
This article is licensed under a Creative Commons Attribution-NonCommercial 3.0 Unported Licence.

conditions.[81,82] Environmental conditions influence both the rhizobial response and the host, resulting in a decline in the efficiency of symbiotic N_2 activation.[83] The extent of this reduction is contingent on how microorganisms thrive, live, and survive in diverse conditions, considering the dynamic nature of stress influenced by collective conditions of salinity, temperature, pesticides, soil pH, drought, or nutrient deficiency.[84] This symbiotic process is influenced by prominent factors shown in Fig. 8.

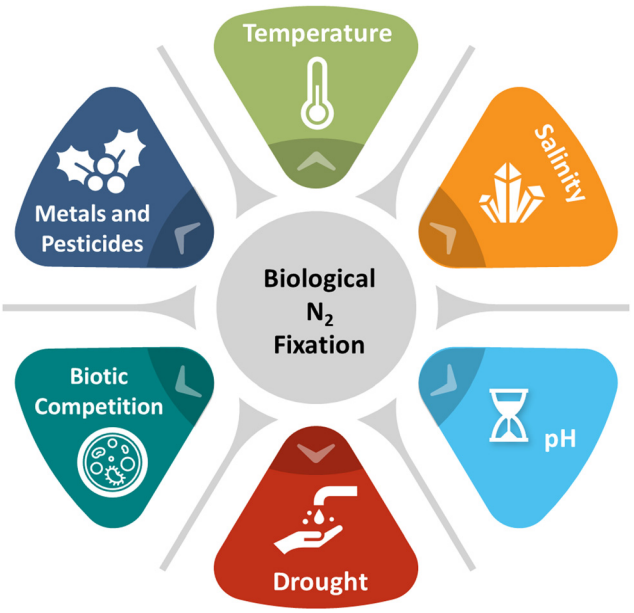

Fig. 8 Factors significantly influencing the efficiency of biological nitrogen activation in symbiosis.

Nitrogenase is the only known biological enzyme responsible for the biogenic reduction of atmospheric N_2 to NH_3 at ambient temperature and pressure.[85] Nitrogenase is produced by certain diazotrophic microorganisms, such as cyanobacteria, also known as blue-green bacteria, and rhizobacteria, a symbiotic diazotroph associated with root nodules of legume plants.[65,86] The nitrogenase family has three known isozymes, Mo-nitrogenase, V-nitrogenase, and Fe-nitrogenase, with Mo-nitrogenase being the most widespread and largest contributor to the nitrogen cycle and the best-studied among three isozymes.[87] Nitrogenase is usually an assembly of two components; the electron-delivery Fe–protein, which is responsible for the supply of electrons, and a catalytic FeM (M = Mo, V, Fe) protein which uses the electrons provided to reduce N_2 to NH_3.[77,80,88,89] A schematic diagram of N_2 activation in nitrogenase is shown in Fig. 9, respectively. The overall reaction for nitrogenase catalyzed N_2 activation can be written as:

$$N_2 + 8H^+ + 8e^- + 16ATP \rightarrow 2NH_3 + H_2 + 16ADP + 16P_i \quad (13)$$

In the reaction above, ATP represents adenosine triphosphate, ADP and P_i represent adenosine diphosphate and inorganic phosphate, respectively. ATP provides the necessary energy to drive the various enzymatic reactions in nitrogen activation from the free energy released when ATP is converted to ADP and P_i.

Biological N_2 activation operates under ambient conditions but requires a substantial energy input in the form of ATP, with approximately 16 ATP molecules needed per N_2 molecule

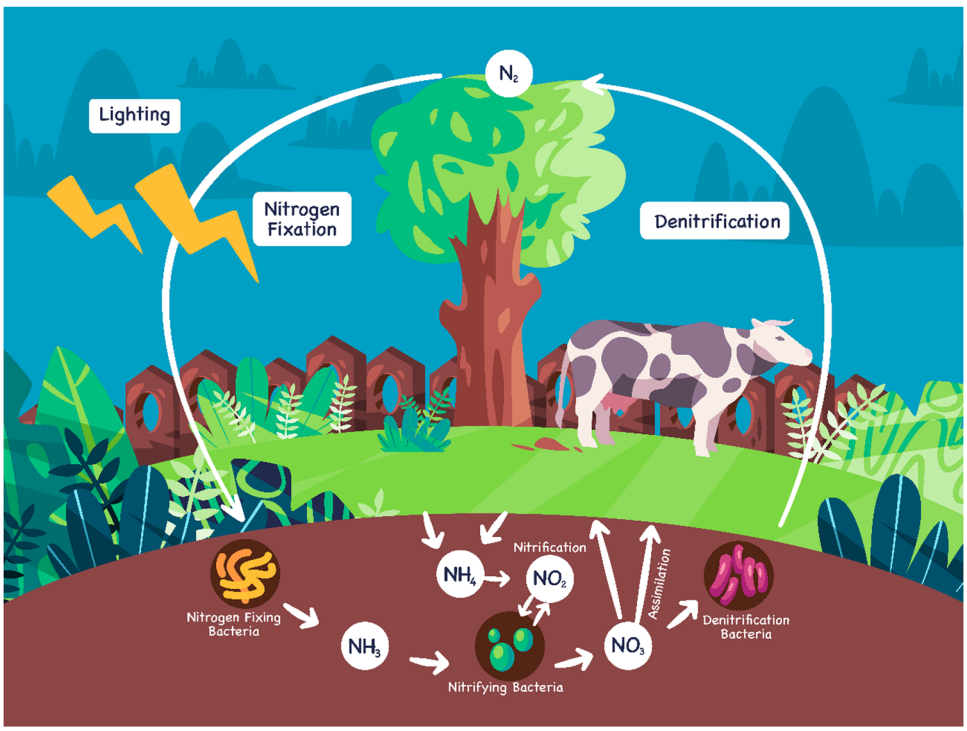

Fig. 9 N_2 activation in N cycle.

© 2025 The Author(s). Published by the Royal Society of Chemistry

Open Access Article. Published on 24 4 2025. Downloaded on 2026-02-14 8:12:44.
This article is licensed under a Creative Commons Attribution-NonCommercial 3.0 Unported Licence.

reduced to NH_3 shown in eqn (13). In biological N_2 activation, six out of eight electrons are used to reduce N_2, while the remaining two contribute to the unavoidable production of H_2, resulting in an electron efficiency of 75%. ATP, often referred to as the cell's energy currency, can be used to express the energy demand of N_2 activation in conventional units. The hydrolysis of ATP to ADP under biological conditions has been measured at 55 kJ mol^{-1} and 48–63 kJ mol^{-1}.[90,91] Assuming similar energy is needed for ATP regeneration, the total energy required to fix $\frac{1}{2}N_2$ molecule is estimated at 0.38 MJ mol^{-1}, which is slightly lower than the 0.48 MJ mol^{-1} used in the Haber–Bosch process.[92] More precise calculations by Alberty research group,[93] considering factors like pH, ionic strength, and Mg^{2+} concentration, have shown that the Gibbs free energy for ammonia formation varies between 63.2 and 180 kJ mol^{-1}, further emphasizing the complexity of biological nitrogen fixation efficiency. This translates to an energy requirement of 0.38–0.77 MJ mol^{-1} NH_3, depending on ATP synthesis efficiency and cellular metabolism. In comparison, the Haber–Bosch process, despite its high temperature (400–500 °C) and pressure (150–300 bar), consumes approximately 0.48 MJ mol^{-1} NH_3, making it slightly more energy-efficient in direct thermodynamic terms. Biological N_2 activation avoids fossil fuel dependency and integrates with natural ecosystems, making it more sustainable. Despite its ATP cost, biological N_2 activation remains crucial in agriculture, particularly for legume-based cropping systems, which reduce reliance on synthetic fertilizers and associated environmental impacts.[62,92]

From an industrial standpoint, biological N_2 activation can be evaluated based on energy efficiency, considering inherent energy losses in metabolic processes. The oxidation of one glucose molecule is commonly estimated to generate up to 36 ATP molecules, though recent studies suggest a more accurate value of 29.85 ATP per glucose. Given that the complete oxidation of glucose releases approximately 2.87 MJ mol^{-1}, each ATP molecule effectively stores around 96 kJ mol^{-1}. This translates to an estimated 0.77 MJ mol^{-1} of NH_3 produced *via* biological fixation. Real-world efficiency may be lower, with some studies indicating that 20–30 ATP molecules may be required instead of the theoretical minimum of 16 ATP. Additionally, nitrogenase enzymes exhibit varying electron efficiencies: Mo-nitrogenase (70%), V-nitrogenase (40%), and Fe-nitrogenase (20%), further influencing overall energy use. Comparatively, biological N_2 activation approaches the energy efficiency of the Haber–Bosch process, though nitrogen-fixing bacteria tend to activate this pathway only when no alternative nitrogen sources are available. The key environmental advantage of biological N_2 activation lies in its self-regulating nature, relying on renewable carbon sources like carbohydrates rather than fossil fuels. Enhancing natural plant-microbe symbiosis could reduce reliance on synthetic fertilizers and mitigate associated inefficiencies. Additionally, biological N_2 activation presents opportunities for sustainable waste management, where agricultural or forestry by-products serve as feedstocks for nitrogen fixation, further integrating biological processes into circular economy models.[62,92]

2.2.6. Lowe–Thorneley kinetic model. The Lowe–Thorneley (LT) kinetic model is a simplified model proposed to describe the reduction of nitrogen to NH_3 by nitrogenase in biological nitrogen activation. This model was developed by David R. Lowe and Roger N. Thorneley and was published in 1984.[94] The reduction of nitrogen to NH_3 by nitrogenase on the Fe–M protein (represented by E_n) is a complex process involving multiple electron transfers and chemical reactions. The Lowe–Thorneley kinetic model breaks down this complex process into a series of simpler steps and provides equations that describe the rates of these individual steps. The model involves eight steps, which include the transfer of eight electrons and protons. The first half of the model (E_0–E_4) describes the accumulation of multiple electrons and protons at the active site of FeM before N_2 can bind, showing the kinetics of transformations among catalytic intermediates between the resting state of the enzyme before catalysis begin (E_0) and the ''Janus Intermediate'' where N_2 is bound to the MoFe protein (E_4).[95] The bonded N_2 is followed by a series of nitrogen protonation steps to complete the model, resulting in NH_3 synthesis. The first half of the mechanism is better understood, and researchers are relatively confident regarding the structures of the first four intermediates (E_0–E_4). On the other hand, the exact pathway for the second half of the LT kinetic scheme remains ambiguous.

Over the years, two major competing pathways have been proposed: the ''distal'' and the ''alternating'' pathway.[96–98] These reaction pathways for N_2 reduction begin with the Janus state (E_4). In the distal pathway utilized by N_2 fixation in inorganic Mo complexes and suggested to apply in reaction at Mo of FeMo, the terminal nitrogen of N_2 is hydrogenated in three steps until the first NH_3 is liberated, then the remaining nitrido-N is hydrogenated three more times to yield the second NH_3. In the alternating pathway, one hydrogen is added to the terminal nitrogen; then, one hydrogen is added to the nitrogen directly bonded to the metal. This alternating pattern continues until NH_3 is released.[85,99,100]

Distal pathway	Alternating pathway
$FeM–N_2 + H + e^- \rightarrow FeM–N–NH$	$FeM–N_2 + H + e^- \rightarrow FeM–N–NH$
$FeM–N–NH + H + e^- \rightarrow FeM–N–NH_2$	$FeM–N–NH + H + e^- \rightarrow FeM–NH–NH$
$FeM–N–NH_2 + H + e^- \rightarrow FeM–N–NH_3$	$FeM–NH–NH + H + e^- \rightarrow FeM–NH–NH_2$
$FeM–N + H + e^- \rightarrow FeM–NH$	$FeM–NH–NH_2 + H + e^- \rightarrow FeM–NH_2–NH_2$
$FeM–NH + H + e^- \rightarrow FeM–NH_2$	$FeM–NH_2–NH_2 + H + e^- \rightarrow FeM–NH_2 + NH_3$
$FeM–NH_2 + H + e^- \rightarrow FeM + NH_3$	$FeM–NH_2 + H + e^- \rightarrow FeM + NH_3$

2.3. Homogeneous and metallocomplex N_2 activation

2.3.1. Metal complexes for homogeneous catalytic N_2 activation. As Fe, V, and Mo are known components of nitrogenases, the process of catalytic nitrogen activation is not

Open Access Article. Published on 24 4 2025. Downloaded on 2026-02-14 8:12:44.
This article is licensed under a Creative Commons Attribution-NonCommercial 3.0 Unported Licence.

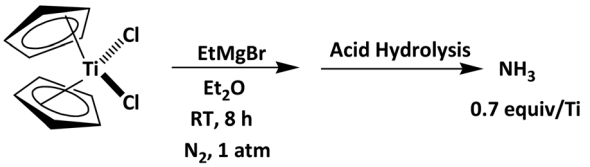

Scheme 1 N_2 activation by transition-metal complexes in moderate reaction operating conditions applying EtMgBr and Cp_2TiCl_2.[102]

solely constrained to these transition metals.[101] During the 1960s, Vol'pin and Shur reported that by subjecting a mixture of titanocene dichloride, *i.e.*, Cp_2TiCl_2 (Cp is C_5H_5) and EtMgBr to acid hydrolysis in Et_2O under atmospheric pressure shown in Scheme 1, they were able to produce 0.7 equivalents of NH_3 per titanium atom.[102] Additionally, in 1972, Shiina observed that the silylation of N_2 into $N(SiMe_3)_3$ (silylamine) shown in Scheme 2, an alternative form of nitrogen activation, could be catalyzed by $CrCl_3$.[103] These findings showcase the capacity of metals that are not biologically significant to facilitate nitrogen activation with modest reaction operating environments. A high rate of NH_3 production of 9.5×10^{-10} mol cm^{-2} s^{-1} MCp_2TiCl_2 was reported at -1 V in H_2O, with a faradaic efficiency of $\approx$0.95% achieved at -2 V in tetrahydrofuran. Theoretical calculations using density functional theory (DFT) recommended that electrochemically reduced $[Cp_2Ti]$- and/or $[Cp_2TiCl]$- based groups could substantially lower the activation energy for the protonation of dinitrogen. The activation of dinitrogen by Cp_2TiCl_2 proceeded through the formation of a Cp_2TiClN_2 intermediate. Initially, H_2O was split to generate H^+ ions on the catalyst surfaces. Then, gaseous dinitrogen is weakly bound to Cp_2TiCl_2 to make the Cp_2TiClN_2 intermediate. Subsequently, H^+ ions diffused to Cp_2TiClN_2 and fragmented on the bonded dinitrogen, resulting in dinitrogen dissociation and subsequent hydrogenation to form NH_3.[104,105]

A significant breakthrough occurred when the molecular $[Ru(NH_3)_5(N_2)]^{2+}$ was synthesized, challenging the belief that N_2 was too stable to react in modest conditions. This breakthrough sparked hope for developing a transition metal mimicking nitrogenase in a homogeneous system.[106] Transition metal complexes, like the aforementioned $[Ru(NH_3)_5(N_2)]^{2+}$, are considered excellent catalysts due to their unique configuration that allows for easy interchange of oxidation states. Inspired by the enzyme nitrogenase structure, chemists have explored Fe and Mo-based metal complexes, such as *trans*-$[Mo(N_2)_2(depf)_2]$, for catalytic N_2 activation.[107] For instance, *trans*-$[Mo(N_2)_2(depf)_2]$ demonstrated N_2 catalysis in the presence of Me_3SiCl and metallic Na as a stoichiometric reductant.[108] The $N(SiMe_3)_3$ intermediate, synthesized in the process, was treated with hydrogen chloride. This treatment released ammonium chloride (NH_4Cl) and completed the catalytic cycle.[109] Other studies

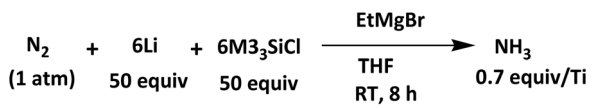

Scheme 2 Catalytic silylation of N_2 with the help of transition metals catalysts.[103]

have shown that transient molybdenum species can dissociate N_2 and form undesired terminal nitride complexes after N_2 cleavage.[108] To address this issue, late transition metal complexes with weak coordination to N_2 were designed, such as $[HIPTN_3N]Mo$ and $[Mo(PNP)(N_2)_2]_2(\mu\text{-}N_2)$. These complexes were found to activate N_2 insufficiently but still continuously produce NH_3.[110]

In a different approach, Schrock and Yandulov developed a Mo-based homogeneous catalytic system for converting N_2 to NH_3. This system involved $[LutH][BAr_4]$ as the proton source and decamethylchromocene as the electron source.[111] Exploring the captivating realm of nitrogen activation, this intricate mermaid code delves into the complexities of catalytic cycles and complexes. It sheds light on the groundbreaking discovery and development of iron-based systems that have successfully converted N_2 into NH_3, marking a significant breakthrough in recent years. The code discusses the synthesis of diverse Fe-based complexes with various ligands, each contributing to the advancement of the nitrogen transfer reaction cycle. Noteworthy achievements include the complete stoichiometric N_2 activation in 2011 and the design of a tris(phosphine)borane-supported iron complex that catalyzes the reduction of N_2 to NH_3 under mild conditions. It also touches upon the investigation of Fe coordination complexes to gain insights into the potential role of the interstitial C atom in the FeMo cofactor. Furthermore, the code highlights the growing interest in multinuclear uranium and iron complexes for N_2 cleavage and binding due to their remarkable capability to weaken and break the N_2 triple bond. Ultimately, this mermaid code offers a comprehensive overview of the advancements, challenges, and potential future targets in the field of N_2 activation.[108]

Apart from the Mo- and Fe-based complexes mentioned earlier, other well-precise transition metal complexes have been developed as effective homogeneous types of catalysts for N_2 activation. Nishibayashi's research group developed co-nitrogen complexes with an anionic polyvinylpyrrolidone-type (PVPtype) pincer ligand. These complexes exhibited remarkable activity in directly converting N_2 gas into NH_3 under mild conditions due to stabilizing the PVP ligand to the Co center in various oxidation states.[112] Mock and his colleagues also demonstrated that Cr–N_2 complexes act as mediators for N_2 reduction through three routes at room temperature.[113] Nishibayashi *et al.*[114] also successfully fabricated V–N_2 complexes, representing the first examples of V-catalyzed N_2 conversion into NH_3 in modest conditions. Moreover, Mizobe and his team reported the isolation of the first cubane-type ruthenium metal complex to bind N_2. They estimated the catalytic cycle of the pathways for the N_2 activation with the help of DFT.[115] These outcomes provide valuable understanding for the design of new homogeneous catalysts for N_2 activation. It is worth noting that separating the generated products poses a challenge and requires more streamlined operations.

Homogeneous electrocatalysts used for nitrogen reduction typically consist of molecular complexes with metal centers of transition metals. These catalysts are dissipated in acidic medium electrolytes and undergo reduction on the electrode surface during reactions where the electrodes remain inactive. The cyclic reaction pathway of homogeneous electrocatalytic

© 2025 The Author(s). Published by the Royal Society of Chemistry

Open Access Article. Published on 24 4 2025. Downloaded on 2026-02-14 8:12:44.
This article is licensed under a Creative Commons Attribution-NonCommercial 3.0 Unported Licence.

reactions involves the coordination of reactants by metal centers, storing charges attained from electrodes, and the conversion of reactants into products. The products are discharged, and the catalysts revert to their initial pattern. In addition, Chatt *et al.*[116] reported the protolysis of a N_2 complex *cis*-$[W(N_2)_2(PMe_2Ph)_4]$, inspired the investigations of molecular complexes with an $[MP_4]$ core (*i.e.*, M = W or Mo) for nitrogen reduction. The $[MP_4]$ complexes have been used as mediators for the cyclic conversion of dinitrogen to NH_3.[117] W/Mo complexes containing N_2 ($[M(N_2)_2(dppe)_2]$, M = W or Mo) or hydrazido(2-) ligands ($[M(X)(NNH_2)(dppe)_2]X$, M = W or Mo, X = BF_4, Br, or HSO_4) have reported NH_3 production rates ranging from 1.3% to 35.8% per mol of the complexes.[117] These complexes rarely produce NH_3 exclusively, and by-products like N_2H_4 and N_2H_2 have been occasionally detected. The ligands organized to the metal centers and the arrangement of the molecular complexes are believed to influence the selectivity towards different types of products. On Mo(III)–Mg^{2+}–R_3P–phospholipid, for example, both hydrazine and NH_3 were synthesized at a ratio of 1/10.[105]

In 1989, Furuya *et al.*[118] discovered that the metal phthalocyanine catalyzes electrochemical nitrogen reduction in an ambient environment. When Fe-phthalocyanine was used as the catalyst, a faradaic efficiency of approximately 1.6% for the NH_3 production rate was accomplished at −0.6 V *vs.* RHE during the initial electrolysis stage. The anode was a platinized gas-diffusion electrode, and the electrolyte was 1 M Na_2SO_4. Fe-phthalocyanine proved unstable in the reaction conditions, with the faradaic efficiency dropping sharply to $<0.1\%$ after approximately 10 minutes of electrolysis. The stability and efficiency of phthalocyanine-based catalysts were found to be dependent on the center metals of the phthalocyanines and electrolytes. A mixture of KOH and $KHCO_3$ as electrolytes enhanced Fe-phthalocyanine's faradaic efficiency and stability, compared to Na_2SO_4 as an electrolyte. Among the series of metal phthalocyanine catalysts tested, Sn-phthalocyanine exhibited the highest stability and activity.[118] The estimated faradaic efficiencies (FE) were ranked as follows: H (a free base phthalocyanine) > Fe, Ti > Pd > Co > Pt > In, Ni > Pb > Cu > Zn > Sn, Ga > Pb.[119]

Active catalysts for electrochemical nitrogen reduction reaction have been reported in the form of a group of Sacconi-type tetradentate ligands, abbreviated as P_3^E, where three phosphine donors (P) are attached to a central atom over an *ortho*-phenylene linker (E = C, B, Si).[120] Notably, iron-based Sacconi-type tetradentate ligands, known as P_3^EFe (E = C, B, Si), have demonstrated the ability to synthesize NH_3 in the presence of dinitrogen. Specifically, it has been reported that P_3^BFe can yield 64 equivalents of NH_3/Fe site, while P_3^CFe can produce 47 equivalents of NH_3 per Fe site. These ligands have also shown good permanence during various reaction series.[120] Conventional and *in situ* characterization techniques have recommended an electrochemical dinitrogen introduction progression reaction mechanism in which P_3^BFe–N_2^- acts as the catalyst and the Fe-borohydrido-hydride complex serves as the supporting state. Similarly, P_3^ECo (E = C, B, Si) complexes have demonstrated the capability to promote the activation and binding of dinitrogen in electrochemical nitrogen reduction reactions.[120]

Catalytic N_2 reduction into silylamines has been accomplished in modest reaction conditions with the help of various metal complexes such as Mn, Re, Ti, Cr, W, Ir, Ni, Co, U, and Rh. Co derivatives have exhibited superior catalytic activity among these metal complexes, producing up to 320 equivalents of silylamines/catalyst or 270 equivalents/metal. Meanwhile, the yield of silylamine has been constrained to 50% due to the formation of silicon-containing by-products. Although silyl radicals are commonly believed to be the reactive species in the catalytic reaction, experimental evidence is lacking.[101] Further mechanistic studies are needed to improve more effective reaction methods. Developing selective and efficient metal complex catalytic techniques for synthesizing valuable N-containing composites is the subsequent focus of research in this field.

2.3.2. Understandings of mechanism. A comprehensive understanding of the N_2 reduction mechanism is essential in the search for novel and extra-effective molecular catalysts. While there are multiple pathways for N_2 reduction, the initial and crucial step involves binding dinitrogen to one or more metal centers to activate its triple bond through reduction (Fig. 10). This coordination can be achieved through the direct reaction of N_2 with a precursor complex that contains strongly donating co-ligands and/or metals in a low oxidation state. Another approach involves coordinating dinitrogen after the reductive removal of H_2 from a metal-hydride complex. In this case, the M–H bonds present electron density for metal p-backbonding to N_2. H_2/N_2 exchange has been observed on the surfaces of the Haber–Bosch catalyst and the biological FeMoco site (Janus intermediate) and in some molecular complexes. The most common coordination modes for N_2 include terminal bridging end-on, end-on, bridging side-on, and bridging side-on-end-on.

Among these modes, the terminal end-on mode is the most prevalent in catalytic systems. In contrast, the bridging side-on and terminal modes generally demonstrate higher reactivity than bridging end-on N_2. After the coordination of N_2, substrate reduction can proceed through two different pathways: an associative mechanism or a dissociative mechanism.

2.3.2.1. Dissociative mechanism for N_2 activation. The N–N triple bond undergoes direct reductive dissociation, which necessitates a significant energy input to permeate the high kinetic barrier of the reaction. This process can occur under extreme Haber–Bosch conditions, leading to the creation of surface-bound Fe–nitrides. These nitrides are subsequently rapidly hydrogenated, resulting in the release of NH_3.[121] Several molecular complexes can also facilitate direct N_2 cleavage, forming distinct molecular nitrides. It is worth noting that only one known instance of a homogeneous catalyst operates through this particular mechanism.

Cummins *et al.*[122] reported metal-assisted N_2 reductive scission. They used a Mo^{III}-trisamide complex $[(NR,Ar)_3Mo]$ to coordinate N_2, forming a μ-η^1:η^1-N_2 bridged dimer at low-temperature Fig. 11(a). After warming, the N_2 split to yield two terminal Mo^{VI}–nitride complexes. This process was facilitated by the π^{10} (end-on) electronic configuration of the Mo_2N_2 core, as recommended by DFT studies. Unlike other metal–nitride

Open Access Article. Published on 24 4 2025. Downloaded on 2026-02-14 8:12:44.
This article is licensed under a Creative Commons Attribution-NonCommercial 3.0 Unported Licence.

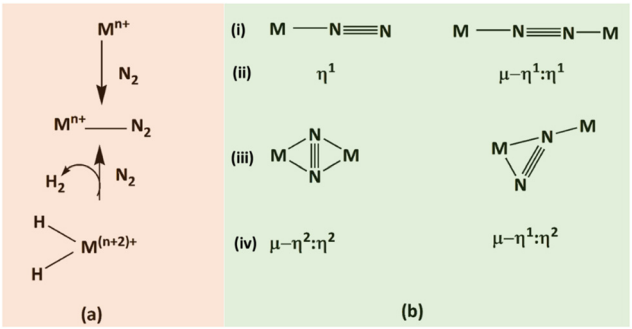

Fig. 10 (a) Binding schemes for dinitrogen to a metal (M), and (b) primary coordination approaches of N_2.

complexes, the Cummins MVI–nitride adduct was too stable to liberate NH_3 through protonation. Later, Nishibayashi's group discovered that the $PN^{PH,tBu}MoI_3$ complex, supported by a pincer ligand, can directly produce a Mo^{IV}–nitride adduct by adding $CoCp^*_2$ under N_2 atmosphere Fig. 11(b). This complex also acts as an effective catalyst for reducing N_2 to NH_3.[123] Kinetic and DFT studies recommend that the rate-determining step in this catalytic process is the direct "proton-unassisted" dinitrogen splitting reaction, which is unique compared to other reported catalytic systems. The nitride adduct can release NH_3 and regenerate a Mo–N_2 adduct by accepting electrons and protons. Iodide co-ligands play a role in the distinct reactivity of $PN^{PH,tBu}MoI_3$ compared to other complexes. These iodides stabilize a transient N_2-bridged MoI dimer, which further splits into Mo^{IV}–nitrides, rather than forming a m-N_2 bridged dinuclear Mo^0 complex. In the case of PPPMo, no Mo^0–N_2 dimers are detected, suggesting a dissociative N_2 reduction mechanism.

In addition, N_2 cleavage was achieved through collaboration between multiple metal centers studied by Holland and Murray research groups in 2011 and 2015, respectively (Fig. 11(c) and (d)).[125,126] Holland demonstrated that the *b*-diketiminate dinuclear $[(b\text{-diketim})Fe^{II}Cl]_2$ complex reacts with KC_8 under a N_2 environment to develop a dinitride-bridged tetranuclear complex.[126] The rational steric bulk of the supplementary ligand and the interaction between the Fe-bound nitrides and the K^+ cation are crucial in facilitating N_2 rupture. Likewise, Murray illustrated a triiron(II) complex assisted by a *b*-diketiminate cyclophane ligand, $[(chp^{b\text{-diketim}})Fe^{II}{}_3Br_3]$, which also splits N_2 after reduction with the help of KC_8. The subsequent trinuclear mixed valence $Fe^{II/III}$ complex comprises three protonated N-atom bridges, with the source of protons not yet fully understood. Adding acids to the N-atom bridged complexes developed by Holland and Murray, (sub)stoichiometric quantities of NH_3 can be released, although the process is non-catalytic.

As mentioned earlier, the studies emphasize the necessity of two or more metal centers to facilitate N_2 splitting through a dissociative pathway. This requirement arises because a single metal center cannot provide the six electrons needed, and the involvement of more than two metal atoms complicates the catalytic process's advancement. Protonation, which is likely to remove the N-atom bridges, could potentially lead to the collapse of the polynuclear structure, making the initial complex's regeneration difficult. Thus, achieving a catalytic process becomes quite challenging in such cases.

2.3.2.2. Associative mechanism for N_2 activation. The N_2 reduction mechanism in nitrogenase and many metal complexes (shown in Fig. 12) includes the stepwise addition of electrons and protons to split the N≡N bond and establish N–H bonds.[77] This hydrogenative cleavage likely supports an associative mechanism, which allows for N–N bond rupture without the involvement of a neighboring metal center. This mechanism helps to reduce the kinetic barrier for the reduction of N_2. Notably, when the proton and electron transfer steps co-occur, either through hydrogen-atom transfer (HAT) or proton-coupled electron transfer (PCET), the formation of N–H bonds is facilitated without high-energy intermediates.[124]

Given negligible kinetic barriers for HAT/PCET reactions, the thermodynamic feasibility of every individual N–H bond configuration *via* HAT/PCET can be assessed. This involves comparing the intensity of the N–H bond, which is established during the NH_3 production process through the D–H bond from the HC donor (D), as shown in eqn (14):

$$\text{D–H} + [\text{N}] = [\text{N–H}] + \text{D} \quad (14)$$

Eqn (14) defines [N] as the nitrogen substrate (*e.g.*, M–NH_2 or M–N_2), with [N–H] representing the subsequent HC adduct (*e.g.*, M–NH_3 or M–N═N–H). The intensity of N–H and D–H bonds can be assessed through bond dissociation enthalpies (BDE) or free energies of bond dissociation, incorporating the effects of entropy.[124] For a successful PCET/HAT, an N–H bond forms only if the D–H bond is ineffective, *i.e.*, when $BDE_{D–H}$ is lower than $BDE_{N–H}$. The stability of the N–H bond depends on the comparative strength of these bonds. The H atom donor's nature is crucial, and the three primary options include (i) H_2 ($BDE_{H–H}$ = 104 kcal mol^{-1}), (ii) metal-hydrides, or (iii) a sequence of reducing agents and acids.

Utilizing distinct electron and proton donors can trigger a multi-site PCET pathway, forming a transient species, *i.e.*, D–H, that may serve as a potential source of HC. In such instances, the adequate bond dissociation energy (*i.e.*, $BDE^{eff}_{H^+/e^-}$) can be determined through experimental or theoretical means. This involves incorporating the acid's dissociation constant (pK_a) and the reductant's standard reduction potential (E^0 *vs.* Fc^+/Fc) into the Bordwell equation (eqn (15), where *C* is a constant dependent on solvent). Consider the case where a potent acid (with a low value of pK_a) is paired with a robust reducing agent (having a low value of E^0). This combination results in a diminished $BDE^{eff}_{H^+/e^-}$ value, anticipating both (i) the sequential creation of N–H bonds from N_2 and (ii) a concurrent enhancement in the energy expenditure of the reaction.[124]

$$BDE^{eff}_{H^+/e^-} = 1.37pK_a + 23.06E^0 + C \quad (15)$$

In terms of mechanism, both pathways, *i.e.*, dissociative and associative, have proven effective for complex metal systems. While the dissociative reduction of N_2 necessitates the collaboration of multiple metal centers, the associative pathway minimizes the kinetic requirements by facilitating multiple hydrogen atom additions to the metal–N_2 adduct. The associative route appears more manageable, allowing for the promotion of PCET events, and is advantageous in avoiding the formation of unreactive multimetallic N-bridged products.

© 2025 The Author(s). Published by the Royal Society of Chemistry

Open Access Article. Published on 24 4 2025. Downloaded on 2026-02-14 8:12:44.
This article is licensed under a Creative Commons Attribution-NonCommercial 3.0 Unported Licence.

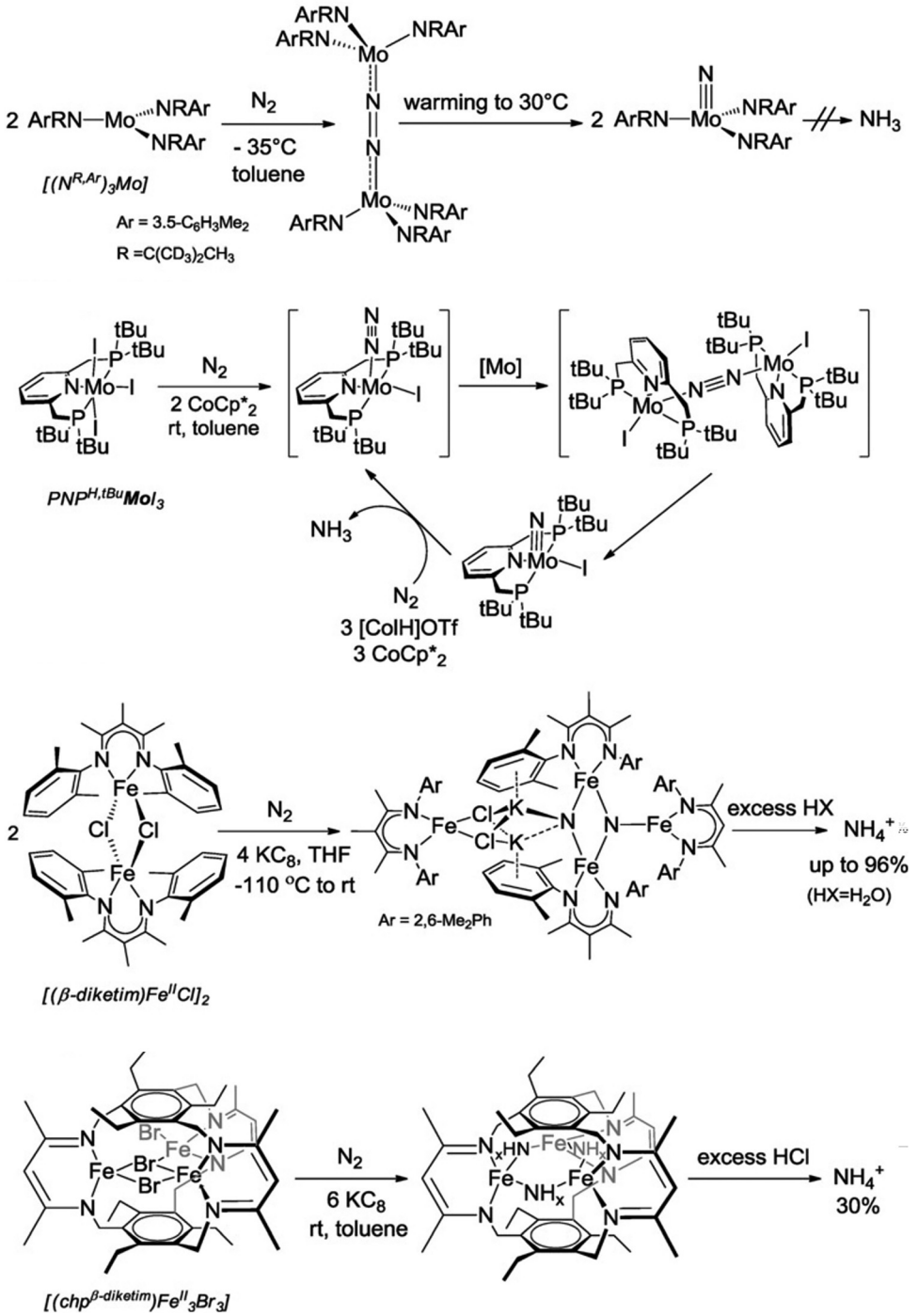

Fig. 11 Examples of dissociative mechanism for N_2 activation. Reproduced with permission from John Wiley & Sons. Copyright © 1999–2023 John Wiley & Sons.[124]

2.4. Thermal and non-thermal plasma mediated N_2 activation

Plasma N_2 fixation was inspired by lightning and thunder, which have enough energy and heat to break the strong bond in nitrogen gas that supports nitrogen molecules to contact with oxygen, forming NO_x.

2.4.1. Thermal plasma N_2 activation. The first method of plasma N_2 activation was provided by Henry Cavendish in 1784 who used electric arcs to reach the same energy and heat as lightning, allowing nitrogen to react with oxygen.[127] After a century, in 1903, these electric arcs were improved by Kristian Birkeland and Sam Eyde, known as the Birkeland–Eyde (B–E) process.[127] The details of the B–E process are shown in Fig. 13.

In the B–E process, air quickly flows through the electric arc furnace and is heated to 3000 °C by using a high electric voltage alternating current between two water-cooled copper

Open Access Article. Published on 24 4 2025. Downloaded on 2026-02-14 8:12:44.
This article is licensed under a Creative Commons Attribution-NonCommercial 3.0 Unported Licence.

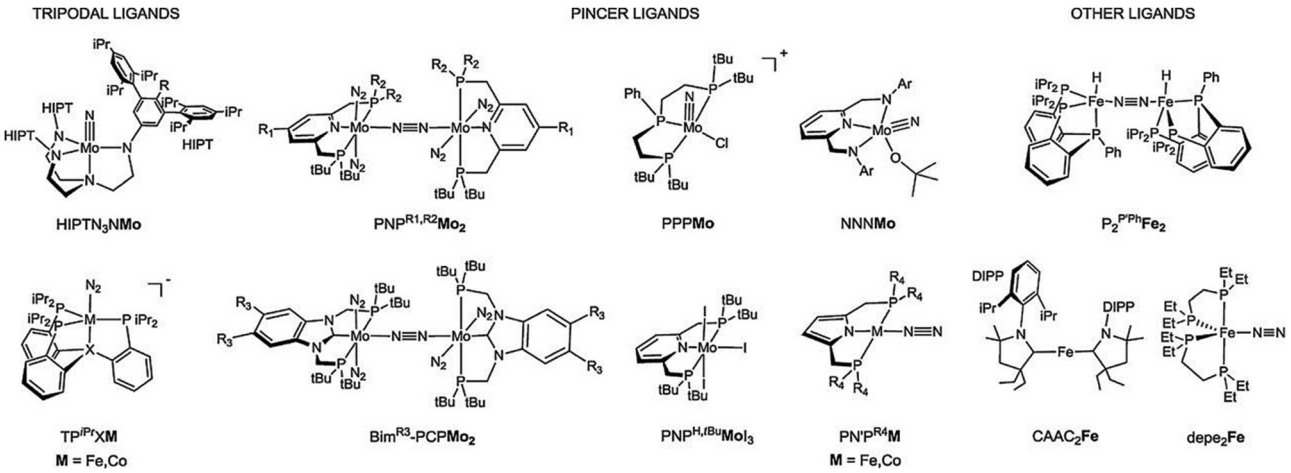

Fig. 12 Metal complexes for N_2 activation through its reduction (X = C, B, Si; Br, R = H; R1 = H, *t*Bu, Me, OMe, Ph, Fc, Me_3Si; Ad, R2 = *t*Bu; R3 = H, Me; R4 = *t*Bu, Cy; Ar = 2,6-diisopropylphenyl). Reproduced with permission from John Wiley & Sons. Copyright © 1999–2023 John Wiley & Sons.[124]

electrodes. At 3000 °C and 1 atm, nitrogen in the air combines with oxygen to reach the maximum 6.5% NO concentration. Next, the cooling chamber decreases the temperature to 1100 °C to avoid the reverse reaction.[127] The remaining heat is gathered in the waste heat boilers for future use. Then, the gases in the cooling chamber are moved to a large oxidation chamber for oxidizing NO to NO_2. Since the absorption rate increases with decreasing temperature, the temperature of NO and NO_2 mixture is dropped from 1100 °C to around 200 °C. The temperature further decreases to 50 °C before NO_x enters the absorption tower. Finally, inside the absorption tower, NO_2 is absorbed in water to produce a solution that contains approximately 30% concentrated nitric acid. The remaining NO_X enters the alkaline absorption columns for further absorption, and 3% of NO_X escapes the atmosphere even after the second absorption.

The first commercial B–E process was built in Niagara Falls, as the waterfall could produce enough hydronic power for the process. According to the study of Rouwenhorst's and Patil's team, the plant consumes 175-ton air to obtain 1-ton N. The energy consumption reaches 15 MW h per ton of nitric acid, which indicates that the B–E process is highly energy intensive. Numerous improvements have been found in the process, including using a 50–50% mixture of N_2 and O_2, preheating the reaction gas, and increasing the pressure in the furnace. Further studies need to be done to reduce energy consumption, use catalysts, and save heat energy to keep plasma-based nitric oxide production commercially reliable.

2.4.2. Non-thermal plasma N_2 activation. After a few decades, in the 1990s, a new theory was developed, which is called non-thermal plasma (NTP).[129] Non-thermal plasma differs from traditional thermal equilibrium systems as the electron temperature can be significantly higher than that of neutral gas molecules. This unique property enables the generation of high-energy species capable of activating N_2 molecules while maintaining a relatively low overall reaction temperature and energy consumption. A key mechanism in this process involves vibrational excitation of ground-state dinitrogen (N_2*), which occurs through collisions with energetic electrons. The energy stored in vibrational modes facilitates chemical reactions by overcoming high activation barriers shown in eqn (16)–(18).[92,130–132]

$$e^- + N_2 \rightarrow e^- + N_{2*} \quad (16)$$

$$O + N_2{}^* \rightarrow NO + N^* \quad (17)$$

$$O_2 + N^* \rightarrow NO + O \quad (18)$$

During NTP (Fig. 14a) for NH_3 synthesis, the reaction depends on the plasma discharge to dissociate the reactants and produce NH_3 with catalysts. Different sources, such as microwave and dielectric barrier discharge, can be utilized to form plasma essential for the synthesis. Finally, the NH_3 product will be collected, and the unreacted reactants will be recycled (Fig. 14b).[129] Generally, NTP refers to any plasma that is not in thermodynamic equilibrium. This can occur either when the ion temperature differs from the electron temperature or when the velocity distribution of one of the species deviates from a Maxwell–Boltzmann distribution. The most notable feature is that the temperature of the electrons can be several orders of magnitude higher than that of the surrounding gas. Therefore, electrons in NTP are promising high-energy species for activating reactants. The energy from their electronic vibration modes can be utilized in nitrogen activation reactions to achieve the significant activation energy required. Compared to thermal plasma N_2 activation, the NTP has lower temperature and pressure and relatively clean, carbon-free production, making NTP environmentally friendly recently. Additional research is required due to the small scale and lower efficiency.

To achieve high energy efficiency in N_2 fixation, Rusanov *et al.*[130] identified several crucial experimental conditions. First, a substantial amount of vibrationally excited N_2 molecules must be generated using non-thermal plasma, with electron temperatures reaching at least 10 000 K. Second, the

© 2025 The Author(s). Published by the Royal Society of Chemistry

Open Access Article. Published on 24 4 2025. Downloaded on 2026-02-14 8:12:44.
This article is licensed under a Creative Commons Attribution-NonCommercial 3.0 Unported Licence.

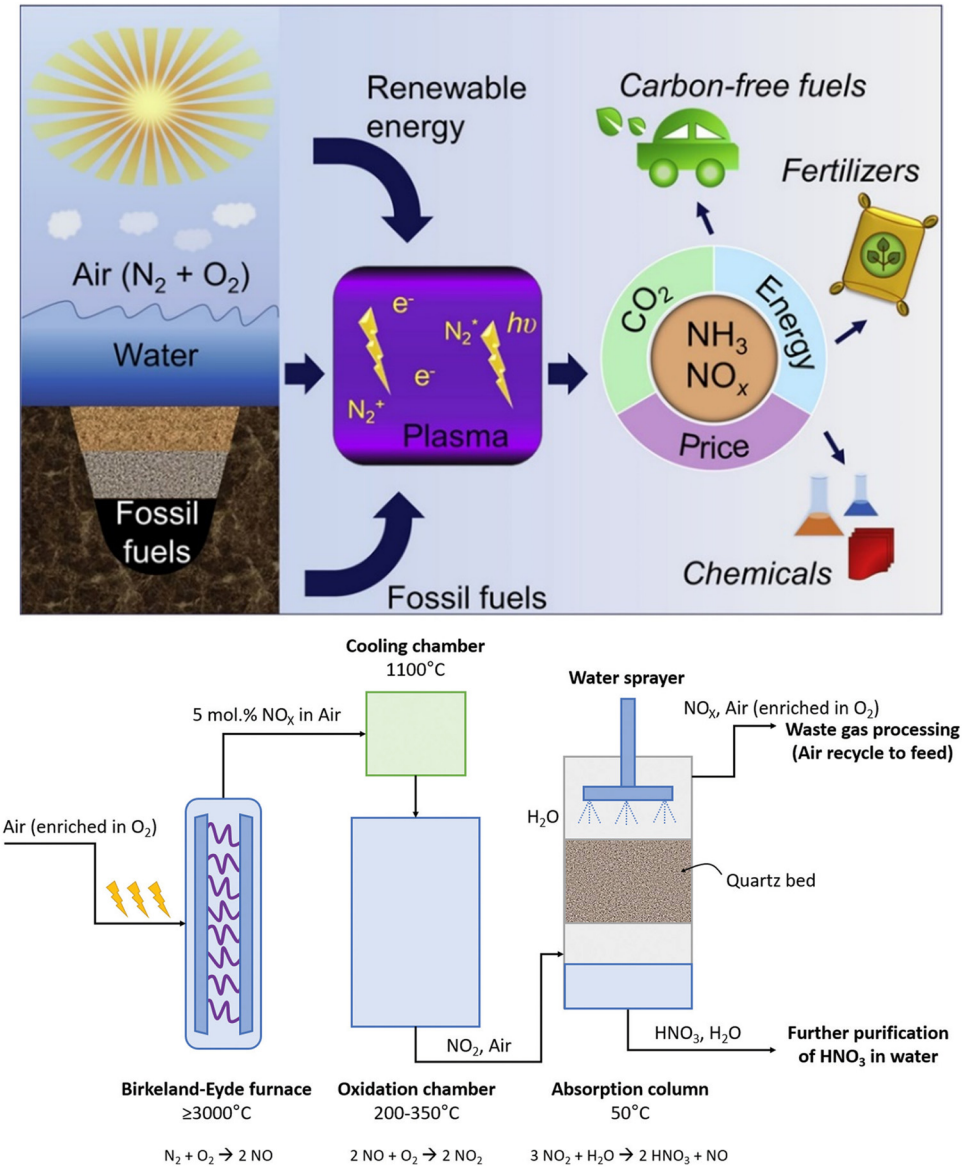

Fig. 13 (a) Plasma-activated nitrogen activation. Figure has been reproduced from ref. 128 with permission from Elsevier, © 2020 Elsevier. (b) Process scheme for the Birkeland–Eyde industrial nitrogen-activation process.[127] Figure has been reproduced from ref. 127 with permission from the Royal Society of Chemistry, © 2021 openly licensed *via* CC BY 3.0.

process should be conducted under moderate pressure, typically between 0.1 and 130 kPa. Third, the temperature of the resulting gas must remain low to prevent equilibrium-driven limitations that would otherwise reduce product yield and efficiency. Azizov *et al.*[134] demonstrated nitrogen oxidation *via* microwave-induced plasma, reporting an energy consumption of 0.29 MJ mol^{-1}, which remains higher than that of the Haber–Bosch process. Vibrational excitation lowers activation barriers in gas-phase reactions and heterogeneous catalysis, where catalysts enhance plasma-driven N_2 activation by activating oxygen or hydrogen. Eremin *et al.*[135] achieved the highest efficiency using a MoO_3 catalyst, reducing energy consumption by 35% to 0.86 MJ mol^{-1}. However, plasma-catalyst interactions remain unclear, as excited nitrogen species often lose energy before reaching the catalyst. Van Durme *et al.*[136] proposed that microscopic plasma channels near catalyst surfaces improve efficiency. A key challenge is the volatility of MoO_3, which can vaporize in plasma, acting as a gas-phase oxidation catalyst. Understanding these interactions is essential for optimizing catalyst performance in nitrogen fixation.

Nonthermal plasma N_2 activation presents environmental and efficiency advantages by utilizing widely available raw materials like air and electricity while generating minimal by-products. Theoretical calculations suggest that the energy consumption for nitrogen oxidation could be as low as 0.2 MJ mol^{-1}, making it potentially over 2.5 times more efficient than the Haber–Bosch process.[92,130] Several challenges remain before this method can be industrially viable, including improving

Open Access Article. Published on 24 4 2025. Downloaded on 2026-02-14 8:12:44.
This article is licensed under a Creative Commons Attribution-NonCommercial 3.0 Unported Licence.

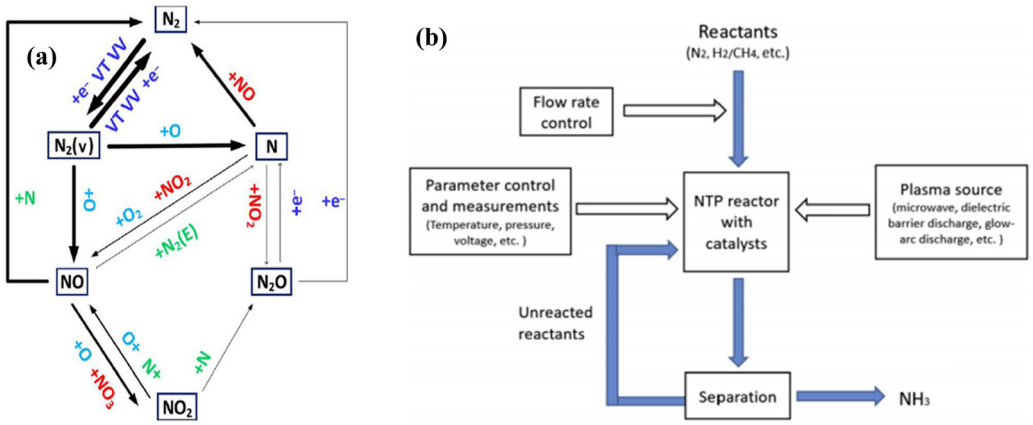

Fig. 14 (a) Summative scheme of the main reactions between molecules and atoms. Figure has been reproduced from ref. 133 with permission from Wiley © 2019 Wiley-VCH Verlag GmbH & Co. KGaA, Weinheim. (b) A flow diagram of the non-thermal plasma NH_3 synthesis process.[129] Figure has been reproduced from ref. 129 with permission from Elsevier © 2018 Elsevier.

energy efficiency, understanding plasma-catalyst interactions, and optimizing catalyst stability for long-term operation. For future advancements in N_2 activation, non-thermal plasma stands out as a promising approach, as it can circumvent thermodynamic constraints by selectively channeling energy into a specific reaction pathway. Efficiency is maximized when sufficient vibrationally excited N_2 forms, gas temperatures remain low to prevent decomposition, and reactions proceed along optimal routes. This targeted energy distribution enables more effective N_2 activation than conventional methods.[92]

2.4.3. Understanding the molecular orbital theory of plasma N_2 activation. Starting with the electronic configurations of N_2 and O_2 (Fig. 15), the HOMO of N_2 is the 2σg orbital with anti-symmetry, while the LUMO of O_2 consists of half-filled πg orbitals with symmetry, which means the distinct symmetries prevent electron transfer from N_2 to O_2. The symmetry of the LUMOs (1πg) of N_2 aligns with the LUMOs (1πg) of O_2. While electron density could theoretically flow from the half-filled 1πg orbital of O2 to the LUMOs of N_2, this violates the electronegativity tendencies of atoms.[137] Hence, the reaction occurs if electrons undergo excitation from the HOMO of N_2 to the LUMO and then proceed to flow into the LUMO of O_2. Plasma is used to provide sufficient energy to excite nitrogen and initiate the reaction.

2.4.4. Potential barriers of thermal and non-thermal N_2 fixation. Thermo plasma N_2 activation faces several practical barriers, including reactor design challenges and cost considerations. Current plasma reactors, such as gliding arc (GA) and microwave (MW) plasmas, require further optimization to reduce energy consumption from around 2.4 MJ mol^{-1} N to the target of 0.7 MJ mol^{-1} N for competitiveness. Efficient gas contacting and rapid quenching are essential to prevent NO decomposition, and scalability remains an issue due to inefficient energy transfer. In terms of cost, plasma reactors currently have a capital expenditure of approximately €0.90 per W, which could decrease to €0.05 per W with large-scale deployment, potentially making the total cost lower than the electrolysis-based Haber–Bosch and Ostwald processes. Operational costs

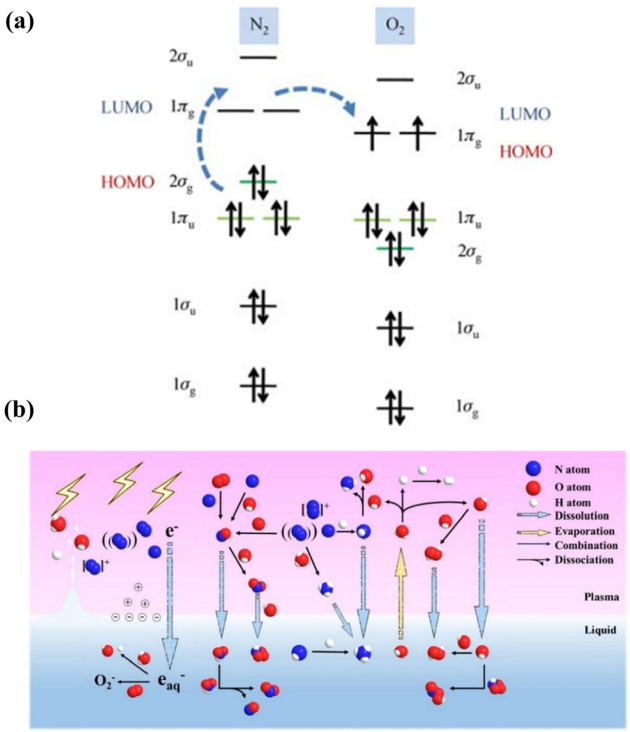

Fig. 15 (a) Scheme of molecular orbits of N_2 and O_2, reproduced form ref. 137 with permission from Springer Nature, Copyright © 2018, Higher Education Press and Springer-Verlag GmbH Germany, part of Springer Nature (b) schematic showing the fundamental processes in N_2 plasma. Reproduced form ref. 138 with permission from Elsevier, © 2023 licensed *via* CC BY-NC-ND 4.0.

remain high, with electricity being a significant factor; for plasma-based NO_X synthesis to be viable, energy consumption must drop below 0.7 MJ mol^{-1} N. Electricity costs should be around €5–10 per MW h. While the Haber–Bosch process remains dominant due to its lower energy consumption (~0.6 MJ mol^{-1} N) and established infrastructure, plasma technology could be applied for decentralized production if efficiency can be improved. Future advancements should focus on integrating

© 2025 The Author(s). Published by the Royal Society of Chemistry

Open Access Article. Published on 24 4 2025. Downloaded on 2026-02-14 8:12:44.
This article is licensed under a Creative Commons Attribution-NonCommercial 3.0 Unported Licence.

catalysts to enhance reaction selectivity, optimizing reactor designs for better gas mixing and power transfer, and leveraging low-cost renewable energy sources to improve overall feasibility.[127]

Non-thermal plasma N_2 activation presents several practical barriers to reactor design and cost analysis. While this method operates at lower temperatures and pressures than the Haber–Bosch process, challenges include nitrogen fixation efficiency and preventing back reactions that decompose ammonia post-synthesis. Reactor design must optimize plasma discharge to enhance nitrogen dissociation and ammonia formation while integrating rapid separation mechanisms to avoid decomposition. The cost structure also plays a crucial role, as non-thermal plasma technology can lower capital expenditures by eliminating the need for high-pressure systems. In contrast, operational expenses remain high due to energy requirements. Efficient catalysts with vigorous plasma synergistic activity, such as ruthenium-based materials with promoters, are essential to improving ammonia yield and reducing energy consumption. Additionally, integrating this technology with renewable energy sources, such as wind or solar, presents an opportunity for decentralized and sustainable ammonia production. Further research is needed to enhance energy efficiency, scale-up feasibility, and overall economic viability.[129]

2.5. Electrochemical N_2 activation

Electrochemical N_2 activation (reduction and oxidation) is attractive as excess renewable energy can produce valuable chemicals decentralized by using air and water as feedstocks.[139–142] In theory, N_2 can be electrochemically reduced to NH_3 and N_2H_4. Also, N_2 can be electrochemically oxidized to various NO_x products such as NO, NO_2, N_2O_4, N_2O_5, N_2O, and HNO_3. Table 5 denotes the electrochemical reactions with standard equilibrium potentials for various N_2 oxidation and reduction products. Though thermodynamically possible to reduce or oxidize N_2 electrochemically, it is challenging due to the competing hydrogen evolution reaction (HER) and oxygen evolution reaction (OER) shown in Table 6. The standard equilibrium potential of the NH_3 formation reaction from N_2 is very close to HER. Hydrazine formation reaction has a slightly higher overpotential. The N_2 oxidation reactions (NORs) have a standard thermodynamic equilibrium potential higher than the OER's. N_2 is in the gas phase with very low solubility in water, making it even more challenging to activate N_2 in aqueous media. Furthermore, N_2 is inert with very high dissociation energy of the N≡N (941 kJ mol^{-1}), N_2 does not have a permanent dipole, has low proton affinity (493.8 kJ mol^{-1}), has negative electron affinity (−1.90 eV), has high ionization potential (15.84 eV), and has a large energy gap between the (highest occupied molecular orbital) HOMO and (lowest unoccupied molecular orbital) LUMO levels. Hence, it is highly challenging to activate N_2 in aqueous medium not just electrochemically but also thermochemically.

Table 6 Competing electrochemical reactions to N_2 reduction and oxidation reactions

S. no.	Electrochemical reaction	Standard equilibrium potential (E^0, V *vs.* RHE)	Product
1	$2H^+ + 2e^- \rightarrow H_{2(g)}$	0	Hydrogen
2	$2H_2O_{(l)} \rightarrow 4H^+ + 4e^- + O_{2(g)}$	1.23	Oxygen

Electrocatalysts that are active, selective, and stable for NORs and NRRs and are inactive towards HER and OER are needed. Experimental screening of candidate catalysts would be a trial-and-error approach, and it is also time-consuming. Computational methods could provide an opportunity to discover and design candidate catalysts that are selective towards NORs and NRRs. The most active catalysts predicted theoretically for N_2 reduction to NH_3 are Mo,[143,144] Fe, Rh, and Ru, but these catalysts are more active for HER, and hence, the NH_3 faradaic efficiency will be very low. Interestingly, Ru[143] instead of Fe on MoS_2 was experimentally discovered as an active catalyst for ENRR, as shown in Fig. 16A. On the other hand, early transition metal catalyst surfaces such as Sc, Y, Ti, and Zr bind the H-adatoms weakly in comparison to N-adatoms. Hence, they were predicted to produce more NH_3 than H_2 at a high negative bias of −1 V to −1.5 V *vs.* SHE. The conclusion was made based on the binding energies of N-adatoms, and several other factors were neglected, such as the solvation effects, potential dependent activation barriers, and lateral interactions among the adsorbates. There are no reliable experimental studies that reported high NH_3 FE in comparison to H_2 on Sc, Y, Ti, and Zr.

Similar trends were observed on transition metal nanoclusters with Fe, Mo, and Ru on top of the volcano when an associative mechanism was considered for the N_2 reduction,[146] but these catalysts were more active for HER than NRR. Montaya *et al.* performed DFT calculations on various transition metal surfaces and found that the linear scaling between the adsorption energies of two main intermediates of NRR, such as N_2H and NH_2, would need at least −0.5 V. All transition metal catalysts suffer from this scaling relation, and an ideal catalyst should break the scaling relation by selectively stabilizing N_2H or by destabilizing NH_2 to

Table 5 Electrochemical reactions denoting N_2 reduction and oxidation to various products with standard equilibrium potentials

S. no.	Electrochemical reaction	Standard equilibrium potential (E^0, V *vs.* RHE)	Product
1	$\frac{1}{2}N_{2(g)} + 3H^+ + 3e^- \rightarrow NH_{3(g)}$	−0.042	Ammonia
2	$N_{2(g)} + 4H^+ + 4e^- \rightarrow N_2H_{4(l)}$	−0.39	Hydrazine
3	$\frac{1}{2}N_{2(g)} + H_2O \rightarrow 2H^+ + 2e^- + NO_{(g)}$	1.68	Nitric oxide
4	$\frac{1}{2}N_{2(g)} + 2H_2O \rightarrow 4H^+ + 4e^- + NO_{2(g)}$	1.36	Nitrogen dioxide
5	$N_{2(g)} + 4H_2O \rightarrow 8H^+ + 8e^- + N_2O_{4(g)}$	1.36	Dinitrogen tetroxide
6	$N_{2(g)} + 5H_2O \rightarrow 10H^+ + 10e^- + N_2O_{5(g)}$	1.35	Dinitrogen pentoxide
7	$N_{2(g)} + H_2O \rightarrow 2H^+ + 2e^- + N_2O_{(g)}$	1.77	Nitrous oxide
8	$\frac{1}{2}N_{2(g)} + 3H_2O \rightarrow 5H^+ + 5e^- + HNO_{3(l)}$	1.31	Nitric acid

Open Access Article. Published on 24 4 2025. Downloaded on 2026-02-14 8:12:44.
This article is licensed under a Creative Commons Attribution-NonCommercial 3.0 Unported Licence.

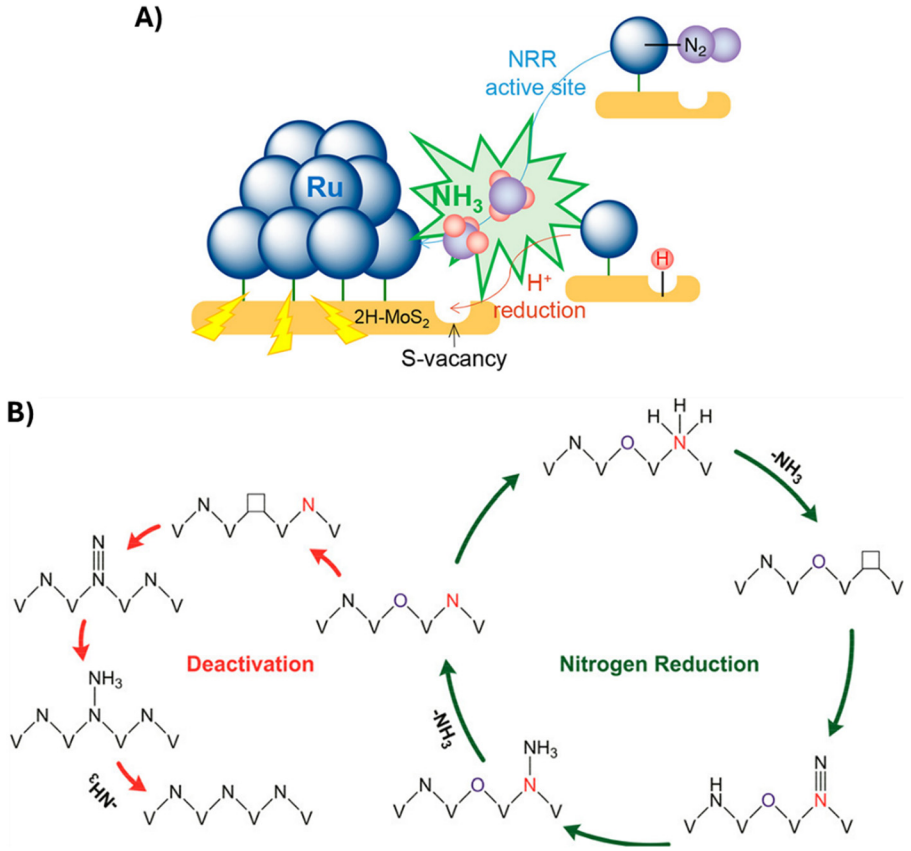

Fig. 16 (A) Ru/MoS_2 catalyzes the eNRR process, with the Ru cluster serving as the active site for nitrogen reduction, while the sulfur vacancy (S-vacancy) in MoS_2 functions as the hydrogenation site.[143] Figure has been reproduced from ref. 143 with permission from American Chemical Society Copyright © 2019 American Chemical Society. (B) NRR pathway on the surface of $VN_{0.7}O_{0.45}$ through a Mars–van Krevelen (MvK) mechanism, along with the catalyst deactivation process.[145] Figure has been reproduced from ref. 145 with permission from American Chemical Society Copyright © 2018, American Chemical Society.

have higher activity and selectivity towards NH_3. Bimetallic catalysts or high entropy alloys that simultaneously bind N_2H and NH_2 onto multiple sites could overcome this problem. Anand *et al.*[147] investigated the NOR mechanisms on a suitable OER catalyst, IrO_2, and a poor OER catalyst, TiO_2, and found that NOR activity is poor on the studied catalysts. In a recent study, Olusegun *et al.*[148] reported that dynamic potential control could be a promising scheme to improve NOR activity by potentially suppressing the oxygen evolution reaction (OER) and facilitating N_2 adsorption. As of now, there are no catalysts predicted by the theory that can activate N_2 electrochemically in an aqueous medium. Experimentally, numerous catalysts, including their oxides, nitrides, sulfides, carbides, and phosphides of various morphologies, have been tested for N_2 reduction to NH_3 in aqueous medium. One good example was demonstrated by vanadium nitride (VN) NPs, where surface $VN_{0.7}O_{0.45}$ acted as the active phase,[145] as shown in Fig. 16B. A detailed review of them is provided by Qing *et al.*[149] None of the published works report an NH_3 current density > -1 mA cm^{-2}. Most of the works are not reproducible as the NH_3 quantification protocols are not rigorous, and the N_2 feed used for the reactions is not pure and has some forms of reactive nitrogen, such as NO_x and NH_3, which leads to false positives for electrochemical N_2 reduction activity. Similar challenges exist for the N_2 oxidation.

The commonly used NH_3 quantification methods in the literature are Nessler's reagent and indophenol blue methods. Both methods are highly unreliable as they are sensitive to pH, counter-cation or anion interferences, and time. Using these methods could lead to the over-estimation of the formed NH_3. These methods are economical and easily accessible across labs. Hence, the methods must be benchmarked with ^{1}H-NMR for reliable quantification. The calibration graphs must be prepared using the electrolyte used, and quantification must be performed at constant pH to ensure the reliability of the method. The electrocatalysts can leach into the solution, interfere with the quantification method, and lead to an overestimation of NH_3. Therefore, N-15 isotope labeling experiments have to be performed for at least two different conditions, and the measured $N^{15}H^3$ should match within the error bars (±5%) with the N-14 experiments. It is a known fact that the N-containing compounds in the catalyst, support, and electrolyte could produce NH_3 and lead to a false positive. Hence, steps should be undertaken to avoid false positives. Andersen *et al.*[150] provide a rigorous quantification procedure for electrochemical N_2 reduction experiments. NO_x contamination, either in the form of gaseous forms (NO, NO_2, and N_2O) or ionic forms (NO_2^- and NO_3^-), could lead to false positives of N_2 reduction

© 2025 The Author(s). Published by the Royal Society of Chemistry

Open Access Article. Published on 24 4 2025. Downloaded on 2026-02-14 8:12:44.
This article is licensed under a Creative Commons Attribution-NonCommercial 3.0 Unported Licence.

or oxidation. Choi *et al.*[151] provide a detailed protocol for avoiding NO_x contamination in the reactant feed, electrolyte, and electrochemical setups.

2.5.1. Understanding electrochemical N_2 activation from a molecular orbital theory perspective. The adsorption of N_2 onto electrocatalyst surfaces occurs at electron-deficient active sites. These sites include transition metal centers with unoccupied d orbitals or heteroatoms with sp^2 orbitals capable of binding N_2. As illustrated, unoccupied d orbitals of transition metals accept electrons from N_2 to form a σ-bond, while occupied d orbitals transfer electrons back into the N_2 π* antibonding orbital. This reciprocal electron transfer, known as the "donor–acceptor" mechanism, weakens and activates the triple bond, ensuring that the N_2 molecule remains stably adsorbed on the active site. Similarly, nonmetal-based catalysts with vacant sites or Lewis acid sites can interact with N_2. These sites accept electrons to form a σ-bond and simultaneously transfer electrons from neighboring orbitals into the N_2 π* orbital, further facilitating triple bond activation. The donor–acceptor mechanism serves as a foundational concept for designing electrocatalysts, both metal and nonmetal, that exhibit enhanced N_2 adsorption and activation capabilities, paving the way for more efficient nitrogen reduction processes. The electrochemical nitrogen reduction reaction (eNRR) involves N_2 into NH_3 through multiple pathways, each characterized by distinct activation and reduction steps (Fig. 17(A) and (B)). Understanding these mechanisms is critical for catalyst design and optimizing reaction conditions. The primary mechanisms include the dissociative, associative, Mars–van Krevelen (MvK), and lithium-mediated NH_3 synthesis (LiMAS) pathways[152,153] as depicted in Fig. 17C.

2.5.1.1. Dissociative mechanism. The dissociative mechanism involves the direct cleavage of the N≡N triple bond before hydrogenation occurs. The nitrogen molecule adsorbs onto the catalyst surface in this pathway, where the strong triple bond is broken into two nitrogen atoms. These nitrogen atoms then undergo stepwise protonation to form NH_3. This mechanism is thermodynamically demanding due to the high bond dissociation energy of N_2 (941 kJ mol^{-1}).[154] Transition metals like ruthenium (Ru) and iron (Fe), which exhibit strong nitrogen binding energies, are effective for this pathway as they can stabilize the intermediate nitrogen atoms during reduction.[36,139,152,153,155,156] The dissociative mechanism is less favorable under ambient conditions because of the significant energy required to break the N≡N bond. The kinetic barrier for this process is high, often necessitating elevated temperatures or pressures, as in the traditional Haber–Bosch process. Thus, while effective at catalyzing NH_3 synthesis, catalysts that follow the dissociative pathway may struggle to achieve high efficiencies in mild conditions without significant advancements in catalyst design.[152]

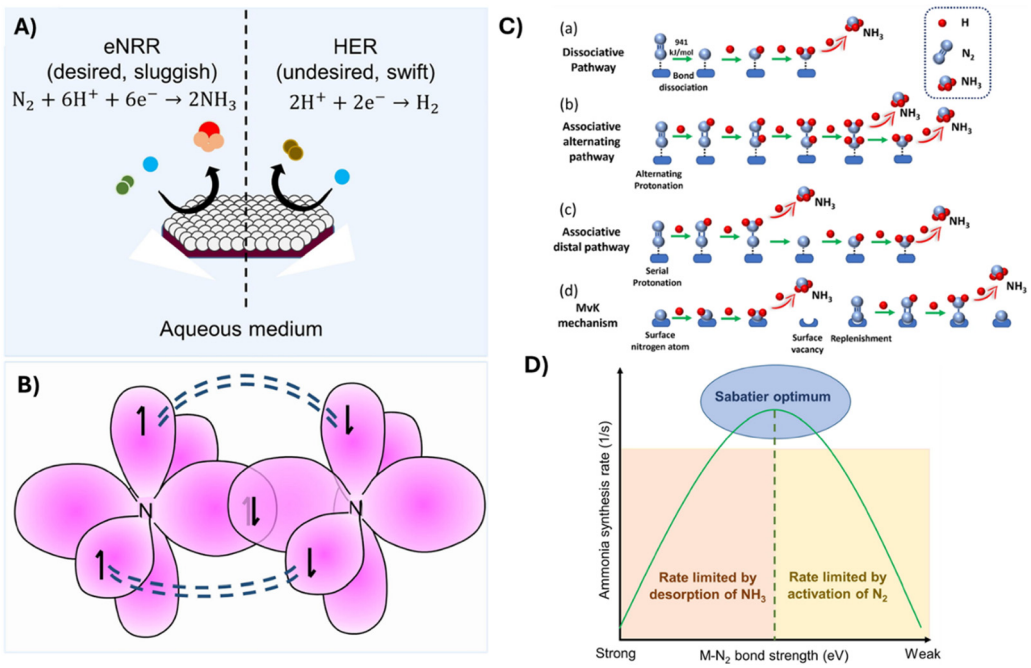

Fig. 17 (A) Competitive hydrogen evolution reaction (HER) on the electrocatalyst surface suppresses the electrochemical nitrogen reduction reaction (eNRR), reducing selectivity toward nitrogen molecules and resulting in low faradaic efficiency and decreased NH_3 production.[152] (B) The highly inert nature of the nitrogen molecule is attributed to its triple bond structure, which contributes to its significant stability.[152] (A) and (B) Have been reproduced from ref. 152 with permission from Elsevier Copyright © 2024 Elsevier. (C) Reaction scheme representing various eNRR mechanisms: a dissociative, b alternating associative, c distal associative, d and MvK mechanism.[153] Figure has been reproduced from ref. 153 with permission from Springer Nature, Copyrigh © 2023, openly licensed *via* CC BY 4.0. (D) Sabatier plot showing the optimal conditions for N_2 adsorption on the catalyst surface (M), where the interaction is balanced to avoid hindering product dissociation or limiting N_2 activation. Figure has been reproduced from ref. 152 with permission from Elsevier Copyright © 2024 Elsevier.

Open Access Article. Published on 24 4 2025. Downloaded on 2026-02-14 8:12:44.
This article is licensed under a Creative Commons Attribution-NonCommercial 3.0 Unported Licence.

2.5.1.2. Associative mechanism. The associative mechanism retains the N≡N bond during the initial steps of the reaction, allowing the molecule to undergo sequential proton–electron transfer events. This pathway is particularly suitable for ambient conditions as it avoids the high energy barrier associated with triple-bond cleavage. It distributes activation energy across intermediate steps, enabling nitrogen reduction at ambient conditions. Effective nitrogen adsorption on the catalyst surface is essential, guided by the Sabatier principle, which emphasizes an optimal interaction strength of neither too strong nor too weak between the catalyst and nitrogen molecule, as shown in Fig. 17D. The associative mechanism is further categorized into two sub-pathways:[157,158]

- Associative alternating pathway: hydrogenation alternates between the two nitrogen atoms. Each atom sequentially gains protons and electrons until NH_3 is formed on both ends. This balanced hydrogenation process ensures that both nitrogen atoms remain partially bonded until the final stages of the reaction.[111,159]
- Associative distal pathway: hydrogenation occurs primarily on one nitrogen atom until the first NH_3 molecule is formed and released. The second nitrogen atom is then protonated to form another NH_3 molecule. This stepwise approach reduces interactions between intermediates and may be advantageous for certain catalyst configurations.[160–162]

The associative mechanism generally exhibits lower kinetic barriers than the dissociative pathway, making it more feasible under mild conditions. Electrocatalysts that promote the end-on adsorption of N_2, such as transition metals with optimized d-orbital interactions, are well-suited for this mechanism.[152,153]

2.5.1.3. Mars–van Krevelen (MvK) mechanism. The Mars–van Krevelen (MvK)[163] mechanism involves nitrogen atoms that are already part of the catalyst's structure, such as transition metal nitrides (TMNs). In this pathway, the nitrogen atoms on the catalyst surface are first protonated to form NH_3, leaving behind vacancies on the surface, as shown in Fig. 18A. These vacancies are subsequently replenished by nitrogen gas from the surrounding environment. Alternatively, nitrogen from the bulk of the material migrates to the surface to fill the vacancies, enabling further reduction cycles.[164] While the MvK mechanism is efficient in utilizing surface nitrogen, the migration of bulk nitrogen to the surface can degrade the catalyst structure over time, impacting stability and reusability. Catalysts following this mechanism are typically robust and suitable for continuous operation, but maintaining structural integrity remains challenging. The MvK mechanism is particularly relevant for nitrogen-rich materials, where surface activity can be replenished.[165,166]

2.5.1.4. Lithium-mediated NH_3 synthesis (LiMAS). The lithium-mediated NH_3 synthesis (LiMAS) mechanism is a unique approach that utilizes non-aqueous electrolytes and lithium as an intermediate as shown in Fig. 18C and D. In this process, lithium reacts with N_2 to form lithium nitride (Li_3N).[152,167–170] The nitride is then protonated to produce NH_3, regenerating lithium for subsequent reactions. This pathway effectively suppresses the hydrogen evolution reaction (HER) because it operates in non-aqueous media, where protons are supplied by sacrificial donors like alcohol. LiMAS offers high faradaic efficiency, and NH_3 yields due to the absence of competing

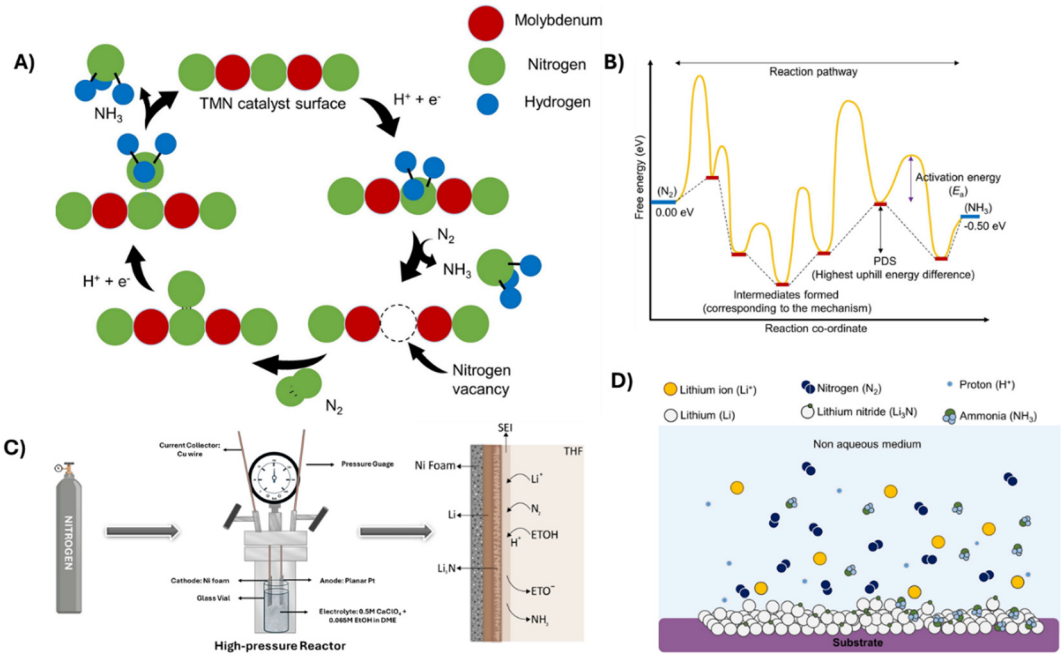

Fig. 18 (A) Schematic representation of the Mars–van Krevelen mechanism for eNRR on the molybdenum nitride catalyst surface.[152] (B) Typical density functional theory (DFT) graph for electrochemical nitrogen reduction reaction.[152] (A) and (B) Have been reproduced from ref. 152 with permission from Elsevier Copyright © 2024 Elsevier. (C) LiMAS experimental set up representation and proposed mechanism.[167] Figure has been reproduced from ref. 167 with permission from American Chemical Society Copyright © 2024 American Chemical Society. (D) The electrochemical nitrogen reduction reaction pathway facilitated by lithium.[152] Figure has been reproduced from ref. 152 with permission from Elsevier Copyright © 2024 Elsevier.

© 2025 The Author(s). Published by the Royal Society of Chemistry

Open Access Article. Published on 24 4 2025. Downloaded on 2026-02-14 8:12:44.
This article is licensed under a Creative Commons Attribution-NonCommercial 3.0 Unported Licence.

HER, but it faces scalability and energy efficiency challenges. The process is energetically intensive and relies on sacrificial reagents, which limits its practicality for large-scale applications. Moreover, the regeneration of lithium adds complexity to the overall system, requiring further innovation to make it commercially viable. Each eNRR mechanism has distinct advantages and challenges, influenced by the nature of the catalyst, electrolyte, and operating conditions. While the dissociative and associative mechanisms are widely explored in aqueous systems, the MvK and LiMAS pathways offer unique opportunities in specific configurations. Advancing the understanding of these mechanisms is essential for developing catalysts and systems capable of overcoming the intrinsic challenges of N_2 activation and achieving efficient, scalable NH_3 synthesis.[152,153,171]

2.5.2. Mechanistic understanding of NRR

2.5.2.1. Reaction mechanism of NRR on heterogeneous catalysts. Similar to homogeneous catalysts, heterogeneous catalysts predominantly follow the associative mechanism for nitrogen reduction reactions. Consequently, most theoretical studies have focused on this pathway. Unlike homogeneous catalysts that primarily involve single-metal sites or small clusters, metal surfaces in heterogeneous catalysis can dissociate the N–N bond without requiring simultaneous proton and electron addition.[172]

A computational study on NRR over ruthenium (Ru) surfaces revealed that multiple pathways involving different N–N bond dissociation steps can achieve activity comparable to the associative mechanism, with similar limiting potentials.[172,173] This finding highlights the necessity of considering alternative reaction pathways beyond the conventional associative model. For instance, intermediates such as $*NNH_2$, $*NHNH_2$, and $*NH_2NH_2$ can undergo dissociation to yield $*N + *NH_2$, $*NH + *NH_2$, and $*NH_2 + *NH_2$, respectively, with low activation energy (0.20–0.52 eV). These steps, absent in the traditional associative mechanism, were also confirmed through *in situ* surface-enhanced infrared absorption spectroscopy (SEIRAS), which detected N_2H_2 (diazene) as an intermediate. This compound can either decompose or be further protonated to ammonia, supporting the argument that additional reaction pathways must be considered to fully understand NRR mechanisms on heterogeneous catalysts.[173]

To design more efficient NRR catalysts, it is crucial to consider the overall reaction equilibrium and limiting steps. The conversion of N_2 to NH_3 requires six proton–electron pairs:[172]

$$N_2 + 6\,(H^+ + e^-) \rightarrow 2NH_3\ (E^\circ = 0.05\ \text{V}\ \textit{vs.}\ \text{NHE}) \quad (19)$$

Although forming NH_3 from N_2 and H_2 is slightly exothermic (with a Gibbs free energy change of -16.4 kJ mol^{-1}), NRR is hindered by the negative equilibrium potentials of its intermediates, particularly the first protonation step forming $*N_2H$.[172,174,175] Theoretical studies and volcano plots indicate that this step is the thermodynamic bottleneck for most catalysts. Catalysts that stabilize $*N_2H$ enhance NRR performance, whereas those that destabilize $*NH_2$ help lower the overpotential.[172,174,175] For weak nitrogen-binding metal surfaces, the limiting step is the initial protonation ($*N_2 \rightarrow *N_2H$), while for strong nitrogen-binding metals, the final protonation ($*NH_2 \rightarrow NH_3$) is the most challenging step.[172,174,175]

Recent research suggests an alternative surface-hydrogenation mechanism for noble-metal catalysts like palladium (Pd) and gold (Au).[176] In this mechanism, nitrogen activation occurs through hydrogen atoms adsorbed on the catalyst surface rather than directly on the metal. Theoretical calculations indicate that forming N_2H_2 *via* surface hydrogenation ($N_2 + 2H \rightarrow *N_2H_2$) requires lower activation energy compared to the conventional *NNH formation ($N_2 + [H^+ + e^-] \rightarrow *NNH$).[176] This pathway is energetically favorable, leading to NRR at reduced overpotentials. Once $*N_2H_2$ is formed, subsequent protonation steps proceed exothermically, further supporting this alternative pathway for efficient NRR on noble metals.[172,176]

2.5.2.2. NRR mechanism on transition metal nitrides. The nitrogen reduction reaction on transition metal nitrides follows a different pathway than pure or alloyed transition metals.[172] Unlike metal surfaces, transition metal nitrides have pre-existing nitrogen atoms incorporated into their structure. This enables them to participate in nitrogen reduction through both the direct reduction of N_2 gas and the reduction of surface nitride species.[172,177]

This process follows the Mars–van Krevelen mechanism, a well-established concept in catalytic oxidation on transition metal oxides. This mechanism initially reduces surface-bound nitrogen atoms to ammonia, creating nitrogen vacancies.[172] Subsequently, atmospheric N_2 replenishes these vacancies, restoring the surface nitride composition and enabling further ammonia synthesis.[172]

This mechanism operates based on the redox cycling of the catalyst surface, where oxygen vacancies play an important role in facilitating the reaction. In the first step, an oxygen atom from the catalyst's surface is removed (often due to interaction with N_2 or other species in the environment), creating an oxygen vacancy on the surface. This oxygen vacancy allows for further reaction steps. The nitrogen molecule then adsorbs onto the catalyst's surface at the location of the oxygen vacancy. The interaction between N_2 and the active site (the oxygen vacancy) facilitates breaking the $N{\equiv}N$ triple bond, which is a key step in N_2 reduction. Once adsorbed, the nitrogen undergoes reduction, where electrons are transferred to the adsorbed N_2 molecule, which is reduced to form ammonia.[47,152,178]

Computational studies by Skúlason and colleagues identified several transition metal nitrides, including chromium nitride (CrN) and vanadium nitride (VN), as promising catalysts for electrochemical nitrogen reduction *via* this mechanism.[175] Density functional theory (DFT) calculations suggest that these materials facilitate nitrogen reduction at low potentials. More recently, a combination of ^{15}N isotope labeling experiments and DFT simulations provided strong evidence that VN follows the Mars–van Krevelen mechanism for ammonia synthesis.[145]

2.5.2.3. High-entropy alloys (HEAs) for nitrogen reduction reaction (NRR). High-entropy alloys (HEAs) catalysts have been

Open Access Article. Published on 24 4 2025. Downloaded on 2026-02-14 8:12:44.
This article is licensed under a Creative Commons Attribution-NonCommercial 3.0 Unported Licence.

proposed as promising strategies for nitrogen reduction reaction (NRR) to overcome the scaling relations between N_2H and NH_2 adsorption energies; their effectiveness remains contingent mainly on specific elemental compositions and local electronic structures. Christensen *et al.*[179] investigation of AuCoFeMoRu HEAs demonstrates that these materials can, to some extent, circumvent traditional scaling constraints by introducing a heterogeneous distribution of adsorption sites. Their findings suggest that a complete decoupling of transition-state and final-state energetics remains fundamentally restricted. Microkinetic modeling reveals that although specific HEA compositions exhibit up to a twofold improvement over monometallic surfaces, these enhancements are incremental rather than groundbreaking.[179]

The assumption that HEAs can universally overcome linear scaling relationships is an oversimplification. Research on high-entropy catalysts for NRR suggests that although their atomic diversity results in a broader range of adsorption energies, they do not fundamentally break the thermodynamic constraints imposed by scaling relations. Instead of entirely decoupling key reaction intermediates, these materials expand the energetic distribution, indicating that while HEAs and bimetallic catalysts provide avenues for incremental performance gains, they do not constitute a definitive solution to the scaling limitation problem. This raises a crucial critique of the prevailing discourse in the field. HEAs and bimetallic catalysts are often credited with capabilities that are overstated in theoretical studies and lack robust experimental confirmation. Consequently, rather than considering these materials as a conclusive breakthrough, future research should prioritize a more systematic approach integrating experimental validation, refined electronic structure tuning, and *operando* characterization to rigorously evaluate their catalytic viability.[179,180]

In addition, optimizing N_2 adsorption and activation while suppressing the competing HER remains a central challenge. Theoretical studies suggest that Fe, Mo, Ru, and Rh are promising catalytic centers for NRR; their strong hydrogen adsorption frequently results in HER side reactions, reducing selectivity. Incorporating transition metals such as Zr, Ti, Y, and Sc has been proposed as a strategy to modulate adsorption energetics and mitigate HER competition. RuFeCoNiCu HEAs have demonstrated significant NH_3 production at low overpotentials, achieving notable activity at 0.05 V *versus* the reversible hydrogen electrode (RHE). DFT calculations indicate that Fe when integrated within a multi-component system, serves as an optimal N_2 activation site, while Ni–Ru and Co–Cu interactions enhance surface hydrogenation at minimal overpotentials. Furthermore, boron doping in FeCoNiCuPd HEAs has been shown to fine-tune electronic structures, leading to a dual-phase material with enhanced electrochemical NRR performance, boasting a FE of $\approx$40% and NH_3 production rates of $\approx$25 μmol h^{-1} cm^{-2}. These findings highlight the potential of compositional tuning in HEAs to push the boundaries of conventional catalytic limitations and improve efficiency and selectivity in ammonia synthesis. Continued experimental validation and advanced theoretical modeling remain imperative to assess their practical viability.[180–182]

2.5.2.4. In situ and operando studies. In situ surface-enhanced infrared absorption spectroscopy (SEIRAS) has been employed to identify reaction intermediates and elucidate the NRR mechanism on various catalysts. For example, SEIRAS studies on Au thin films detected IR bands corresponding to H–N–H bending, $-NH_2$ wagging, and N–N stretching of $*N_2H_y$ $(3 \leq y \leq 4)$ species, confirming the presence of an alternative associative pathway involving N_2H_4 as an intermediate.[158] In contrast, SEIRAS analysis of Ru surfaces in acidic media revealed IR signals of $*N_2H_x$ $(0 \leq x \leq 2)$ species, with an N=N stretching mode appearing at potentials below 0.2 V in 0.1 M $HClO_4$, indicating the involvement of N_2H_2 as the key intermediate.[183] These signals were absent in alkaline electrolytes, suggesting poor N_2 adsorption on Ru under such conditions. Unlike Ru, Rh exhibited strong IR signals corresponding to end-on $*N_2H_x$ species in alkaline solutions, indicating an associative two-electron transfer pathway where N_2H_2 decomposes to form NH_3.[184] Similar SEIRAS studies on NiFe–MoS_2 nanocubes,[185] Fe-doped ReS_2,[186] and Al-doped Co_3O_4[187] have further supported associative NRR mechanisms, while phosphorus-doped carbon nanotubes were found to follow a distal pathway.[172]

In situ Raman spectroscopy has been widely utilized to identify reaction intermediates and elucidate the N_2 reduction pathway. For instance, Raman analysis of Re_2MnS_6 revealed a prominent peak at 658 cm^{-1}, corresponding to the N–H stretching mode of $*NH_2$–NH_2 species, confirming that the NRR follows an associative alternating pathway facilitated by dual-metal sites.[172,188] In contrast, ReS_2 exhibited a blue-shifted peak at 709 cm^{-1}, attributed to $*NNH_2$, suggesting a distal pathway over single-metal active sites. Similarly, Bi-based metal–organic frameworks underwent electrochemical transformation into Bi nanoparticles at potentials more negative than −0.5 V, as evidenced by *in situ* Raman spectroscopy,[189] indicating the formation of active Bi species during NRR. Given that Raman spectroscopy relies on laser excitation, which may influence intermediate formation, near-infrared lasers are often preferred to minimize fluorescence and optical interference from catalysts.[172]

Online differential electrochemical mass spectrometry (DEMS) enables real-time monitoring of volatile intermediates and products during the NRR process, providing direct insights into the reaction mechanism.[172,189] The presence of mass-to-charge ratio (m/z) signals at 27, 30, 31, and 33 confirms the formation of N_2H_4. In contrast, the signal at 15 is attributed to either NH_3 or N_2H_4. Although NH_3 and water exhibit overlapping signals (m/z = 17 and 16, respectively), the NH_3 signal varies with applied potential, distinguishing it from water. Recently, Shao *et al.*[184] identified N_2H^+ (m/z = 29) alongside H_2 (m/z = 2) at potentials below −0.3 V on Rh, while $N_2H_2^+$ (m/z = 30) and $N_2H_3^+$ (m/z = 31) were undetectable, suggesting a two-step reaction pathway involving an initial two-electron transfer to form N_2H_2, which subsequently decomposes in KOH electrolyte to generate NH_3.[172,184]

Operando X-ray absorption spectroscopy (XAS) provides information on the electronic structure, coordination environment, and oxidation state of catalysts during NRR.[172] XAS studies on VN revealed that the position and intensity of the

© 2025 The Author(s). Published by the Royal Society of Chemistry

Open Access Article. Published on 24 4 2025. Downloaded on 2026-02-14 8:12:44.
This article is licensed under a Creative Commons Attribution-NonCommercial 3.0 Unported Licence.

vanadium K-edge white line remained constant at −0.1 and −0.2 V (*versus* RHE).[145] A pre-edge peak at 5468.4 eV indicated the formation of oxynitride species ($VN_{0.7}O_{0.45}$), which gradually weakened over time, suggesting its transformation to VN. This conversion accelerated with increasing overpotential, reaching 57.8% after 1 hour at −0.2 V. These findings support the hypothesis that $VN_{0.7}O_{0.45}$ acts as the active site for NRR, with its gradual reduction to VN leading to catalyst deactivation.[145,172]

In situ X-ray photoelectron spectroscopy (XPS) enables real-time tracking of catalyst valence states and adsorbed intermediates during NRR. Valov *et al.*[190] demonstrated electrochemical activation of N_2 at the interface between an iridium microelectrode and (111)-oriented 9.5 mol% yttria-stabilized zirconia (YSZ) at 450 °C and 10^{-5} Pa. Under cathodic voltages more negative than −1.5 V, a broad N 1s XPS peak at 397–398 eV emerged, which deconvoluted into three components: an N^{3-} ion (397.2 eV) and N_2 species in more positive oxidation states (397.7 and 398.6 eV).[172,190] The reversibility of the N 1s peak suggested that the reduced nitrogen species accumulated only in the top monolayers and desorbed upon voltage removal. At potentials below −2.0 V, reduction of the solid electrolyte was observed, as indicated by the emergence of lower formal charge Zr 3d and Y 3d components.[172,190]

2.5.3. Potential barriers of electrochemical N_2 fixation. Electrochemical nitrogen fixation, while promising as a more sustainable alternative to the Haber–Bosch process, faces several practical barriers, particularly in reactor design, cost, faradaic efficiency (FE), and current density. In terms of reactor design, choice of catalyst, electrolyte, creating systems that can effectively maintain stable solid electrolyte interphase (SEI),[191] and conditions like temperature and pressure, is challenging, as these factors are critical for optimizing the nitrogen reduction reaction (NRR). Currently, only Li-mediated ammonia synthesis is well explored, and recent studies showed the potential of Ca and Mg-mediated ammonia synthesis.[170,191] The high energy input required to initiate Li plating on the electrode remains a considerable roadblock.[192] Electrochemical reactors must efficiently manage mass transport and maintain long-term stability under operating conditions. Cost is another significant barrier, as the materials used in electrochemical cells, such as catalysts and electrodes, can be expensive, especially when rare or specialized materials are required for optimal NRR performance. Faradaic efficiency, which refers to the percentage of the applied current that results in the desired nitrogen fixation reaction, remains relatively low for electrochemical N_2 fixation. This reduces the overall efficiency and viability of the process compared to more established methods. Furthermore, achieving high current densities without sacrificing efficiency is difficult, as higher currents can lead to side reactions and lower FE, making it harder to scale the technology for industrial use. Overcoming these barriers will require advancements in catalyst development,[193] reactor design, and process optimization to improve efficiency and make electrochemical nitrogen fixation a competitive alternative for large-scale ammonia production.

The decomposition of NH_3 into N_2 and H_2 also presents a significant challenge in NH_3 synthesis, as it competes with the forward reaction and reduces overall yield. This endothermic reaction becomes increasingly favorable at high temperatures, necessitating effective inhibition strategies to maintain ammonia concentrations. The mechanism of NH_3 decomposition involves sequential dehydrogenation steps, where NH_3 dissociates into NH_2, NH, and ultimately atomic nitrogen, recombining to form N_2, while H atoms form H_2. The efficiency of these steps is primarily dictated by catalyst properties, particularly the adsorption characteristics of nitrogen species. Several strategies have been proposed to mitigate ammonia decomposition. Modifying the catalyst surface by incorporating elements with strong nitrogen affinity, such as certain high-entropy alloys (HEAs), has been shown to stabilize nitrogen intermediates and suppress N_2 formation. Optimizing reaction conditions, such as lowering reaction temperatures, increasing system pressure, and maintaining a high H_2 partial pressure, can shift the equilibrium toward ammonia synthesis, thereby reducing decomposition rates. The introduction of promoters like potassium (K) has also been found to enhance catalytic performance for NH_3 synthesis while selectively inhibiting decomposition pathways. Recent studies have further demonstrated that tuning catalyst supports, such as Ni-based materials with enhanced metal–support interactions and oxygen vacancies, can significantly impact NH_3 decomposition kinetics. The design of HEA catalysts with optimized compositions has exhibited high catalytic activity for ammonia synthesis while concurrently suppressing its reverse reaction. These findings underscore the importance of an integrated approach combining catalyst engineering, reaction condition optimization, and selective inhibition strategies to effectively counteract NH_3 decomposition and improve ammonia synthesis efficiency.[194,195]

2.5.4. Future outlook. Electrochemical nitrogen activation presents an opportunity for sustainable NH_3 production, addressing the limitations of the energy-intensive Haber–Bosch process and realizing its full potential demands, overcoming significant scientific and technical challenges. Future research must focus on multiple fronts to enhance the feasibility and scalability of eNRR.[167,170] Developing catalysts with high selectivity and activity remains a priority. Catalysts must promote effective N_2 adsorption and activation and suppress competing reactions, particularly the HER. Machine learning and computational tools like density functional theory can accelerate the discovery of new catalysts by predicting their interaction with N_2 and the associated reaction energetics.[152,153] DFT calculations for eNRR evaluate all possible mechanisms for a given catalyst, producing distinct graphs of intermediates and their free energies. The step with the highest uphill energy, the potential-determining step (PDS), dictates the mechanism, with the lowest PDS pathway being the most favorable for N_2 reduction, as illustrated in Fig. 18B.[152,153]

Innovative electrolyte systems that optimize proton availability and suppress HER are crucial. Non-aqueous systems and hybrid approaches involving ionic liquids or sacrificial proton donors can provide an alternative to traditional aqueous setups, offering improved FEs and NH_3 yields. Future work should explore such systems' scalability and environmental impact to

Open Access Article. Published on 24 4 2025. Downloaded on 2026-02-14 8:12:44.
This article is licensed under a Creative Commons Attribution-NonCommercial 3.0 Unported Licence.

ensure commercial viability. Understanding the fundamental mechanisms of eNRR, including dissociative, associative, and Mars–van Krevelen pathways, is essential for tailoring reaction conditions. Real-time spectroscopic and electrochemical techniques can provide deeper insights into intermediate species and reaction kinetics, guiding the rational design of more effective systems.[152,153]

Moreover, Li-mediated nitrogen reduction reaction faces challenges such as poor energy efficiency, notably lower than the traditional Haber–Bosch process, due to lithium's highly reducing electroplating potential (~ -3.04 V *vs.* SHE). Additionally, the long-term stability of Li-NRR is compromised by electrolyte degradation, which affects lithium recovery, and the high cost of lithium salts makes the process economically unfeasible. To enhance energy efficiency, exploring metals with lower electroplating potentials could offer significant improvements. Li-NRR proceeds through electrochemical and chemical steps, with lithium's unique properties, such as stable nitride decomposition and an optimal SEI, contributing to its excellent selectivity. Key criteria for effective NH_3 electrosynthesis mediators include spontaneous nitride formation, stable surface nitrogen vacancies, exergonic binding of N_2, solubility of mediator salts in non-aqueous electrolytes, and facile nitrogen diffusion. Calcium and magnesium were identified as promising alternatives, meeting these criteria alongside lithium. Calcium (~ -2.87 V *vs.* SHE) has shown favorable performance, with a faradaic efficiency (FE) of 50% for NH_3 production using calcium perchlorate and dimethoxy ethane as the electrolyte.[170] Magnesium has also demonstrated potential, with an FE of 27%[170] in preliminary studies, although recent work by Krebsz *et al.* reported a lower FE of 7%.[196]

Integrating eNRR with renewable energy sources such as solar, wind, or hydropower could enhance its sustainability. Coupling eNRR with CO_2 reduction or other value-added processes can create multifunctional systems that optimize resource utilization. For instance, hybrid systems that simultaneously address environmental challenges like CO_2 sequestration and NH_3 synthesis could yield synergistic benefits. Scaling up eNRR technologies to meet industrial demands requires addressing technical bottlenecks like mass transfer limitations and operational stability. Designing continuous flow reactors, improving catalyst durability, and optimizing reaction conditions will be critical. Lifecycle assessments and cost analyses will help ensure the developed processes are economically competitive and environmentally sustainable. The potential applications of eNRR extend beyond NH_3 synthesis. Emerging technologies like metal–N_2 batteries highlight the versatility of nitrogen reduction in energy storage and conversion systems.[152,153] Future research could explore innovative applications of N_2 activation in producing other nitrogen-based compounds and energy carriers.

2.6. Thermo-electrochemical N_2 activation

The predominant approach in industrial NH_3 synthesis involves the Haber–Bosch process, where NH_3 is generated through the chemical reaction of N_2 and H_2 under the influence of iron or ruthenium-based catalysts.[197] Generally, the Haber–Bosch process with Fe-based catalysts operates at 300–500 °C temperatures and 130–170 bar pressures.[198] To achieve NH_3 synthesis under milder conditions, Ru-based catalysts have been used to operate the Haber–Bosch process at relatively low pressures ($\leq$100 bar).[159] Despite these efforts, the thermodynamic conversion remains low (around 10–15%), consuming 1–2% of the worldwide annual energy.[199]

As the global demand for NH_3 continues to rise, driven by a decrease in fossil fuels and a simultaneous increase in greenhouse gas emissions, there is a growing imperative to develop more sustainable and cost-effective methodologies for NH_3 synthesis.[200] Recognizing the limitations of the Haber–Bosch process, recent research endeavors are increasingly directed toward optimizing NH_3 production across various temperature conditions. The experimental studies are categorized based on their operating temperature into three groups: (a) high temperature (above 500 °C), (b) intermediate temperature (between 500 °C and 100 °C), and (c) low temperature (below 100 °C).[200] Currently, most of the research in NH_3 production is concentrated on achieving low-temperature synthesis (below 100 °C) in water-based solutions.[201] Studies also explore intermediate-temperature methods (from 200 °C to 500 °C) using molten salt electrolytes and high-temperature approaches (above 400 °C) with solid-state electrolytes.[200] The high-temperature route could be significant by reducing the energy required due to lower kinetic barriers and improving the efficiency of NH_3 formation by enhancing catalytic activity. Both solid-state electrolytes, characterized by their robustness and stability, and molten electrolytes, known for their high ionic conductivity, play pivotal roles in facilitating effective electrochemical pathways at elevated temperatures for NH_3 synthesis.[200] Fig. 19 provides a temperature-classified map offering detailed insights.[202] The red region (above 500 °C) in the center of Fig. 19(A) shows a narrow range of current densities, largely independent of efficiency, which in some cases approaches the practical threshold. The blue region (below 100 °C) features points clustered at lower efficiencies (below 20%) and fails to reach the reaction rates achieved at higher temperatures. Meanwhile, the orange region (100–500 °C) is more scattered, indicating the potential for achieving high energy efficiency or high current densities, though not both simultaneously.

2.6.1. High temperature NH_3 synthesis. An electrochemical cell utilizing solid electrolytes allows for a wide operational temperature range from near room temperature to 700–800 °C, dictated by the electrolyte membrane type.[203,204] The NH_3 electrocatalytic synthesis involves a reaction pathway where $N_2 + 6H^+ + 6e^- \rightarrow 2NH_3$ occurs, with H^+ generated at the anode/electrolyte interface and transferred to the cathode *via* the electrolyte to yield NH_3. The application of high-temperature protonic conductors in NH_3 synthesis circumvents the limitations of the Haber–Bosch process, exhibiting catalytic activity enhancements of up to 1300% by integrating catalysts with proton conductors.[205] Fig. 20(A) and (B) show that NH_3 yield exceeds 98% at $\sim$50 °C regardless of pressure,[41,206] with minimal differences observed below this temperature. Lower temperatures favor higher yield and reduced energy consumption, but conventional catalysts lose activity for

© 2025 The Author(s). Published by the Royal Society of Chemistry

Open Access Article. Published on 24 4 2025. Downloaded on 2026-02-14 8:12:44.
This article is licensed under a Creative Commons Attribution-NonCommercial 3.0 Unported Licence.

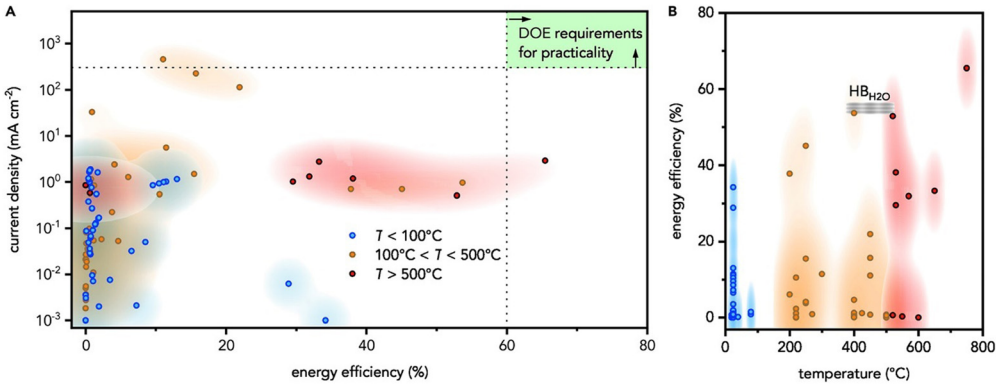

Fig. 19 Performance maps of electrocatalytic nitrogen reduction reactions across temperature regimes. (A) Current density *versus* energy efficiency, with the DOE target zone highlighted in green. (B) Energy efficiency as a function of temperature, with the mixed water-splitting Haber–Bosch process (HBH_2O) indicated in gray. Background color intensity reflects data density from kernel density analysis. Figures have been reproduced from ref. 202 with permission from Elsevier Copyright © 2018 Elsevier Inc.

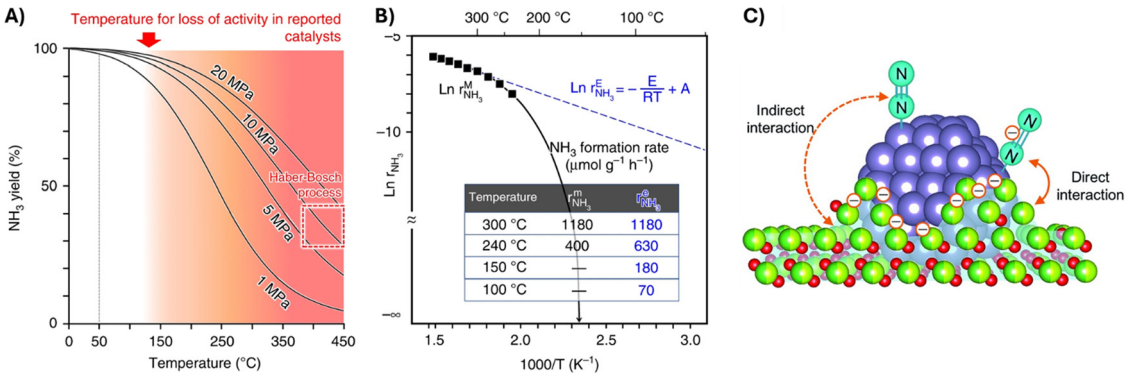

Fig. 20 (A) Relationship between NH_3 yield and varying temperature and pressure.[41,206] (B) Arrhenius plots illustrating NH_3 synthesis kinetics over a commercial Fe catalyst. (A) and (B) Have been reproduced from ref. 206 with permission from Springer Nature, Copyright © 2020, openly licensed *via* CC BY 4.0. (C) Possible mechanism of N_2 activation over $Ru/Ce_{0.5}La_{0.5}O_{1.75}$–650red.[210] Figure has been reproduced from ref. 211 with permission from the Royal Society of Chemistry, Copyrigh © 2018, openly licensed *via* CC BY 3.0.

N_2 and H_2 conversion between 100–200 °C. Reducing the temperature for catalytic activity loss below 50 °C could significantly improve NH_3 synthesis efficiency at low temperatures (<300 °C). While homogeneous systems using specific reagents achieve NH_3 synthesis below room temperature, strategies for lowering the activity loss temperature in N_2 and H_2 systems remain unclear. Marnellos *et al.* illustrated this process, converting 78% of delivered H_2 into NH_3 at 570 °C and atmospheric pressure.[203,207] Perovskite materials are commonly used as electrolytes, with some studies exploring fluorite or pyrochlore structures. Notably, a composite electrolyte of YDC combined with calcium–potassium phosphate demonstrated high NH_3 rates in one study.[200,208,209] When the electrolyte is a proton conductor, the electrochemical reactions at the two electrodes involve the anode reaction and the cathode reaction, combining to form the overall reaction aligning with the traditional Haber–Bosch process.[200]

Most of the reactions at the anode and cathode involved gaseous H_2 and N_2, respectively. Pd-containing catalysts, especially Ag–Pd electrodes, exhibited high reaction rates and FE.[200] The introduction of water vapor (steam) was found to enhance protonic conductivity in perovskite electrolytes. When barium cerate-based electrolytes operated with wet hydrogen over the anode, higher reaction rates and FEs were observed.[212,213]

In contrast to the industrial process, the electrochemical synthesis process bypasses the need for purified gaseous H_2, relying on protons (H^+) conducted through the solid electrolyte. This approach opens the possibility of using any hydrogen-containing compound, eliminating the extensive purification required in traditional methods.[200] Notably, studies demonstrated the feasibility of solid state ammonia synthesis (SSAS) from steam and nitrogen using a solid electrolyte cell with an Ag–Ru/MgO catalyst (cathode).[211] Fig. 20(C) illustrates the two modes of N_2 adsorption:[210] direct interaction, where N_2 adsorbs on Ru atoms strongly coupled with the reduced support through strong metal–support interaction (SMSI), and indirect interaction, where N_2 adsorbs on Ru atoms with weak coupling to the reduced support. Moreover, an oxygen-ion (O_2^-) conductor can be employed for SSAS, synthesizing NH_3 from gaseous nitrogen and steam. Reaction rates in O_2^- cells were notably lower than those in proton-conducting cells, potentially due to oxygen-containing compounds at the cathode. The use of gaseous fuel at the anode in O_2^- cells could potentially reduce energy requirements for *in situ* hydrogen production.[211]

Open Access Article. Published on 24 4 2025. Downloaded on 2026-02-14 8:12:44.
This article is licensed under a Creative Commons Attribution-NonCommercial 3.0 Unported Licence.

In industrial processes, a substantial portion of the overall cost is associated with preparing and purifying hydrogen feed gas, making the electrochemical synthesis approach an attractive alternative. Specific studies, such as Wang *et al.*,[209] reported high reaction rates in SSAS using different electrolytes and hydrogen sources (natural gas, CH_4).

Several issues in NH_3 synthesis have been identified, such as limitations in proton transport rates and catalyst modification due to ion spillover from the solid electrolyte.[205,214] The utilization of water as a proton source resolves problems related to impurity-induced catalyst poisoning.[215] Electrochemical NH_3 synthesis from steam and N_2 *via* solid-state proton-conducting electrolytes, exemplified by $SrCe_{0.95}Yb_{0.05}O_{3-\delta}$, displayed promising outcomes, producing NH_3 at notable rates.[211] Reducing the operating temperature to 400 °C significantly boosted NH_3 production from wet N_2, although concerns regarding proton conductivity and resistance loss emerged.[216] Thinner electrolyte membranes are crucial for practical applications, given that bulk proton conductors are relatively thick and sintered at high temperatures. Thin proton-conducting membranes showed reduced resistance and improved NH_3 formation rates.[212] The electrochemical NH_3 synthesis process using solid electrolytes exhibits significant potential, especially when employing high-temperature protonic conductors. There are several challenges also which persist regarding temperature optimization and membrane thickness.[205,207–209,212,217]

2.6.2. Intermediate temperature NH_3 synthesis. The electrochemical synthesis of NH_3 using a molten salt electrolyte operates within a temperature range of 300 to 500 °C. Converting N_2 to NH_3 faces the challenge of breaking the robust triple bond of N_2. One effective approach is through a lithium-mediated pathway, where metallic lithium reacts with N_2 to form lithium nitride (Li_3N) as an intermediate.[168] This pathway, initially proposed by Tsuneto *et al.*,[169] demonstrated a maximum efficiency of 59% at 50 atm of N_2 and requires high-pressure and non-water-derived electron donors. Building on this concept, Murakami *et al.* employed a LiCl–KCl–CsCl electrolyte and utilized nitride ions from Li_3N to synthesize NH_3 electrochemically under atmospheric pressure.[218] Using this system, NH_3 was produced at a rate of 201.96 μg cm^{-2} h^{-1} with a current efficiency of 72% at 400 °C.[218] Subsequent experiments explored methane as a hydrogen source, showcasing NH_3 and carbon formation at 500 °C.[219] At 400 °C, the NH_3 synthesis rate was hampered due to the minimal decomposition rate of methane. To enhance NH_3 production, steam was employed as a hydrogen source, resulting in NH_3 production at an average rate of 1224 μg h^{-1} cm^{-2} with a 23% efficiency at 300 °C.[220,221] This process involved a carbon anode, which, unfortunately, was consumed due to the reaction between carbon and oxide ions, releasing CO_2.[220] To mitigate this issue, researchers adopted a non-consumable B-doped diamond anode for NH_3 synthesis under atmospheric pressure.[221]

Although this adjustment yielded reduced NH_3 yields, hinting at potential NH_3 reactions with oxygen ions.[221] Subsequent studies introduced nanoparticle catalysts within molten NaOH/KOH electrolytes, enhancing NH_3 formation rates albeit with voltage considerations and catalyst particle size being key factors determining activity.[200,222] Parallel advancements explored composite electrolytes, combining solid oxides with eutectic mixtures of alkali metal salts, primarily aiming to enhance ionic conductivity and lower operating temperatures for hydrogen fuel cells within the 400 °C to 800 °C range.[200] Amar *et al.* assessed these composite electrolytes for solid-state NH_3 synthesis (SSAS) in cell configurations akin to earlier designs.[223] Their exploration involving a mixture of $(Li/Na/K)_2CO_3$ and $LiAlO_2$ revealed varied catalysts and hydrogen sources, identifying Co_3Mo_3N as the most promising catalyst, achieving significant rates at 450 °C albeit with relatively lower efficiencies, primarily attributed to rapid hydrogen evolution.[223] Noteworthy enhancements in reaction rates were observed with alterations in electrolyte composition, emphasizing the potential of $(Li,Na,K)_2CO_3$-SDC as an electrolyte, showcasing an augmented reaction rate compared to prior electrolytes.[203,218–221,224]

2.6.3. Low temperature NH_3 synthesis. NH_3 synthesis at low temperatures (below 100 °C) utilizes proton-conducting electrolytes like Nafion and sulfonated polysulfone (SPSF).[200] Operating at these lower temperatures offers two distinct advantages: firstly, the reaction becomes spontaneous, and secondly, the proton conductivity of low-temperature electrolytes, such as Nafion, significantly surpasses that of counterparts at intermediate and high temperatures.[225,226] Despite these benefits, reaction kinetics tend to be sluggish at lower temperatures. The inaugural report on low-temperature NH_3 synthesis surfaced in 2000 by Kordali *et al.*, employing a Nafion electrolyte alongside an alkaline solution to generate NH_3 from water and nitrogen within temperatures up to 100 °C.[227] Their setup featured a Pt anodic electrode immersed in a KOH solution, separated by a Nafion membrane, while the cathode was a carbon cloth housing a Ru catalyst where gaseous N_2 was introduced. The reactions at the electrodes and within the KOH solution delineate the overall reaction.[227]

Low-temperature experiments for NH_3 synthesis relied on either gaseous H_2[228,229] or H_2O as the hydrogen source, following similar cell configurations as depicted in Fig. 16 and 17, respectively. Varied cathode materials were explored, and noteworthy high reaction rates were observed on mixed oxide and perovskite cathodes.[229,230] For instance, Xu *et al.* reported a notably high rate of 1.13×10^{-8} mol s^{-1} cm^{-2} and an exceptional faradaic efficiency of 90.4% using an SFCN electrode.[231] Although Lan *et al.* employed Pt electrodes and operated at 25 °C, achieving a reaction rate and faradaic efficiency not among the highest (1.14×10^{-9} mol s^{-1} cm^{-2} and 0.55, respectively), their work significantly contributed to advancing the electrochemical synthesis of NH_3 by utilizing abundant reactants (water and air) at ambient conditions (25 °C and atmospheric pressure).[232]

2.6.4. Understanding thermo-electrochemical N_2 activation with molecular orbital theory. The mechanisms governing N_2-to-NH_3 conversion can be categorized into dissociative and associative pathways.[161,233,234] In the dissociative pathway, similar to the Haber–Bosch process, high-energy input initially breaks the N≡N triple bond to yield isolated N atoms, which then react with H atoms to form NH_3 molecules. In the associative pathway, hydrogenation occurs while the N_2 molecule remains bonded, either in end-on or side-on configurations, to active sites.[233,234]

© 2025 The Author(s). Published by the Royal Society of Chemistry

Open Access Article. Published on 24 4 2025. Downloaded on 2026-02-14 8:12:44.
This article is licensed under a Creative Commons Attribution-NonCommercial 3.0 Unported Licence.

The end-on configuration involves bonding of one N atom of N_2 to active sites, whereas in the side-on configuration, both N atoms bond to active sites.[235] The end-on pathway offers distal and alternating pathways for NH_3 production, while the side-on pathway primarily follows an enzymatic pathway.[233,234] In the distal pathway of the end-on configuration, proton–electron pairs initially attack the N atom furthest from the active site, leading to N_2 reduction to NH_3.[235] The key step involves facilitating electron exchange between N_2 and the catalyst, where N_2 initially donates electrons from its bonding orbitals to generate NH_3 and subsequently attacks the other N atom of N_2.[235] In the alternating pathway, proton–electron pairs alternately attack both N atoms of N_2, resulting in sequential NH_3 release.[235] The enzymatic pathway parallels the alternating pathway in its hydrogenation process.[233,234]

In electrochemical NRR, ATP-hydrolysis electrons are replaced by those from an external electrode. Regardless of the method, essential steps include N_2 adsorption, activation, hydrogenation, and NH_3 desorption.[235] Effective N_2 adsorption in electrochemical NRR involves selecting catalysts with favorable active sites, similar to the biological FeMo cofactor, and other transition metals known for their N_2 adsorption and activation capabilities using d-orbital electrons.[236,237] Additionally, strategies such as vacancy engineering, edge adsorption, heterojunction, and heteroatoms doping can enhance N_2 adsorption by redistributing catalyst charge density.[235,238] Furthermore, catalysts with high specific surface areas enhance N_2 adsorption by providing more exposed active sites.[235,239] The concentration of N_2 in the reaction solvent also affects adsorption rates through gas–liquid–solid interface exchange.[235,240]

N_2 activation typically involves a donation-acceptance process, often requiring a negative electrode potential to inject electrons into N_2's antibonding π^* orbital.[108] Other methods include photo-induced and plasmon-driven hot electrons for electron injection.[234,241] At this activation step, a free energy increase often occurs, involving $*N_2$ or $*N_2H$ formation.[234] During hydrogenation, the catalytic environment influences pathways and orders, yielding products like NH_3, N_2H_4, and H_2.[108] NH_3 desorption, crucial for catalytic cycle efficiency, is facilitated by destabilizing $*NH_2$ on strong-binding sites, reducing free energy during $*NH_3$ formation and desorption.[234]

Produced NH_3 readily dissolves in water, facilitating active site release for subsequent cycles. Ensuring electron exchange throughout the NRR process necessitates a conductive catalyst substrate to support continuous electron injection to active sites.[108,242] Fig. 21 presents various electrochemical setups for NH_3 synthesis, each utilizing different approaches to nitrogen reduction. Panel A shows a solid-state proton-conducting cell that produces NH_3 from steam (H_2O) and nitrogen (N_2). Panel B[5,242] depicts an electrochemical membrane reactor where NH_3 is synthesized using methane (CH_4), steam (H_2O), and nitrogen (N_2). Panel C[243] illustrates a molten salt (NaOH-KOH) cell that facilitates NH_3 production through the reaction of hydrogen (H_2) with N^{3-} ions. In panel D, a hydrochloric acid (HCl)[244] cell is shown, where NH_3 is synthesized on a VN/TM (VN on titanium mesh) catalyst *via* the Mars–van Krevelen mechanism.

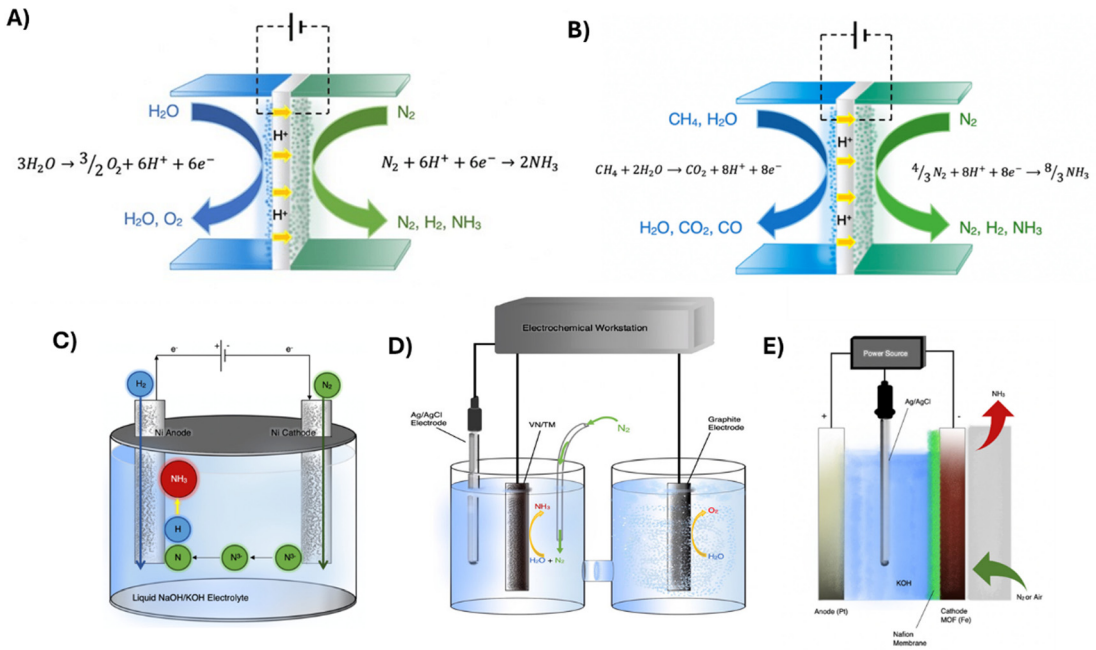

Fig. 21 (A) Schematic of a solid-state proton-conducting cell showing the process of NH_3 synthesis using steam (H_2O) and N_2.[242] (B) Schematic of an electrochemical membrane reactor illustrating NH_3 synthesis using CH_4, H_2O, and N_2.[242] (C) Schematic of a molten salt (NaOH-KOH) cell where NH_3 is produced from the reaction of H_2 with N_3^- ions.[242,243] (D) Schematic of a HCl cell where NH_3 is produced on a VN/(titanium mesh) (VN/TM) catalyst *via* a Mars–van Krevelen mechanism.[242,244] (E) Diagram of the KOH cell where NH_3 production was catalyzed by metal–organic frameworks (MOFs) of Fe, Cu, and Co.[242] Figures have been reproduced with permission from ref. 242 © 2019 by the authors. Licensee MDPI, Basel, Switzerland, openly licensed *via* CC BY 3.0.

© 2025 The Author(s). Published by the Royal Society of Chemistry

Open Access Article. Published on 24 4 2025. Downloaded on 2026-02-14 8:12:44.
This article is licensed under a Creative Commons Attribution-NonCommercial 3.0 Unported Licence.

Finally, panel E presents a KOH cell catalyzed by metal–organic frameworks (MOFs) made of Fe, Cu, and Co,[245] highlighting a diverse range of electrolyte and catalyst designs aimed at enhancing NH_3 synthesis efficiency. These schematics underscore the evolving strategies across different reaction environments for sustainable NH_3 production.

Addressing practical challenges includes overcoming low NH_3 yield and Faraday efficiency (FE). Challenges include the competitive hydrogen evolution reaction (HER) at similar standard potentials, hindering electron availability for NRR.[246] High energy barriers associated with N-related intermediates during hydrogenation or NH_3 desorption can also impede active sites and promote HER.[235] Catalyst properties such as intrinsic activity, porosity, specific surface area, and substrate conductivity also influence NH_3 production efficiency.

2.6.5. Decarbonization in ammonia production. Decarbonizing ammonia production is imperative, given the significant greenhouse gas (GHG) emissions associated with the conventional Haber–Bosch process. High-temperature electrochemical ammonia synthesis has emerged as a potential low-carbon alternative. However, its widespread adoption remains hindered by high energy consumption, low conversion efficiency, and competitive hydrogen evolution reactions. A multifaceted approach is required to mitigate these challenges and reduce carbon emissions, encompassing renewable energy integration, process optimization, and advanced catalyst development. A primary strategy involves replacing fossil fuel-derived hydrogen with electrochemically produced hydrogen from renewable energy sources such as solar, wind, or hydroelectric power. Life cycle assessment (LCA) studies indicate that this transition can significantly lower the carbon footprint of ammonia production compared to conventional methods. Operating under milder conditions-such as lower temperatures and pressures, further enhances energy efficiency and reduces overall emissions. Solid oxide electrolysis cells (SOECs) have demonstrated superior efficiency in hydrogen generation, offering a promising route to improve the sustainability of electrochemical ammonia synthesis. Catalyst advancements play a crucial role in enhancing process efficiency and minimizing emissions. Recent studies have demonstrated that transition-metal-free catalysts, including nitrogen-doped carbons and black phosphorus, exhibit enhanced nitrogen fixation capabilities while reducing energy intensity.[247–250]

2.6.6. Divergence between simulations and experimental NRR. Bridging the gap between theoretical predictions, particularly those from DFT simulations, and experimental observations remains a significant challenge in electrocatalysis, especially for the NRR and related catalytic processes. While DFT provides critical insights into reaction energetics and intermediate states, its reliance on idealized conditions often leads to discrepancies compared to actual experimental outcomes. Factors such as catalyst deactivation, solvent effects, and competing side reactions, including hydrogen evolution, are frequently overlooked in conventional computational models. The inability of standard DFT approaches to accurately capture dynamic electrode potential shifts, explicit solvation effects, and catalyst surface reconstructions under operating conditions further complicates the alignment between theory and experiment. In the case of NRR, catalysts predicted to be highly selective in theoretical studies often degrade rapidly in practical applications due to by-product adsorption or structural transformations that are inadequately represented in conventional models. Long-term stability predictions remain challenging as computational methods struggle to incorporate degradation mechanisms such as metal leaching or oxide formation. Addressing these limitations requires a multifaceted approach, integrating advanced computational techniques such as molecular dynamics simulations, explicit solvation models, and machine learning-enhanced DFT to improve predictive accuracy. Refining experimental methodologies to ensure kinetic control and proper normalization of catalytic activity is essential for meaningful comparisons. By fostering closer collaboration between theorists and experimentalists and leveraging emerging computational advancements, a more accurate and reliable framework for catalyst design can be established, ultimately driving progress in ammonia synthesis and broader electrocatalytic applications.[149,251–253]

2.6.7. Future outlook. The future of high-temperature NH_3 synthesis depends on several key advancements and strategic considerations. One pivotal advantage lies in the electrochemical process's ability to bypass extensive hydrogen purification, a significant cost in conventional NH_3 production methods reliant on natural gas. Using protons as the hydrogen source eliminates the need for purification, enhancing the overall economic viability of this approach.[203] The pursuit of scaling up this electrochemical process necessitates achieving high FEs and reaction rates. Presently, FEs at low temperatures tend to be notably low due to sluggish reaction kinetics, while at high temperatures, FEs are acceptable, a considerable fraction of produced NH_3 gets lost due to reverse reactions. The challenge here lies in finding solid-state materials that exhibit robust mechanical properties and high protonic conductivity within the critical temperature range of 250 °C to 450 °C.[203]

Advancing this field requires a collaborative effort encompassing both theoretical and practical dimensions. A thorough comprehension of the high-temperature electrocatalytic NH_3 synthesis mechanism across diverse electrocatalysts is imperative. This involves conducting experimental and theoretical studies to explore reaction pathways on various active surfaces, from precious metals to metal nitrides and perovskite oxides. Leveraging advanced characterization techniques like *in situ*/in *operando* spectroscopy can offer deeper insights into these processes, and innovative electrode design is also paramount. Relying on precious metal-based electrodes might be rethought in favor of novel electrocatalysts that can sustain high activity while suppressing dominant hydrogen evolution reactions. Computational studies hint at transition metal nitrides significantly impacting nitrogen reduction for NH_3 synthesis *via* specific mechanisms.[254] Resolving debates around nitrogen source origins requires meticulous isotope labeling experiments, clarifying whether reported production values stem from potential contamination or the materials themselves.

© 2025 The Author(s). Published by the Royal Society of Chemistry

Open Access Article. Published on 24 4 2025. Downloaded on 2026-02-14 8:12:44.
This article is licensed under a Creative Commons Attribution-NonCommercial 3.0 Unported Licence.

3. Summary and overall outlook

This review offers an in-depth exploration of the challenges and recent advancements in nitrogen activation, focusing on the activation and catalytic transformation of atmospheric N_2 into biologically and industrially valuable compounds, such as NH_3 and nitrates. Nitrogen activation is central to global agriculture, chemical production, and ecological balance, as it provides reactive nitrogen essential for fertilizers, fine chemicals, and biological processes. The Haber–Bosch process, a century-old innovation, continues to dominate industrial nitrogen activation due to its efficiency and scalability. Its high energy consumption, reliance on fossil fuels, and significant carbon emissions have driven research into alternative methods. Emerging approaches are being developed to address these limitations, including biological nitrogen activation, plasma-assisted processes, electrochemical and thermochemical methods, and homogeneous catalysis.

Biological nitrogen activation, mediated by nitrogenase enzymes, operates under ambient conditions and provides a sustainable pathway for nitrogen conversion. The process is inherently energy-intensive, as it requires substantial ATP to overcome the stability of the N≡N triple bond. Similarly, mechanistic insights into catalytic nitrogen activation reveal the complexity of breaking the triple bond, with transition metals playing a pivotal role by facilitating back-donation of electrons into nitrogen's antibonding orbitals. Novel catalyst designs, such as Ru-based systems and metal hydrides, can help reduce the reaction barriers. Furthermore, homogeneous catalytic systems inspired by enzymatic structures have demonstrated significant progress, with molybdenum- and iron-based complexes achieving selective N_2 reduction under mild conditions.

A significant focus in recent research has been on advancing sustainable hydrogen sources to support nitrogen activation processes. Innovations in methane pyrolysis and direct seawater electrolysis aim to reduce carbon emissions associated with hydrogen production. These technologies provide greener alternatives and integrate well with emerging electrochemical nitrogen activation methods. Non-thermal plasma techniques have also garnered attention for their ability to activate nitrogen under atmospheric conditions, offering a potential route for decentralized, non-thermal nitrogen activation. Achieving selectivity and minimizing by-products in alternative catalytic methods remain active research areas. Optimizing catalytic systems to reduce reaction conditions, improving the energy efficiency of hydrogen production, and leveraging the insights from biological nitrogen activation are critical steps for progress.

4. Conclusions

This review highlights the different dinitrogen (N_2) activation methods that offer a transformative pathway for developing energy-efficient ammonia synthesis and other nitrogen-based chemical products. We have seen that N_2's inertness stems from its high bond dissociation energy, large HOMO–LUMO gap, and minimal polarity factors demanding extraordinary reaction conditions or specialized catalysts to achieve practical conversion into valuable products such as ammonia, nitrates, urea, or other nitrogen-containing compounds. The substantial energy requirements of Haber–Bosch process, its reliance on fossil-derived hydrogen, and inevitable CO_2 emissions have stimulated extensive research into alternative pathways and catalysts.

We surveyed an array of emerging strategies for nitrogen fixation using nitrogenase enzymes, homogeneous and metallocomplex routes leveraging transition-metal complexes, plasma-based activation inspired by lightning, electrochemical approaches driven by renewable electricity, and integrated thermo-electrochemical processes that combine the best of both high-temperature and electrochemical methods. Each route presents specific benefits and challenges: biological systems can circumvent harsh industrial conditions but face scalability limits; homogeneous catalysts enable selective transformations yet often struggle with product separation; plasma processes provide high reactivity but can be energy-intensive; electrochemical methods offer greener, on-demand synthesis but require breakthroughs in catalyst selectivity to overcome competing side reactions such as the hydrogen evolution reaction; and thermo-electrochemical platforms aim to capitalize on robust materials and high protonic conductivity but must still balance reaction kinetics and energy costs.

Collectively, these insights highlight that no single method offers a universal solution. Instead, future progress will depend on converging multiple innovations: designing catalysts that selectively favor N_2 activation over undesired reactions, enhancing active-site density *via* advanced nanostructures or single-atom approaches, coupling reaction systems with renewable energy sources, improving our mechanistic understanding of elementary reaction steps through *in situ*/*operando* techniques, and employing rigorous protocols (including isotope labeling) to validate performance. Successful breakthroughs in these areas could ultimately transform nitrogen fixation into a more sustainable, decentralized, and energy-efficient process. As research accelerates in catalysis, materials science, and process engineering, the collective goal remains clear: to unlock the full potential of N_2 as a readily available feedstock for vital chemicals and clean energy carriers, thereby contributing to a more resilient and sustainable global economy.

Data availability

No primary research results, software or code have been included and no new data were generated or analysed as part of this review.

Conflicts of interest

The authors declare no competing financial interest.

Acknowledgements

This material is based on the work performed in the Materials and Systems Engineering Laboratory at the University of Illinois

Open Access Article. Published on 24 4 2025. Downloaded on 2026-02-14 8:12:44.
This article is licensed under a Creative Commons Attribution-NonCommercial 3.0 Unported Licence.

Chicago (UIC) and the Gauthier Laboratory at Texas Tech University (TTU). The authors used 'Generative AI on text selection' by 'Grammarly' to improve readability and language of the article. This material is based upon work supported by the National Science Foundation (NSF) Engineering Research Center for Advancing Sustainable and Distributed Fertilizer Production (CASFER) under Grant No. 2133576. S. A. O. and J. A. G. gratefully acknowledge support from The Welch Foundation under Grant NumberD-2188-20240404.

References

1 H. Iriawan, S. Z. Andersen, X. Zhang, B. M. Comer, J. Barrio, P. Chen, A. J. Medford, I. E. Stephens, I. Chorkendorff and Y. Shao-Horn, *Nat. Rev. Methods Primers*, 2021, **1**, 56.
2 B. Chang, H. Zhang, S. Sun and G. Zhang, *Carbon Energy*, 2024, **6**, e491.
3 University *Chemistry, 4/E*, Pearson Education, 2009.
4 A. O'Connor, *The Undergraduate Historical Journal at UC Merced*, 2014, 2.
5 A. Rovaletti, L. De Gioia, C. Greco and F. Arrigoni, *Dalton Trans.*, 2023, **52**, 7966–7974.
6 J. D. Cox, D. D. Wagman and V. A. Medvedev, CODATA—Key Values for Thermodynamics, aus der Reihe: CODATA, Series on Thermodynamic Properties, in *Berichte der Bunsengesellschaft für physikalische Chemie*, Hemisphere Publishing Corporation, New York, Washington, Philadelphia, London, 1989, DOI: 10.1002/bbpc.19900940121.
7 B. L. Oberholtzer, Publications of the National Bureau of Standards, U.S. Department of Commerce, 1970, p. 378.
8 H.-P. Jia and E. A. Quadrelli, *Chem. Soc. Rev.*, 2014, **43**, 547–564.
9 D.-Y. Hwang and A. M. Mebel, *J. Phys. Chem. A*, 2003, **107**, 2865–2874.
10 Y. Huang, D. D. Babu, Z. Peng and Y. Wang, *Adv. Sci.*, 2020, **7**, 1902390.
11 A. Shilov, *Russ. Chem. Bull.*, 2003, **52**, 2555–2562.
12 K. H. R. Rouwenhorst, P. M. Krzywda, N. E. Benes, G. Mul and L. Lefferts, *Techno-Economic Challenges of Green Ammonia as an Energy Vector*, 2021, pp. 41–83.
13 C. Smith, A. K. Hill and L. Torrente-Murciano, *Energy Environ. Sci.*, 2020, **13**, 331–344.
14 T. D. Rapson and C. C. Wood, *Catalysts*, 2022, **12**, 844.
15 R. K. Sharma, H. Patel, U. Mushtaq, V. Kyriakou, G. Zafeiropoulos, F. Peeters, S. Welzel, M. C. Van De Sanden and M. N. Tsampas, *ACS Energy Lett.*, 2020, **6**, 313–319.
16 M. K. Sosna, Y. A. Sokolinskii, D. Khudyakov and A. Lapidus, *Solid Fuel Chem.*, 2022, **56**, 456–461.
17 V. Smil, *Nature*, 1999, **400**, 415.
18 J. G. Speight, *Kirk-Othmer Encycl. Chem. Technol.*, 2000, DOI: 10.1002/0471238961.0701190519160509.a01.
19 F. Haber, *Nobel Lect.*, 1920, **2**, 1.
20 A. Frank and N. Caro, DE88363, 1895.
21 The Rjukan–Notodden Industrial World Heritage Site, https://ra.brage.unit.no/ra-xmlui/bitstream/handle/11250/177016/Verdensarv_norsk_industriarv_submission_nov_2009.pdf?sequence=1&isAllowed=y.
22 A. Silverman, *J. Chem. Educ.*, 1938, **15**, 289.
23 R. Oesper, *J. Chem. Educ.*, 1948, **25**, 531.
24 A. Vojvodic, A. J. Medford, F. Studt, F. Abild-Pedersen, T. S. Khan, T. Bligaard and J. Nørskov, *Chem. Phys. Lett.*, 2014, **598**, 108–112.
25 G. Ertl, *Angew. Chem., Int. Ed.*, 2008, **47**, 3524–3535.
26 T. Zambelli, J. Trost, J. Wintterlin and G. Ertl, *Phys. Rev. Lett.*, 1996, **76**, 795.
27 R. Imbihl, R. J. Behm, G. Ertl and W. Moritz, *Surf. Sci.*, 1982, **123**, 129–140.
28 F. Bozso, G. Ertl, M. Grunze and M. Weiss, *J. Catal.*, 1977, **49**, 18–41.
29 G. Ertl, *Catal. Rev.:Sci. Eng.*, 1980, **21**, 201–223.
30 S. Dahl, A. Logadottir, R. Egeberg, J. Larsen, I. Chorkendorff, E. Törnqvist and J. K. Nørskov, *Phys. Rev. Lett.*, 1999, **83**, 1814.
31 G. Ertl, M. Weiss and S. Lee, *Chem. Phys. Lett.*, 1979, **60**, 391–394.
32 B. A. Rohr, A. R. Singh and J. K. Nørskov, *J. Catal.*, 2019, **372**, 33–38.
33 G. P. Connor and P. L. Holland, *Catal. Today*, 2017, **286**, 21–40.
34 M. Kitano, Y. Inoue, Y. Yamazaki, F. Hayashi, S. Kanbara, S. Matsuishi, T. Yokoyama, S.-W. Kim, M. Hara and H. Hosono, *Nat. Chem.*, 2012, **4**, 934–940.
35 Y. Inoue, M. Kitano, K. Kishida, H. Abe, Y. Niwa, M. Sasase, Y. Fujita, H. Ishikawa, T. Yokoyama and M. Hara, *ACS Catal.*, 2016, **6**, 7577–7584.
36 Y. Kobayashi, Y. Tang, T. Kageyama, H. Yamashita, N. Masuda, S. Hosokawa and H. Kageyama, *J. Am. Chem. Soc.*, 2017, **139**, 18240–18246.
37 W. Gao, P. Wang, J. Guo, F. Chang, T. He, Q. Wang, G. Wu and P. Chen, *ACS Catal.*, 2017, **7**, 3654–3661.
38 A. Cao, V. J. Bukas, V. Shadravan, Z. Wang, H. Li, J. Kibsgaard, I. Chorkendorff and J. K. Nørskov, *Nat. Commun.*, 2022, **13**, 2382.
39 S. Hagen, R. Barfod, R. Fehrmann, C. J. Jacobsen, H. T. Teunissen, K. Ståhl and I. Chorkendorff, *Chem. Commun.*, 2002, 1206–1207.
40 M. Kitano, Y. Inoue, H. Ishikawa, K. Yamagata, T. Nakao, T. Tada, S. Matsuishi, T. Yokoyama, M. Hara and H. Hosono, *Chem. Sci.*, 2016, **7**, 4036–4043.
41 M. Hattori, T. Mori, T. Arai, Y. Inoue, M. Sasase, T. Tada, M. Kitano, T. Yokoyama, M. Hara and H. Hosono, *ACS Catal.*, 2018, **8**, 10977–10984.
42 P. Wang, F. Chang, W. Gao, J. Guo, G. Wu, T. He and P. Chen, *Nat. Chem.*, 2017, **9**, 64–70.
43 T.-N. Ye, S.-W. Park, Y. Lu, J. Li, M. Sasase, M. Kitano, T. Tada and H. Hosono, *Nature*, 2020, **583**, 391–395.
44 T.-N. Ye, S.-W. Park, Y. Lu, J. Li, M. Sasase, M. Kitano and H. Hosono, *J. Am. Chem. Soc.*, 2020, **142**, 14374–14383.
45 Z. Ma, X. Xiong, C. Song, B. Hu and W. Zhang, *RSC Adv.*, 2016, **6**, 51106–51110.
46 V. Shadravan, A. Cao, V. J. Bukas, M. K. Grønborg, C. D. Damsgaard, Z. Wang, J. Kibsgaard, J. K. Nørskov and I. Chorkendorff, *Energy Environ. Sci.*, 2022, **15**, 3310–3320.

© 2025 The Author(s). Published by the Royal Society of Chemistry

Open Access Article. Published on 24 4 2025. Downloaded on 2026-02-14 8:12:44.
This article is licensed under a Creative Commons Attribution-NonCommercial 3.0 Unported Licence.

47 S. Wu, Y.-K. Peng, T.-Y. Chen, J. Mo, A. Large, I. McPherson, H.-L. Chou, I. Wilkinson, F. Venturini and D. Grinter, *ACS Catal.*, 2020, **10**, 5614–5622.
48 T. Brown, *Chem. Eng. Prog.*, 2019, **115**, 47–53.
49 M. Khan, T. Al-Attas, S. Roy, M. M. Rahman, N. Ghaffour, V. Thangadurai, S. Larter, J. Hu, P. M. Ajayan and M. G. Kibria, *Energy Environ. Sci.*, 2021, **14**, 4831–4839.
50 M. F. Lagadec and A. Grimaud, *Nat. Mater.*, 2020, **19**, 1140–1150.
51 S. r Dresp, F. Dionigi, M. Klingenhof and P. Strasser, *ACS Energy Lett.*, 2019, **4**, 933–942.
52 S. T. Wismann, J. S. Engbæk, S. B. Vendelbo, F. B. Bendixen, W. L. Eriksen, K. Aasberg-Petersen, C. Frandsen, I. Chorkendorff and P. M. Mortensen, *Science*, 2019, **364**, 756–759.
53 D. C. Upham, V. Agarwal, A. Khechfe, Z. R. Snodgrass, M. J. Gordon, H. Metiu and E. W. McFarland, *Science*, 2017, **358**, 917–921.
54 C. Palmer, M. Tarazkar, H. H. Kristoffersen, J. Gelinas, M. J. Gordon, E. W. McFarland and H. Metiu, *ACS Catal.*, 2019, **9**, 8337–8345.
55 D. Kang, N. Rahimi, M. J. Gordon, H. Metiu and E. W. McFarland, *Appl. Catal., B*, 2019, **254**, 659–666.
56 D. A. Zuberer, *Principles and applications of soil microbiology*, Elsevier, 2021, pp. 423–453.
57 R. C. Burns and R. W. F. Hardy, *Nitrogen Fixation in Bacteria and Higher Plants, Molecular Biology, Biochemistry and Biophysics*, Springer Berlin Heidelberg, Germany, 2012.
58 A. Adeniyi, I. Bello, T. Mukaila, N. C. Sarker and A. Hammed, *BioTech*, 2023, **12**, 41.
59 C. C. Cleveland, A. R. Townsend, D. S. Schimel, H. Fisher, R. W. Howarth, L. O. Hedin, S. S. Perakis, E. F. Latty, J. C. Von Fischer and A. Elseroad, *Global Biogeochem. Cycles*, 1999, **13**, 623–645.
60 D. Fowler, M. Coyle, U. Skiba, M. A. Sutton, J. N. Cape, S. Reis, L. J. Sheppard, A. Jenkins, B. Grizzetti and J. N. Galloway, *Philos. Trans. R. Soc., B*, 2013, **368**, 20130164.
61 J. K. Ladha, M. B. Peoples, P. M. Reddy, J. C. Biswas, A. Bennett, M. L. Jat and T. J. Krupnik, *Field Crops Res.*, 2022, **283**, 108541.
62 F. J. de Bruijn and M. Hungria, *Good Microbes Med., Food Prod., Biotechnol., Biorem., Agric.*, 2022, 466–475.
63 N. Rascio and N. La Rocca, *Encyclopedia of ecology*, Elsevier, 2008, vol. 1, pp. 412–419.
64 R. H. Burris and G. P. Roberts, *Annu. Rev. Nutr.*, 1993, **13**, 317–335.
65 J. R. Postgate, *Nitrogen fixation*, Cambridge University Press, 1998.
66 J. Young and G. Stacey, in *Phylogenetic Classification of Nitrogen Nitrogen-¢ xing Organism*, ed. G. Stacey, R. H. Burris and H. J. Evans, 1992, pp. 43–86.
67 D. Gadkari, *Catalysts for Nitrogen Fixation: Nitrogenases, Relevant Chemical Models and Commercial Processes*, Springer, 2004, pp. 309–332.
68 M. Ribbe, D. Gadkari and O. Meyer, *J. Biol. Chem.*, 1997, **272**, 26627–26633.
69 D. MacKellar, L. Lieber, J. S. Norman, A. Bolger, C. Tobin, J. W. Murray, M. Oksaksin, R. L. Chang, T. J. Ford and P. Q. Nguyen, *Sci. Rep.*, 2016, **6**, 20086.
70 V. Krewald, *Dalton Trans.*, 2018, **47**, 10320–10329.
71 I. Fischler and E. K. von Gustorf, *Naturwissenschaften*, 1975, **62**, 63–70.
72 L. C. Seefeldt, B. M. Hoffman and D. R. Dean, *Curr. Opin. Chem. Biol.*, 2012, **16**, 19–25.
73 R. Cai and S. D. Minteer, *ACS Energy Lett.*, 2018, **3**, 2736–2742.
74 R. Bjornsson, F. A. Lima, T. Spatzal, T. Weyhermueller, P. Glatzel, E. Bill, O. Einsle, F. Neese and S. DeBeer, *Chem. Sci.*, 2014, **5**, 3096–3103.
75 S. M. Keable, O. A. Zadvornyy, L. E. Johnson, B. Ginovska, A. J. Rasmussen, K. Danyal, B. J. Eilers, G. A. Prussia, A. X. LeVan and S. Raugei, *J. Biol. Chem.*, 2018, **293**, 9629–9635.
76 D. Sippel and O. Einsle, *Nat. Chem. Biol.*, 2017, **13**, 956–960.
77 B. M. Hoffman, D. Lukoyanov, Z.-Y. Yang, D. R. Dean and L. C. Seefeldt, *Chem. Rev.*, 2014, **114**, 4041–4062.
78 T. Spatzal, M. Aksoyoglu, L. Zhang, S. L. Andrade, E. Schleicher, S. Weber, D. C. Rees and O. Einsle, *Science*, 2011, **334**, 940.
79 O. Einsle and D. C. Rees, *Chem. Rev.*, 2020, **120**, 4969–5004.
80 B. K. Burgess and D. J. Lowe, *Chem. Rev.*, 1996, **96**, 2983–3012.
81 G. Koskey, S. W. Mburu, J. M. Kimiti, O. Ombori, J. M. Maingi and E. M. Njeru, *Front. Microbiol.*, 2018, **9**, 968.
82 H. B. Vuong, P. H. Thrall and L. G. Barrett, *J. Ecol.*, 2017, **105**, 540–548.
83 M. Laranjo and S. Oliveira, *Antonie van Leeuwenhoek*, 2011, **99**, 651–662.
84 R. K. Goyal, M. A. Schmidt and M. F. Hynes, *Microorganisms*, 2021, **9**, 125.
85 J. Yang, *Catalysts*, 2019, **9**, 939.
86 F. B. Simpson and R. H. Burris, *Science*, 1984, **224**, 1095–1097.
87 Q. Wang, Y. Guan, J. Guo and P. Chen, *Cell Rep. Phys. Sci.*, 2022, **3**, 100779.
88 F. A. Tezcan, J. T. Kaiser, J. B. Howard and D. C. Rees, *J. Am. Chem. Soc.*, 2015, **137**, 146–149.
89 L. C. Seefeldt, Z.-Y. Yang, D. A. Lukoyanov, D. F. Harris, D. R. Dean, S. Raugei and B. M. Hoffman, *Chem. Rev.*, 2020, **120**, 5082–5106.
90 J. Fiolet, A. Baartscheer, C. Schumacher, R. Coronel and H. Ter Welle, *J. Mol. Cell. Cardiol.*, 1984, **16**, 1023–1036.
91 H. Kammermeier, P. Schmidt and E. Jüngling, *J. Mol. Cell. Cardiol.*, 1982, **14**, 267–277.
92 N. Cherkasov, A. Ibhadon and P. Fitzpatrick, *Chem. Eng. Process.*, 2015, **90**, 24–33.
93 R. A. Alberty, *Arch. Biochem. Biophys.*, 2001, **389**, 94–109.
94 R. N. Thorneley and D. Lowe, *Biochem. J.*, 1984, **224**, 887–894.
95 B. M. Hoffman, D. Lukoyanov, D. R. Dean and L. C. Seefeldt, *Acc. Chem. Res.*, 2013, **46**, 587–595.
96 B. M. Hoffman, D. R. Dean and L. C. Seefeldt, *Acc. Chem. Res.*, 2009, **42**, 609–619.

Open Access Article. Published on 24 4 2025. Downloaded on 2026-02-14 8:12:44.
This article is licensed under a Creative Commons Attribution-NonCommercial 3.0 Unported Licence.

97 F. Neese, *Angew. Chem., Int. Ed.*, 2006, **45**, 196–199.
98 B. Hinnemann and J. K. Nørskov, *Top. Catal.*, 2006, **37**, 55–70.
99 J. Kästner and P. E. Blöchl, *J. Am. Chem. Soc.*, 2007, **129**, 2998–3006.
100 R. R. Schrock, *Acc. Chem. Res.*, 2005, **38**, 955–962.
101 S. Kuriyama and Y. Nishibayashi, *Tetrahedron*, 2021, **83**, 131986.
102 M. Vol'Pin and V. Shur, *Nature*, 1966, **209**, 1236.
103 K. Shiina, *J. Am. Chem. Soc.*, 1972, **94**, 9266–9267.
104 E.-Y. Jeong, C.-Y. Yoo, C. H. Jung, J. H. Park, Y. C. Park, J.-N. Kim, S.-G. Oh, Y. Woo and H. C. Yoon, *ACS Sustainable Chem. Eng.*, 2017, **5**, 9662–9666.
105 H. Liu, L. Wei, F. Liu, Z. Pei, J. Shi, Z.-J. Wang, D. He and Y. Chen, *ACS Catal.*, 2019, **9**, 5245–5267.
106 H. Basch, D. G. Musaev, K. Morokuma, M. D. Fryzuk, J. B. Love, W. W. Seidel, A. Albinati, T. F. Koetzle, W. T. Klooster and S. A. Mason, *J. Am. Chem. Soc.*, 1999, **121**, 523–528.
107 I. Čorić and P. L. Holland, *J. Am. Chem. Soc.*, 2016, **138**, 7200–7211.
108 S. Wang, F. Ichihara, H. Pang, H. Chen and J. Ye, *Adv. Funct. Mater.*, 2018, **28**, 1803309.
109 Y. Nishibayashi, *Dalton Trans.*, 2012, **41**, 7447–7453.
110 K. Arashiba, Y. Miyake and Y. Nishibayashi, *Nat. Chem.*, 2011, **3**, 120–125.
111 D. V. Yandulov and R. R. Schrock, *Science*, 2003, **301**, 76–78.
112 S. Kuriyama, K. Arashiba, H. Tanaka, Y. Matsuo, K. Nakajima, K. Yoshizawa and Y. Nishibayashi, *Angew. Chem., Int. Ed.*, 2016, **55**, 14291–14295.
113 A. J. Kendall, S. I. Johnson, R. M. Bullock and M. T. Mock, *J. Am. Chem. Soc.*, 2018, **140**, 2528–2536.
114 Y. Sekiguchi, K. Arashiba, H. Tanaka, A. Eizawa, K. Nakajima, K. Yoshizawa and Y. Nishibayashi, *Angew. Chem., Int. Ed.*, 2018, **57**, 9064–9068.
115 K. Hashizume, Y. Mizobe and M. Hidai, *Organometallics*, 1996, **15**, 3303–3309.
116 J. Chatt, A. Pearman and R. Richards, *Nature*, 1975, **253**, 39–40.
117 J. Y. Becker and S. Avraham, *J. Electroanal. Chem. Interfacial Electrochem.*, 1990, **280**, 119–127.
118 N. Furuya and H. Yoshiba, *J. Electroanal. Chem. Interfacial Electrochem.*, 1989, **263**, 171–174.
119 N. Furuya and H. Yoshiba, *J. Electroanal. Chem. Interfacial Electrochem.*, 1989, **272**, 263–266.
120 T. J. Del Castillo, N. B. Thompson and J. C. Peters, *J. Am. Chem. Soc.*, 2016, **138**, 5341–5350.
121 T. Li, S. Han, Y. Wang, J. Zhou, B. Zhang and Y. Yu, *Angew. Chem., Int. Ed.*, 2023, **62**, e202217411.
122 C. E. Laplaza and C. C. Cummins, *Science*, 1995, **268**, 861–863.
123 K. Arashiba, A. Eizawa, H. Tanaka, K. Nakajima, K. Yoshizawa and Y. Nishibayashi, *Bull. Chem. Soc. Jpn.*, 2017, **90**, 1111–1118.
124 Y. Roux, C. Duboc and M. Gennari, *ChemPhysChem*, 2017, **18**, 2606–2617.
125 Y. Lee, F. T. Sloane, G. Blondin, K. A. Abboud, R. García-Serres and L. J. Murray, *Angew. Chem., Int. Ed.*, 2015, **54**, 1499–1503.
126 M. M. Rodriguez, E. Bill, W. W. Brennessel and P. L. Holland, *Science*, 2011, **334**, 780–783.
127 K. H. Rouwenhorst, F. Jardali, A. Bogaerts and L. Lefferts, *Energy Environ. Sci.*, 2021, **14**, 2520–2534.
128 L. R. Winter and J. G. Chen, *Joule*, 2021, **5**, 300–315.
129 P. Peng, P. Chen, C. Schiappacasse, N. Zhou, E. Anderson, D. Chen, J. Liu, Y. Cheng, R. Hatzenbeller and M. Addy, *J. Cleaner Prod.*, 2018, **177**, 597–609.
130 V. D. Rusanov, A. Fridman and G. V. E. Sholin, *Sov. Phys.-Usp.*, 1981, **24**, 447.
131 T. Grigoreva, A. Levitskii, S. Macheret, L. Polak, V. Rusanov and A. Fridman, *High Energy Chem.*, 1984, **18**, 268–272.
132 A. Gicquel, S. Cavadias and J. Amouroux, *J. Phys. D:Appl. Phys.*, 1986, **19**, 2013.
133 P. Peng, C. Schiappacasse, N. Zhou, M. Addy, Y. Cheng, Y. Zhang, K. Ding, Y. Wang, P. Chen and R. Ruan, *ChemSusChem*, 2019, **12**, 3702–3712.
134 R. Azizov, V. Zhivotov, M. Krotov, V. Rusanov, Y. Tarasov and A. Fridma, *Khim. Vys. Energ.*, 1980, **14**, 366–368.
135 E. Eremin, V. Belova and A. Mal'tsev, *Zh. Fiz. Khim.*, 1978, **52**, 1679–1682.
136 J. Van Durme, J. Dewulf, C. Leys and H. Van Langenhove, *Appl. Catal., B*, 2008, **78**, 324–333.
137 Y. He, Z. Chen, Z. Li, G. Niu and J. Tang, *Front. Optoelectron.*, 2018, **11**, 92–96.
138 X. Zhao and Y. Tian, *Cell Rep. Phys. Sci.*, 2023, **4**, 101618.
139 D. Liu, H. Yan, J. Lin, S. Lu, Y. Xie, X. Peng, S. Liang and L. Jiang, *Chem. Eng. Sci.*, 2024, **283**, 119448.
140 J. Lin, X. Lin, S. Lu, W. Liao, T. Qi, S. Liang, Z.-J. Zhao and L. Jiang, *Chem. Eng. Sci.*, 2024, **300**, 120664.
141 Z. Sun, J. Lin, S. Lu, Y. Li, T. Qi, X. Peng, S. Liang and L. Jiang, *Langmuir*, 2024, **40**, 5469–5478.
142 W. Liao, L. Qi, Y. Wang, J. Qin, G. Liu, S. Liang, H. He and L. Jiang, *Adv. Funct. Mater.*, 2021, **31**, 2009151.
143 B. H. R. Suryanto, D. Wang, L. M. Azofra, M. Harb, L. Cavallo, R. Jalili, D. R. G. Mitchell, M. Chatti and D. R. MacFarlane, *ACS Energy Lett.*, 2019, **4**, 430–435.
144 W. Liao, K. Xie, L. Liu, X. Wang, Y. Luo, S. Liang, F. Liu and L. Jiang, *J. Energy Chem.*, 2021, **62**, 359–366.
145 X. Yang, J. Nash, J. Anibal, M. Dunwell, S. Kattel, E. Stavitski, K. Attenkofer, J. G. Chen, Y. Yan and B. Xu, *J. Am. Chem. Soc.*, 2018, **140**, 13387–13391.
146 H. Fang, D. Liu, Y. Luo, Y. Zhou, S. Liang, X. Wang, B. Lin and L. Jiang, *ACS Catal.*, 2022, **12**, 3938–3954.
147 M. Anand, C. S. Abraham and J. K. Nørskov, *Chem. Sci.*, 2021, **12**, 6442–6448.
148 S. A. Olusegun, Y. Qi, N. C. Kani, M. R. Singh and J. A. Gauthier, *ACS Catal.*, 2024, **14**, 16885–16896.
149 G. Qing, R. Ghazfar, S. T. Jackowski, F. Habibzadeh, M. M. Ashtiani, C.-P. Chen, M. R. Smith III and T. W. Hamann, *Chem. Rev.*, 2020, **120**, 5437–5516.
150 S. Z. Andersen, V. Čolić, S. Yang, J. A. Schwalbe, A. C. Nielander, J. M. McEnaney, K. Enemark-Rasmussen, J. G. Baker, A. R. Singh and B. A. Rohr, *Nature*, 2019, **570**, 504–508.

© 2025 The Author(s). Published by the Royal Society of Chemistry

Open Access Article. Published on 24 4 2025. Downloaded on 2026-02-14 8:12:44.
This article is licensed under a Creative Commons Attribution-NonCommercial 3.0 Unported Licence.

151 J. Choi, B. H. Suryanto, D. Wang, H.-L. Du, R. Y. Hodgetts, F. M. Ferrero Vallana, D. R. MacFarlane and A. N. Simonov, *Nat. Commun.*, 2020, **11**, 5546.
152 A. U. Shetty and R. Sankannavar, *J. Energy Chem.*, 2024, **92**, 681–697.
153 S. C. Jesudass, S. Surendran, J. Y. Kim, T.-Y. An, G. Janani, T.-H. Kim, J. K. Kim and U. Sim, *Electrochem. Energy Rev.*, 2023, **6**, 27.
154 C. Hu, X. Chen, J. Jin, Y. Han, S. Chen, H. Ju, J. Cai, Y. Qiu, C. Gao, C. Wang, Z. Qi, R. Long, L. Song, Z. Liu and Y. Xiong, *J. Am. Chem. Soc.*, 2019, **141**, 7807–7814.
155 K.-i Aika, *Catal. Today*, 2017, **286**, 14–20.
156 Y. Kobayashi, M. Kitano, S. Kawamura, T. Yokoyama and H. Hosono, *Catal.:Sci. Technol.*, 2017, **7**, 47–50.
157 C. D. Zeinalipour-Yazdi, J. S. J. Hargreaves and C. R. A. Catlow, *J. Phys. Chem. C*, 2018, **122**, 6078–6082.
158 Y. Yao, S. Zhu, H. Wang, H. Li and M. Shao, *J. Am. Chem. Soc.*, 2018, **140**, 1496–1501.
159 M. A. Shipman and M. D. Symes, *Catal. Today*, 2017, **286**, 57–68.
160 C. Yang, Y. Zhu, J. Liu, Y. Qin, H. Wang, H. Liu, Y. Chen, Z. Zhang and W. Hu, *Nano Energy*, 2020, **77**, 105126.
161 X. Cui, T. Cheng and Q. Zhang, *Adv. Energy Mater.*, 2018, **8**, 1800369.
162 J. Kibsgaard, J. K. Nørskov and I. Chorkendorff, *ACS Energy Lett.*, 2019, **4**, 2986–2988.
163 P. Mars and D. W. van Krevelen, *Chem. Eng. Sci.*, 1954, **3**, 41–59.
164 H. Y. Kim and G. Henkelman, *J. Phys. Chem. Lett.*, 2013, **4**, 216–221.
165 S. U. Haq, M. Aghajamali and H. Hassanzadeh, *RSC Adv.*, 2021, **11**, 24387–24397.
166 C. D. Zeinalipour-Yazdi, J. S. J. Hargreaves and C. R. A. Catlow, *J. Phys. Chem. C*, 2015, **119**, 28368–28376.
167 N. C. Kani, I. Goyal, J. A. Gauthier, W. Shields, M. Shields and M. R. Singh, *ACS Appl. Mater. Interfaces*, 2024, **16**, 16203–16212.
168 K. Kim, S. J. Lee, D. Y. Kim, C. Y. Yoo, J. W. Choi, J. N. Kim, Y. Woo, H. C. Yoon and J. I. Han, *ChemSusChem*, 2018, **11**, 120–124.
169 A. Tsuneto, A. Kudo and T. Sakata, *J. Electroanal. Chem.*, 1994, **367**, 183–188.
170 I. Goyal, N. C. Kani, S. A. Olusegun, S. Chinnabattigalla, R. R. Bhawnani, K. D. Glusac, A. R. Singh, J. A. Gauthier and M. R. Singh, *ACS Energy Lett.*, 2024, **9**, 4188–4195.
171 W. Liao, H.-X. Liu, L. Qi, S. Liang, Y. Luo, F. Liu, X. Wang, C.-R. Chang, J. Zhang and L. Jiang, *Cell Rep. Phys. Sci.*, 2021, **2**, 100557.
172 H. Shen, C. Choi, J. Masa, X. Li, J. Qiu, Y. Jung and Z. Sun, *Chem*, 2021, **7**, 1708–1754.
173 S. Back and Y. Jung, *Phys. Chem. Chem. Phys.*, 2016, **18**, 9161–9166.
174 C. J. M. van der Ham, M. T. M. Koper and D. G. H. Hetterscheid, *Chem. Soc. Rev.*, 2014, **43**, 5183–5191.
175 E. Skúlason, T. Bligaard, S. Gudmundsdóttir, F. Studt, J. Rossmeisl, F. Abild-Pedersen, T. Vegge, H. Jónsson and J. K. Nørskov, *Phys. Chem. Chem. Phys.*, 2012, **14**, 1235–1245.
176 C. Ling, Y. Zhang, Q. Li, X. Bai, L. Shi and J. Wang, *J. Am. Chem. Soc.*, 2019, **141**, 18264–18270.
177 Y. Abghoui, A. L. Garden, V. F. Hlynsson, S. Björgvinsdóttir, H. Ólafsdóttir and E. Skúlason, *Phys. Chem. Chem. Phys.*, 2015, **17**, 4909–4918.
178 S. Y. Park, Y. J. Jang and D. H. Youn, *Catalysts*, 2023, **13**, 639.
179 O. Christensen, A.-I. Hutu, H. H. Kristoffersen and J. Rossmeisl, *J. Catal.*, 2024, **436**, 115572.
180 L. Sun, K. Wen, G. Li, X. Zhang, X. Zeng, B. Johannessen and S. Zhang, *ACS Mater. Au*, 2024, **4**, 547–556.
181 D. Zhang, H. Zhao, X. Wu, Y. Deng, Z. Wang, Y. Han, H. Li, Y. Shi, X. Chen and S. Li, *Adv. Funct. Mater.*, 2021, **31**, 2006939.
182 Y. Wen, W. Zhang, X. Wang, S. Lu, F. Duan, H. Zhu and M. Du, *Chem. Commun.*, 2023, **59**, 13371–13374.
183 Y. Yao, H. Wang, X.-Z. Yuan, H. Li and M. Shao, *ACS Energy Lett.*, 2019, **4**, 1336–1341.
184 Y. Yao, S. Zhu, H. Wang, H. Li and M. Shao, *Angew. Chem., Int. Ed.*, 2020, **59**, 10479–10483.
185 L. Zeng, X. Li, S. Chen, J. Wen, W. Huang and A. Chen, *J. Mater. Chem. A*, 2020, **8**, 7339–7349.
186 F. Lai, N. Chen, X. Ye, G. He, W. Zong, K. B. Holt, B. Pan, I. P. Parkin, T. Liu and R. Chen, *Adv. Funct. Mater.*, 2020, **30**, 1907376.
187 X.-W. Lv, Y. Liu, R. Hao, W. Tian and Z.-Y. Yuan, *ACS Appl. Mater. Interfaces*, 2020, **12**, 17502–17508.
188 Y. Fu, T. Li, G. Zhou, J. Guo, Y. Ao, Y. Hu, J. Shen, L. Liu and X. Wu, *Nano Lett.*, 2020, **20**, 4960–4967.
189 D. Yao, C. Tang, L. Li, B. Xia, A. Vasileff, H. Jin, Y. Zhang and S.-Z. Qiao, *Adv. Energy Mater.*, 2020, **10**, 2001289.
190 I. Valov, B. Luerssen, E. Mutoro, L. Gregoratti, R. A. De Souza, T. Bredow, S. Günther, A. Barinov, P. Dudin, M. Martin and J. Janek, *Phys. Chem. Chem. Phys.*, 2011, **13**, 3394–3410.
191 R. Tort, A. Bagger, O. Westhead, Y. Kondo, A. Khobnya, A. Winiwarter, B. J. Davies, A. Walsh, Y. Katayama and Y. Yamada, *ACS Catal.*, 2023, **13**, 14513–14522.
192 H. Jin, S. S. Kim, S. Venkateshalu, J. Lee, K. Lee and K. Jin, *Adv. Sci.*, 2023, **10**, 2300951.
193 Z. Chen, C. Liu, L. Sun and T. Wang, *ACS Catal.*, 2022, **12**, 8936–8975.
194 I. Lucentini, X. Garcia, X. Vendrell and J. Llorca, *Ind. Eng. Chem. Res.*, 2021, **60**, 18560–18611.
195 D. Shlyapin, V. Borisov, V. Temerev, K. Iost, Z. Fedorova and P. Snytnikov, *Kinet. Catal.*, 2023, **64**, 815–825.
196 M. Krebsz, R. Y. Hodgetts, S. Johnston, C. K. Nguyen, Y. Hora, D. R. MacFarlane and A. N. Simonov, *Energy Environ. Sci.*, 2024, **17**, 4481–4487.
197 Y. Bicer and I. Dincer, *J. Electrochem. Soc.*, 2017, **164**, H5036.
198 H. Liu, *Chin. J. Catal.*, 2014, **35**, 1619–1640.
199 I. Rossetti, N. Pernicone and L. Forni, *Catal. Today*, 2005, **102–103**, 219–224.
200 V. Kyriakou, I. Garagounis, E. Vasileiou, A. Vourros and M. Stoukides, *Catal. Today*, 2017, **286**, 2–13.
201 X. Guo, Y. Zhu and T. Ma, *J. Energy Chem.*, 2017, **26**, 1107–1116.
202 A. J. Martín, T. Shinagawa and J. Pérez-Ramírez, *Chem*, 2019, **5**, 263–283.

© 2025 The Author(s). Published by the Royal Society of Chemistry

Open Access Article. Published on 24 4 2025. Downloaded on 2026-02-14 8:12:44.
This article is licensed under a Creative Commons Attribution-NonCommercial 3.0 Unported Licence.

203 R. Zhao, H. Xie, L. Chang, X. Zhang, X. Zhu, X. Tong, T. Wang, Y. Luo, P. Wei, Z. Wang and X. Sun, *EnergyChem*, 2019, **1**, 100011.
204 Á. B. Höskuldsson, Y. Abghoui, A. B. Gunnarsdóttir and E. Skúlason, *ACS Sustainable Chem. Eng.*, 2017, **5**, 10327–10333.
205 C. G. Yiokari, G. E. Pitselis, D. G. Polydoros, A. D. Katsaounis and C. G. Vayenas, *J. Phys. Chem. A*, 2000, **104**, 10600–10602.
206 M. Hattori, S. Iijima, T. Nakao, H. Hosono and M. Hara, *Nat. Commun.*, 2020, **11**, 2001.
207 G. Marnellos and M. Stoukides, *Science*, 1998, **282**, 98–100.
208 B. H. Wang, R. Q. Liu, J. D. Wang, Z. J. Li and Y. H. Xie, *Chin. J. Inorg. Chem.*, 2005, **21**, 1551–1555.
209 B. H. Wang, J. D. Wang, R. Q. Liu, Y. H. Xie and Z. J. Li, *J. Solid State Electrochem.*, 2006, **11**, 27–31.
210 Y. Ogura, K. Sato, S. I. Miyahara, Y. Kawano, T. Toriyama, T. Yamamoto, S. Matsumura, S. Hosokawa and K. Nagaoka, *Chem. Sci.*, 2018, **9**, 2230–2237.
211 A. Skodra and M. Stoukides, *Solid State Ionics*, 2009, **180**, 1332–1336.
212 W. B. Wang, X. B. Cao, W. J. Gao, F. Zhang, H. T. Wang and G. L. Ma, *J. Membr. Sci.*, 2010, **360**, 397–403.
213 C.-H. Chen, S.-J. Chang, S.-P. Chang, M.-J. Li, I. C. Chen, T.-J. Hsueh and C.-L. Hsu, *Chem. Phys. Lett.*, 2009, **476**, 69–72.
214 C. G. Vayenas, M. M. Jaksic, S. I. Bebelis and S. G. Neophytides, in *Modern Aspects of Electrochemistry*, ed. J. O. M. Bockris, B. E. Conway and R. E. White, Springer US, Boston, MA, 1996, vol. 29, pp. 57–202, DOI: **10.1007/978-1-4613-0327-5_2**.
215 S. Giddey, S. P. S. Badwal and A. Kulkarni, *Int. J. Hydrogen Energy*, 2013, **38**, 14576–14594.
216 C. W. Li and M. W. Kanan, *J. Am. Chem. Soc.*, 2012, **134**, 7231–7234.
217 Á. B. Höskuldsson, Y. Abghoui, A. B. Gunnarsdóttir and E. Skúlason, *ACS Sustainable Chem. Eng.*, 2017, **5**, 10327–10333.
218 T. Murakami, T. Nishikiori, T. Nohira and Y. Ito, *J. Am. Chem. Soc.*, 2003, **125**, 334–335.
219 T. Murakami, T. Nohira, Y. H. Ogata and Y. Ito, *Electrochem. Solid-State Lett.*, 2005, **8**, D12–D14.
220 T. Murakami, T. Nohira, T. Goto, Y. H. Ogata and Y. Ito, *Electrochim. Acta*, 2005, **50**, 5423–5426.
221 T. Murakami, T. Nohira, Y. Araki, T. Goto, R. Hagiwara and Y. H. Ogata, *Electrochem. Solid-State Lett.*, 2007, **10**, E4–E6.
222 S. Licht, B. Cui, B. Wang, F. F. Li, J. Lau and S. Liu, *Science*, 2014, **345**, 637–640.
223 I. A. Amar, R. Lan, C. T. G. Petit and S. Tao, *Int. J. Electrochem. Sci.*, 2015, **10**, 3757–3766.
224 I. A. Amar, C. T. G. Petit, L. Zhang, R. Lan, P. J. Skabara and S. Tao, *Solid State Ionics*, 2011, **201**, 94–100.
225 I. Garagounis, V. Kyriakou, A. Skodra, E. Vasileiou and M. Stoukides, *Front. Energy Res.*, 2014, **2**, DOI: **10.3389/fenrg.2014.00001**.
226 I. A. Amar, R. Lan, C. T. G. Petit and S. Tao, *J. Solid State Electrochem.*, 2011, **15**, 1845–1860.
227 V. Kordali, G. Kyriacou and C. Lambrou, *Chem. Commun.*, 2000, 1673–1674, DOI: **10.1039/b004885m**.
228 J. N. Renner, L. F. Greenlee, A. M. Herring and K. E. Ayers, *Electrochem. Soc. Interface*, 2015, **24**, 51–57.
229 Z. Zhang, Z. Zhong and R. Liu, *J. Rare Earths*, 2010, **28**, 556–559.
230 R. Liu and G. Xu, *Chin. J. Chem.*, 2010, **28**, 139–142.
231 G. Xu, R. Liu and J. Wang, *Sci. China, Ser. B:Chem.*, 2009, **52**, 1171–1175.
232 R. Lan, J. T. S. Irvine and S. Tao, *Sci. Rep.*, 2013, **3**, 1145.
233 C. Ling, X. Bai, Y. Ouyang, A. Du and J. Wang, *J. Phys. Chem. C*, 2018, **122**, 16842–16847.
234 Y. Wan, J. Xu and R. Lv, *Mater. Today*, 2019, **27**, 69–90.
235 B. Ma, H. Zhao, T. S. Li, Q. Liu, Y. Luo, C. Li, S. Lu, A. M. Asiri, D. Ma and X. Sun, *Nano Res.*, 2020, **14**, 1–15.
236 J. S. Anderson, G. E. Cutsail, III, J. Rittle, B. A. Connor, W. A. Gunderson, L. Zhang, B. M. Hoffman and J. C. Peters, *J. Am. Chem. Soc.*, 2015, **137**, 7803–7809.
237 Z. Wang, F. Gong, L. Zhang, R. Wang, L. Ji, Q. Liu, Y. Luo, H. Guo, Y. Li, P. Gao, X. Shi, B. Li, B. Tang and X. Sun, *Adv. Sci.*, 2019, **6**, 1801182.
238 F. Lai, J. Feng, X. Ye, W. Zong, G. He, C. Yang, W. Wang, Y.-E. Miao, B. Pan, W. Yan, T. Liu and I. P. Parkin, *J. Mater. Chem. A*, 2020, **8**, 1652–1659.
239 W. Tong, B. Huang, P. Wang, Q. Shao and X. Huang, *Natl. Sci. Rev.*, 2020, **8**, nwaa088.
240 M. Ali, F. Zhou, K. Chen, C. Kotzur, C. Xiao, L. Bourgeois, X. Zhang and D. R. MacFarlane, *Nat. Commun.*, 2016, **7**, 11335.
241 C. Ling, X. Niu, Q. Li, A. Du and J. Wang, *J. Am. Chem. Soc.*, 2018, **140**, 14161–14168.
242 I. Garagounis, A. Vourros, D. Stoukides, D. Dasopoulos and M. Stoukides, *Membranes*, 2019, **9**, 112.
243 Y. Bicer and I. Dincer, *J. Electrochem. Soc.*, 2017, **164**, H5036–H5042.
244 R. Zhang, Y. Zhang, X. Ren, Y. Luo, G. Cui, A. M. Asiri, B. Zheng and X.-P. Sun, *ACS Sustainable Chem. Eng.*, 2018, **6**, 9545–9549.
245 X. Zhao, F. Yin, N. Liu, G. Li, T. Fan and B. Chen, *J. Mater. Sci.*, 2017, **52**, 1–11.
246 L. Zhang, G.-F. Chen, L.-X. Ding and H. Wang, *Chem. – Eur. J.*, 2019, **25**, 12464–12485.
247 H. Ishaq and C. Crawford, *Energy Convers. Manage.*, 2024, **300**, 117869.
248 A. E. Yüzbaşıoğlu, A. H. Tatarhan and A. O. Gezerman, *Heliyon*, 2021, **7**, e08257.
249 C. A. Fernandez, O. Chapman, M. A. Brown, C. E. Alvarez-Pugliese and M. C. Hatzell, *Environ. Sci. Technol.*, 2024, **58**, 6964–6977.
250 A. M. Mohamed, I. G. Economou and Y. Bicer, *Curr. Opin. Green Sustainable Chem.*, 2024, 100947.
251 F. Dominguez-Flores and M. M. Melander, *Curr. Opin. Electrochem.*, 2022, **36**, 101110.
252 J. Resasco, F. Abild-Pedersen, C. Hahn, Z. Bao, M. T. Koper and T. F. Jaramillo, *Nat. Catal.*, 2022, **5**, 374–381.
253 Y. Yang, J. Wang, Y. Shu, Y. Ji, H. Dong and Y. Li, *Phys. Chem. Chem. Phys.*, 2022, **24**, 8591–8603.
254 S. Gunduz, D. J. Deka and U. S. Ozkan, *J. Catal.*, 2020, **387**, 207–216.

© 2025 The Author(s). Published by the Royal Society of Chemistry